National Library
of Canada

Acquisitions and
Bibliographic Services Branch

395 Wellington Street
Ottawa, Ontario
K1A 0N4

Bibliothèque nationale
du Canada

Direction des acquisitions et
des services bibliographiques

395, rue Wellington
Ottawa (Ontario)
K1A 0N4

Your file Votre référence

Our file Notre référence

NOTICE

The quality of this microform is heavily dependent upon the quality of the original thesis submitted for microfilming. Every effort has been made to ensure the highest quality of reproduction possible.

If pages are missing, contact the university which granted the degree.

Some pages may have indistinct print especially if the original pages were typed with a poor typewriter ribbon or if the university sent us an inferior photocopy.

Reproduction in full or in part of this microform is governed by the Canadian Copyright Act, R.S.C. 1970, c. C-30, and subsequent amendments.

AVIS

La qualité de cette microforme dépend grandement de la qualité de la thèse soumise au microfilmage. Nous avons tout fait pour assurer une qualité supérieure de reproduction.

S'il manque des pages, veuillez communiquer avec l'université qui a conféré le grade.

La qualité d'impression de certaines pages peut laisser à désirer, surtout si les pages originales ont été dactylographiées à l'aide d'un ruban usé ou si l'université nous a fait parvenir une photocopie de qualité inférieure.

La reproduction, même partielle, de cette microforme est soumise à la Loi canadienne sur le droit d'auteur, SRC 1970, c. C-30, et ses amendements subséquents.

Canada

Impact of Engineering Modelling Assumptions on Assessing the Seismic Performance of Montgomery Block Building

By

Laith Boussabah

Thesis Submitted
to the School of Graduate Studies
in partial fulfilment of the requirements
for the Master of Applied Science in Civil Engineering
under the auspices of the Ottawa-Carleton
Institute for Civil Engineering

UNIVERSITÉ D' OTTAWA

UNIVERSITY OF OTTAWA

ISBN 0-315-82589-8

UNIVERSITÉ D'OTTAWA
UNIVERSITY OF OTTAWA

To Salah

& Souad

Abstract

This study focuses on the Montgomery Block building, built in 1853 and which survived the 1906 San Francisco earthquake of magnitude 8.3 despite being roughly 15 km from the ruptured San Andreas fault (Freeman 1932).

After a review of the existing literature on the seismic performance of unreinforced masonry structures, a summary of the lessons to be learned and an identification of the areas that require further research is presented. Then, an assessment of the range of predicted seismic capacities as estimated from traditional and conservative methods to the most liberal ones for the selected Montgomery building is conducted. Finally, a comparison of these capacities is performed to illustrate the impact of structural engineering modelling decisions on the predicted seismic performance of URM buildings.

From this study, it is clear that depending on the structural model selected by the engineer, considerable differences of nearly an order of magnitude in some cases may exist in the seismic performance assessments of URM buildings.

Acknowledgments

My special thanks go to my supervisor Dr. Michel Bruneau for his support, advice and patience; without his directions, this thesis could have looked much different and less complete. I would like to thank my professors of the University of Ottawa such as Dr. Murat Saatcioglu for his excellent teaching and pedagogy, Dr. H. Tanaka, Dr. Suter from Carleton University for his useful discussions and all my friends and colleagues for their fruitful discussions and critiques.

I would like to express my gratitude to the Tunisian and Canadian governments for providing the financial support under the scholarship program CIDA/Tunisia. As well, I should acknowledge the financial support of Public Works Canada, the National Research Council of Canada and the Natural Sciences and Engineering Research Council of Canada.

My deep thanks go to my parents, for their patience and support throughout my studies; their advice and encouragement always helped me achieve my goals in life.

Table of Contents

List of Tables

List of Figures

Notations

γ	: Shear strain
Δ	: Lateral floor or master Joint displacement
ξ	: Damping ratio
σ_1	: Principal tensile stress
σ_o	: Peak value of the shear stress
σ_t	: Tensile stress capacity for masonry
σ_x	: Tensile stress in x-direction
σ_y	: Tensile stress in y-direction
τ	: Shear stress
τ_{max}	: Maximum shear stress at failure (fundamental shear stress capacity of masonry in pure shear
τ_{MEAN}	: Maximum average shear stress
τ_u	: Maximum shear stress that can be applied on masonry already stressed by an applied gravity load
2D	: 2 Dimensional
3D	: 3 Dimensional
ABK	: A joint-venture of three Southern Californian engineering consultant firms: Agbabian Associates, S.B. Barnes & Associates, and Kariotis & Associates
b or t	: Thickness of a pier or a shear wall
D or d	: Width of a pier or a shear wall

DCR : Demand-to-Capacity Ratio

E-W : East-West

E_m : Modulus of elasticity

ENA : Eastern North America

EQ : Earthquake

F.C. : Flexural Compression

F.T. : Flexural Tension

f'_m : Ultimate compressive strength of masonry

f_m : Maximum allowable axial or flexural compressive stress

f_t : Maximum allowable direct or flexural tensile stress

F_{wx} : Force applied to a wall or pier al level x

G : Modulus of rigidity (Shear modulus)

H or h : Height of a pier or a shear wall

LLRSE : Lateral-Load-Resistant Structural Element

M.J. : Master Joint

MMI : Mass Moment of Inertia

N-S : North-South

P : Compressive force

P.S. : Pure Shear

P_D : Superimposed dead load at the top of the pier under consideration

PGA : Peak Ground Acceleration

PGD : Peak Ground Displacement

PGV : Peak Ground Velocity

Pr.S. : Precompressed Shear

PSa : Pseudo Spectral acceleration

P_w : Weight of wall or pier

SAP90 : Structural Analysis Program 1990

SDOF : Single Degree Of Freedom system

UCBC :Uniform Code for Building Conservation

URM : Unreinforced Masonry

V : Shear force

v_a : Allowable shear stress for URM

V_a : Shear cracking strength

v_m : Maximum allowable shear stress

V_{max} : Maximum Base shear

V_R : Rocking restoring shear

W : Total weight of a model

W_d : Total dead load tributary to a diaphragm

W_p : Element self-weight

W_{wx} : Dead load of an URM wall assigned to level X halfway above and below the level under consideration

CHAPTER 1

Introduction

1.1. Statement of the problem:

In North America, many old buildings are unreinforced masonry (URM) structures. These buildings, constructed in the absence of mandatory earthquake design requirements, are thought to be the most vulnerable to earthquakes. Yet, many of them have survived strong earthquakes. Investigating the seismic performance of such survivors would definitely help in understanding the behaviour of URM buildings which can translate into savings when seismic retrofit is considered, or even demonstrate in some cases that a building is already capable to withstand a broad range of earthquake ground motion intensities.

1.2. Research objectives:

There is apparently no consensus regarding which of the modelling strategies provides the most realistic appraisal of the true seismic resistance of unreinforced masonry walls in evaluating the in-plane and out-of-plane behaviors of these structures. In order to avoid conservative decisions leading to expensive rehabilitation costs, this research work presents the existing analytical and modelling procedures and assess the effectiveness of some modelling procedures on the predicted performance of an URM building predominantly made of Pier/Spandrel facades with numerous openings and URM shear walls. It is hoped that findings from this case study will provide general knowledge more broadly applicable.

1.3. Selection of the building:

This study focuses on the four-story Montgomery Block building. Built in 1853, this 122 ft 3 in x 137 ft 10 in URM building has a relatively rigid first storey, having more URM shear walls in both perpendicular directions than for the other three storeys of identical floor plan. The thickness of the walls and piers of the studied structure is equal to 0.45 m and is constant for all the elements. The height of the first, second, third and fourth storey are respectively equal to 3.8 m, 3.5 m, 3.2 m and 2.9 m. All the floors and the low attic ceiling of the last floor, which has a height of 0.75 m, are made of wood. This building has an interior court providing natural light, hence surrounded by walls with numerous window openings. Three of the exterior perforated facades are equally perforated walls: The north facade is situated on Washington street, the south facade is situated on Merchant street and the west facade is situated on the Montgomery street. Each perforated facade has 4 ft deep spandrels for the three first storeys and 5.5 ft deep for the fourth storey, with piers continuous from the base to the roof. The east wall is made of three rigid walls at the first storey and a solid wall without any opening for the other storeys. The reconstructed architectural plans are in appendix A. This office building survived the 1906 San-Francisco earthquake of

magnitude 8.3 despite being roughly 15 km from the ruptured San Andreas fault (Freeman 1932). This structure, which was demolished approximately 25 years ago to be replaced by the "Transamerica Pyramid" high-rise, was selected for this research programme because of:

(i) The availability of reconstructed structural drawings.

(ii) The almost regular structural layout of the building.

(iii) The absence of liability problems.

(iv) The fact it surprisingly survived what is considered to be a major earthquake.

1.4. Scope of work:

This research programme consists of four main parts:

- A review of the existing literature on the seismic performance of URM structures, a summary of the lessons to be learned and an identification of the areas that require further research.
- A presentation of existing analytical and modelling procedures assessing the seismic performance of URM buildings, including simplified methods of structural analysis for use with existing codes and structural standards for the design of URM structures and the ABK[1] methodology.
- An assessment of the range of predicted seismic capacities as estimated from traditional and conservative methods to the most liberal ones for the selected Montgomery building. The lateral deformations and fundamental periods of the building are also considered as a function of the various resulting capacities.
- A comparison of these capacities to illustrate the impact of structural engineering modelling decisions on the predicted seismic performance of URM buildings. This is accomplished by interpreting the results in the perspective that the Montgomery Block

[1] ABK is a joint-venture of three Southern Californian engineering consultant firms: Agbabian Associates, S.B. Barnes & Associates, and Kariotis & Associates

Building is known to have survived the 1906 San Francisco earthquake.

1.5. Outline of Thesis:

- Chapter 2 presents the behavior concepts and material properties of URM structures, a review of their seismic performances during some selected earthquakes, and a summary from a literature survey on linear elastic and hysteretic analytical models of URM structures and their seismic performance.
- Chapter 3 presents the 2D-analysis results of the perforated facades, employing the flexible diaphragm hypothesis, by using 2 approaches: Solid pier/Cracked spandrel model and Cracked pier/Solid spandrel model.
- Chapter 4 presents the results of the 3D-analysis, utilizing the rigid diaphragm hypothesis and the previous 2 approaches.
- Chapter 5 presents the results of the UCBC 91 analysis based on the ABK approach.
- Chapter 6 interprets and discusses the results of the procedures used to analyze the Montgomery Block building.
- Chapter 7 presents the conclusions and provides some suggestions for further research and development.

CHAPTER 2

Behavior Concepts, Material Properties and State-of-the-Art on the Seismic Performance of URM Structures

2.1. UCBC concepts:

The Uniform Code for Building Conservation UCBC 1991 is based on the ABK methodology developed as an ultimate strength design procedure. Therefore, as the UCBC is to be used in context with other American working stress design codes, values in the ABK procedure have been reduced to allowable loads, but the concept should be understood in terms of ultimate loads and behaviour. Of particular interest is a special procedure, which allows a non-

conventional analysis of URM buildings.

One of the main assumptions of this special procedure, which will be applied to the Montgomery Block building in chapter 6, is to consider that the URM shear walls are rigid enough to drive each floor with an un-amplified ground motion. Floor diaphragms are assumed to yield at a driving effective ground acceleration of 0.4 g at their edges. Simultaneously, because of diaphragm flexibility, acceleration of 1.0 g could be reached at their middles. URM piers have two modes of behavior. A pier can either fail in shear, with typical "X" crackings, or rock back and forth as a solid block between rigid spandrels. The conversion from the ABK methodology to the allowable loads format underestimates the capacity of a wall system to rock.

The dynamic stability or resistance of normal walls to out-of-plane loading is dependent upon:

- The response velocities imparted by the diaphragms to the URM wall panel.
- The ratio O/W of the overburden weight of the walls above the story under consideration to the weight of the wall panel in that story.
- The slenderness ratio h/t of the wall panel in the story under consideration.

For diaphragms, the demand-to-capacity ratio (DCR) is the ratio of the 1.0 g force level to the diaphragm shear yield capacity. The presence of crosswalls in an URM building serves to couple the deformations of the diaphragms and reduce their deformation demands. Figure A-1-1 of UCBC 91 (reproduced in Figure 2.1), shows the limitations on diaphragm spans and DCRs. The outer curve represents the diaphragm displacement limit of 5 inches. In region 1, crosswalls are needed but not in regions 2 and 3. The analysis of an URM building by the UCBC 1991 special procedure can be achieved by following the flow chart of Figure 2.2.

2.2. Inventory of some selected earthquakes:

In the last decade, seven important earthquakes occurred in North America. Further to a review of published reconnaissance reports, it is noteworthy that the behaviour or the damage of URM buildings does not intrinsically depend on the magnitude of the earthquake. Many other components do have an influence on the degree of damage and life safety.

For those selected earthquakes and another earthquake which took place in Armenia, reported here due to the heavy damage it imparted to URM buildings, Table 2.1 summarizes their general characteristics and describes the seismic performance of typical URM buildings. Out-of-plane and in-plane failures and other important problems are also reported. In that table, the "damage degree" is the writer's subjective evaluation of the damage's severity sustained by the URM buildings. For example, "very high" implies there were many partial or complete collapses. For each earthquake, factors, such as the severity of out-of-plane or in-plane failures, anchorage problems and other reported problems, were all influential in assigning this damage dègree.

2.3. Material characteristics of URM structures:

In this section, URM brick masonry characteristics are presented according to different sources. Suggested values of an old URM building material characteristics are also introduced for the analysis of Montgomery block building.

2.3.1. Modulus of elasticity of URM in compression:

The Young's modulus of a brick masonry may be used up to about 75% of the ultimate strength. Until this limit, the material is treated as linearly elastic one, but, its overall stress-strain relationship is approximately parabolic. Table 2.2 gives an idea about the different

values that can be used, according to many references.

2.3.2. Direct or in-plane allowable tensile stress of URM:

Due to some in-plane loading effects, f_t might play an important role in the design of brickwork. The material characteristics, such as mortar and brick, may have a considerable influence in determining the allowable tensile stress which is generally the most difficult component to determine. According to two different sources, Table 2.3 presents the different values of f_t.

2.3.3. Flexural tensile stress in URM:

The allowable flexural tensile stress of a brick masonry element can be influenced by the brick and mortar characteristics. For example, if the brick-mortar adhesion is good, the bending strength parallel to the bed joint direction will be limited by the flexural tensile strength of the bricks and the failure crack will take the path of least resistance by passing through the head joints and brick units in an almost vertical line. Typically, this is not the case and the tensile strength of the units is strong enough to force the crack to follow the mortar joints around the units. For tension normal to the bed joints, the cracking, which is controlled by the bond between the mortar and the units, almost always occurs at the interface between these two materials. The values of f_t are given in Table 2.4.

2.3.4. Allowable flexural and axial compressive stresses of URM:

Many factors do have an influence on the axial or flexural strength of an URM brick building:

- The compressive strength of the units.
- The eccentricity of the load (type of loading).
- Slenderness of the brickwork.

- Mortar bedding and strength.
- Workmanship.

In structural design, the basic problem is to select an adequate brick-mortar combination that will be suitable to resist the imposed loads. However, in Tables 2.5 and 2.6, the brick or mortar quality does not have an influence in determining the allowable compressive stress. In fact, according to Hendry, Sinha and Davies (1987), the mortar does not have a big influence.

2.3.5. Allowable shear stress in URM:

A lot of care was given to this variable by ABK (1984), Hendry, Sinha and Davies (1987) and ACI committee 530 (1988) (Table 2.7). In fact, according to these references, the allowable shear stress of brick masonry is usually dependent on its concurrently acting vertical compression. But, when the compressive stress attains the crushing strength, the shear stress will fall to zero.

2.3.6. Suggested brick masonry properties for old buildings:

Before 1940, the most used mortars for construction were of types O, K or N and the brick units were having a typical strength of 20 to 40 MPa. For old URM buildings, according to many references, some suggested brick masonry characteristics are summarized in Table 2.8. For the study of the seismic performance of Montgomery Block building, the following values were used:

- Young modulus: E_m = 1000 MPa
- Allowable flexural tensile stress: f_t = .19 MPa
- Allowable flexural compressive stress: f_c = 2.6 MPa
- Allowable shear stress: f_s = 0.24 MPa

These allowable values are used in the study of Montgomery Block building. When an element is overstressed, it is eliminated from the model of the studied case for the next

analysis. Therefore, in chapters 3, 4 and 5, the words "crack", "cracking", "failure" and "rupture" shall be understood in terms of overstress for the working stress analyses, but conceptually correct when interpreted in their ultimate performance and the context of chapter 6.

2.4. State-of-the-art on the seismic performance of URM structures:

2.4.1. Introduction:

The potential vulnerability of old unreinforced masonry (URM) buildings, designed to no or few seismic-design requirements, is well documented. As this type of construction is prevalent in the downtown core of most North American cities exposed to a seismic risk, the districts usually of highest population density, the magnitude of this hazard can be appreciated. In regions of Eastern North America (ENA) where seismic-resistant design requirements have been in effect for a few decades already, some owners are slowly beginning to recognize this seismic-hazard; witnessing the devastating effect recent North American earthquakes have had on older URM buildings, in contrast to buildings designed to modern standards, has undoubtedly been inspirational. This has led, in some instances, to requests for the evaluation of the seismic-resistance adequacy of existing URM structures, the first step of any effective seismic hazard mitigation strategy.

While there is evidence that URM buildings can survive major earthquakes, the conditions to this satisfactory performance are not fully understood and modern analytical tools are unable to discriminate accordingly. Structural engineers retained to investigate the seismic-resistance of various URM facilities promptly discover the limitations of current masonry design standards whose simplistic design guidelines are of little, if any, assistance in formulating a realistic assessment of this resistance. One recent code (and its variations thereof), the 1991

edition of the Uniform Code for Building Conservation (UCBC) (ICBO 1991), is a notable exception which specifically addresses the seismic strengthening of URM bearing wall buildings, and includes a special procedure based on empirical evidence and applicable to certain types of URM buildings. In California, where endorsed by local ordinances mandating the mitigation of seismic hazards from URM buildings, it has already been used to investigate, and retrofit when necessary, thousands of buildings. In absence of such endorsement, and concurrent legal protection, engineers have generally resorted to either conservative methods, the UCBC procedure, or other advanced analytical models. Such engineering decisions are directly related to knowledge of the behavior of URM buildings and their proper modelling, and a review of current research is useful in this respect.

The objective of this section is to summarize the findings from recent analytical research activities on the seismic behavior of URM buildings, and from advances in their modelling.

Existing knowledge on reinforced or partially reinforced masonry is not reviewed, nor is current research on improved determination of various material properties (compressive, tensile, shear strengths of grout, mortar, brick and masonry, friction and bond strength, absorption rates, etc.), and studies of behavior and performance not directly related to seismic response. Findings exclusive to special types of structures (i.e. single story masonry houses or adobe houses) are not reported herein. The special problem of URM used as infill to reinforced concrete or steel frames is also beyond the scope of this study.

2.4.2. Modelling Aspects of URM structures:

It is the prime responsibility of the structural engineer to establish, based on judgement and experience, a realistic structural model of any given URM building. While many engineers will reluctantly depart from proven, albeit conservative, traditional approaches suitable for hand-calculations, others are more inclined to rely on sophisticated, less intuitive, finite element models. The individual engineer's confidence in the reliability of respective

approaches, as well as some non-technical aspects, such as liability and client's sophistication, all influence modelling decisions, particularly in the absence of an "umbrella" ordinance prescribing a specific procedure. Yet, the final judgement on the seismic-adequacy of a given URM building is very much also dependent on the characteristics of the selected model. Some of the modelling approaches proposed in the literature are reviewed following.

2.4.2.1. Out-of-plane Modelling:

Out-of-plane models, suitable for use in a design office, are few. While the dynamic stability concepts exposed previously are simple, the formulation of an analytical model extending beyond purely static stability considerations remain elusive.

Priestley (1985) proposed a hand-calculation method based on energy equivalence for the prediction of the dynamic out-of-plane wall stability. Assuming in-phase floor accelerations and a condition of average constant acceleration acting on walls conservatively taken as spanning in a simply supported fashion between stories, simple relationships of static equilibrium were developed on the rigid-body wall segment post-cracking, as shown in Figure 2.3. Essentially, in this method, the location of the gravity forces (overburden, P, and wall self-weight, W) along the wall, and the reactions forces needed for stability, must be located and calculated, the width of the bearing surface at mid-span must be determined from equilibrium conditions, the displacement conditions for instability must be established from geometry, and finally, the formulation of equilibrium equations allows the expression of the inertia forces as a function of all other variables. The key-equations resulting from all these steps are presented directly in Figure 2.3.

The relationship between the wall's acceleration (i.e. inertia force) and its displacement at mid-height is described as non-linear elastic; it draws a linear curve until first cracking of the wall, reaches a maximum acceleration corresponding to a point of maximum static stability, and progressively returns to zero under much larger displacements. As the area under this curve is associated to the total energy needed to fail the wall, Priestley suggested that a linear

elastic model, whose ultimate limit would be selected to yield the same energy to failure as the actual non-linear model, would be a good indicator of dynamic stability. It is thus assumed that if no single pulse of excitation requires an energy exceeding that required statically to produce collapse, stability is ensured.

In a comprehensive illustrative numerical example of this method as applied to a five-story URM building, Priestley found that high values of accelerations were needed to produce failure, provided good quality masonry and positive anchorages of walls to floors and roof were present. The possible amplifications of the ground acceleration along the height of the building, as normally done for standard buildings, were considered in that example, contrary to the UCBC recommended special procedure. Priestley also reduced gravity loads by an arbitrary allowance to account for vertical accelerations. Hence, assuming that response is dominantly driven by the first fundamental vibration frequency, Priestley found that the lower overburden and least thickness present at the top story of tall bearing-wall structures, where the largest floor accelerations occur, make the out-of-plane failure of URM walls more probable at that top level, as frequently observed following earthquakes. This appealing equivalent-energy method remains to be verified in controlled experiments.

To date, research on Dynamic Stability has concentrated on walls implicitly modeled as continuous vertical slabs supported between floor levels (ABK 1984, Prawel and Lee 1990b) or at their base only (Bariola et al. 1990). The natural "vertical-anchorage" provided by continuity with the other perpendicular walls has been conservatively neglected. This continuity could possibly enhance significantly the out-of-plane resistance of narrow walls. The effect of various boundary conditions on the ultimate out-of-plane strength of URM panels, in a non-seismic context, has received some attention: a fracture-line model applicable to orthotropic brickwork panels of low tensile strength, proposed by Sinha (1978, 1980), is noteworthy (it is not to be confused with the well-known yield-line theory for the analysis of reinforced concrete slabs, although it is conceptually similar). In this upper-bound approach, lines of maximum moment and zero shear are assumed to be linear; the cracking moment is assumed reached simultaneously along these lines, with ensuing rigid-body rotation

of the separated URM panel portions, and failure. The panel's boundary conditions on all sides, for any arbitrary geometry, are directly considered by the method. As with all upper-bound methods, the maximum capacity of the panel is found by finding the path of the fracture-lines allowing failure under the lowest magnitude of applied loads. While Sinha found excellent correlation with experimental results, the URM panels tested were free of concurrent in-plane axial loads. An adaptation of this method into a dynamic stability framework could be of interest.

2.4.2.2. In-plane Modelling:

2.4.2.2.1. Hand-calculation Models:

Various strategies exist to reduce an URM building to a structural model manageable by hand-calculations. A number of these are reviewed following.

(i) Solid-pier/Cracked-spandrel Model:

A legitimate, yet conservative, model is to assume that the spandrel beams will crack under a very low lateral load, leaving the piers alone to resist the lateral loads. This approach is not unlike that recommended by some researchers for the analysis of reinforced masonry walls having numerous opening, where the masonry above and below the openings is neglected (Englekirk and Hart 1984). Although this models the structure at its ultimate state if the spandrels are shallow or not well connected to the piers, it immediately assumes a structure in its degraded condition, neglecting the potentially larger capacity of the structure before cracking.

(ii) Wall Models and Solid-spandrel/Cracked-piers Models:

If the spandrels are deep and/or of short span, the piers may fail first, like walls, in flexural cracking, shear cracking (diagonal tension), or compression crushing. A number of models of

this behavior are suggested.

Traditionally, design standards recommend a no-tension criteria for the design of URM walls in flexure, or alternatively, in the absence of significant axial compression, the design is governed by the allowable tensile stresses, f_t. Resistance to shear stresses is checked independently, against an allowable shear stress enhanced by the presence of axial compression, if present (Bruneau 1992). Thus, elementary equations of mechanics of materials are used, as illustrated in Figure 2.4a.

Many researchers (Mayes and Clough 1975, Turnsek et al. 1978, Zingali 1986, to name a few) have used a shear failure criteria directly related to the diagonal tension capacity by principal stresses relationships. Directly from Mohr's circle, for an URM panel in pure shear by diagonal tension, the normal tensile stress capacity of masonry, σ_t, is equal to the maximum shear stress at failure, τ_{MAX} , where $\tau_{MAX} = 1.5\ \tau_{MEAN}$ for a rectangular cross-section, and τ_{MEAN} is the maximum average shear stress. (Figure 2.4a). The ultimate shear capacity of this same URM panel, stressed in combined shear and axial compression by earthquake excitation and gravity loading respectively, is amenable to a single expression derived from the well known classical expression for principal tensile stresses (Gere and Timoshenko 1984):

$$\sigma_1 = \frac{\sigma_x + \sigma_y}{2} + \sqrt{\left(\frac{\sigma_x - \sigma_y}{2}\right)^2 + (\tau_{xy})^2} \qquad (2.1)$$

Knowing that the principal tensile stress, σ_1, cannot exceed the tensile stress capacity of the masonry, σ_t, for a given magnitude of the applied mean compressive axial stress, σ_o, the peak value of the shear stress, τ_u, that can be sustained at the centre point of the URM panel

(Figure 2.4b) before cracking initiates must satisfy the relationship following:

$$\sigma_1 = \frac{-\sigma_o}{2} + \sqrt{\left(\frac{\sigma_0}{2}\right)^2 + (\tau_u)^2} = \sigma_t = \tau_{MAX} = 1.5\ \tau_{MEAN} \tag{2.2}$$

Rearranging these terms,

$$\tau_u = \sigma_t \sqrt{1 - \frac{\sigma_o}{\sigma_t}} = 1.5\,\tau_{MEAN} \sqrt{1 - \frac{\sigma_o}{1.5\,\tau_{MEAN}}} \tag{2.3}$$

The maximum lateral load, V, that could be applied to this panel would then be:

$$V = \frac{\tau_u A}{1.5} \tag{2.4}$$

For clarity, it is worth re-emphasizing that τ_{MAX} (and correspondingly $1.5\tau_{MEAN}$) is the fundamental shear stress capacity of masonry in pure shear (i.e. a material property), whereas τ_u is the maximum shear stress that can be applied on a given panel already stressed by an applied gravity load. Obviously, in this procedure, the other limiting conditions of flexural cracking and compression crushing at the extreme fibres of the piers would again need to be checked independently.

Some researchers (Sinha and Hendry 1969, Mayes and Clough 1975) have recommended that both the usual Coulomb friction shear strength equation (i.e. the one present in North American codes) and the above formulation be checked: The first reflects that bond and friction between the mortar joints could potentially govern at low axial compressions, whereas for high bond mortar and/or higher axial loads, only the second would be applicable. In addition, Samarasinghe et al. (1981) cautioned that the Coulomb equation is reliable only for panel geometry having length (L) to height (H) ratios in the range $1.2 < L/H < 2.0$, as verified both experimentally and analytically.

The above formulations implicitly postulate that shear strength is exhausted at the onset of

first cracking. This need not be the limiting condition under flexural cracking, considering, even statically, the stabilizing effect of axial loads. Equations have been proposed to assess the ultimate strength of flexurally cracked piers having reserve shear strength capacity. ABK (1984) recommended the following expression for the dynamic restoring shear capacity, V_R, of URM piers:

$$V_R = 0.9 \frac{P \cdot D}{H} \tag{2.5}$$

where P is the axial load on the pier, and D and H are the pier width and height respectively, as shown in Figure 2.4c (the pier's self-weight is neglected in this equation). The value of 0.9 is recommended based on experimental results. Priestley (1985) slightly refined this equation by assuming that the bearing zone resisting overturning is under a uniform compression of 0.85 f'_m.

Finally, Epperson and Abrams (1990) suggested that, for walls flexurally cracked at their base, the compressive strength of masonry at the wall's toe could be reached before overturning and diagonal tension (shear) failures. Assuming a linear distribution of stresses over the uncracked portion of the wall base, as illustrated in Figure 2.4d, and neglecting masonry's tensile strength, the expression derived from statical equilibrium to check for this maximum compressive stress the wall's toe is:

$$f_{max} = \frac{2P}{3b\left(\frac{d}{2} - \frac{Hh}{P}\right)} \leq f_m' \tag{2.6}$$

where, P is the sum of the vertical compressive force acting on the wall, b, d and h are the wall's thickness, width and height respectively, H is the applied horizontal force, and f_m' the ultimate compressive capacity of masonry.

2.4.2.2.2. Finite Element Models:

Linear elastic finite element analyses are becoming popular, particularly in Europe, to establish the state-of-stress in complex URM heritage structures, often built of stone (e.g.

Pistone et al. 1991). However, only a few of the reported studies are concerned with seismic resistance (Elsesser et al. 1991, Quirós Lara and Gutiérrez 1991, Vestroni et al. 1991); most investigate other loading conditions or general structural distress. These linear elastic analyses may be worthwhile to provide some guidance as to the governing failure mode, ultimate elastic capacity, natural frequencies, mode shapes and modal participation factors of uncracked URM buildings, but they provide a limited insight into the ultimate strength and seismic behavior of such structures; the method also produces unavoidable local stress concentrations which require a careful interpretation.

Recognizing these limitations, some researchers have investigated the adequacy of special non-linear and cracking finite elements for studying the ultimate seismic behavior of structures. Both discrete-crack and smeared-crack formulations have been tried.

In the discrete-crack model, a special interface element (also called a "gap" or "gap contact" element), is introduced to allow separation of adjacent elements when the tensile strength of the material at this interface is exceeded. The layered structure of masonry suggests modelling the mortar joints as non-linear gap-elements and the bricks as standard four-node elastic isotropic elements.

Chiostrini et al. (1989) adopted this approach to analytically replicate the ultimate behavior of a masonry panel monotonically tested in shear. Their gap-element consisted of two parallel plane surfaces capable of separating or sliding to break the bond between adjacent brick elements; only compressive normal stresses, by contact, and shear stresses, by Coulomb's friction, can be transferred across this element. The judicious selection of the friction coefficient is partly accountable for the reported excellent agreement with experimental results for which, incidentally, damage was confined to the mortar joints.

Obviously, it is not practical nor desirable to model all bricks and mortar joints to study the seismic response of entire URM buildings. Thus, in a companion study, Chiostrini and Vignoli (1989) used macro-masonry elements, in combination with gap-elements, to model

flexurally dominant cracking modes of piers or spandrels, as well as global overturning; these ultimate collapse mechanisms could be well replicated analytically and their capacities compared satisfactorily with that predicted by other means. However, the discrete-crack strategy presumes prior knowledge of ultimate behavior so that the gap-elements can be located adequately in the model, i.e. where cracking will occur (Chiostrini and Vignoli 1991, Barberis et al. 1991). Results are otherwise unreliable. The model is also unable to model cross-brick cracking.

Alternatively, smeared-crack models were studied. In this model, the non-linear effect produced by the opening and closing of cracks are integrated in the element formulation itself. Essentially, when the tensile strength of the material is exceeded, as determined from the internal state of stresses in a given element, cracking occurs orthogonally to the tension principal stress, and assumed uniformly distributed (i.e. "smeared") over the whole element. Clearly meshing refinements in the zones of cracking improve the reliability of the solution.

However, reported finite element investigations of the behavior of URM structures using smeared-crack models remain few and are mostly concerned with gravity loads. One study addresses the seismic-response of URM walls (Chiostrini and Vignoli 1991); in this limited investigation, the predicted ultimate response and dynamic properties of a wall modeled using plasticity versus smeared-crack elements are compared, and some theoretical developments are presented regarding the addition of geometrical and material non-linearity capabilities to the smeared crack element, aiming at the study of slender URM components. More research is needed to fully assess the potential of this finite element strategy.

The ability to computationally predict the seismic-response of URM structures will obviously improve in parallel with advancements in the modelling of the masonry material itself through finite element analyses. For example, research (Ignatakis et al. 1989) in which masonry units and mortar joints are modeled separately, each with its own tri-dimensional non-linear material characteristics, has been successful in replicating experimentally obtained ultimate loads, displacements, damage pattern and failure mode of URM panels subjected to in-plane

loading. However, as each brick and adjacent mortar bed are individually meshed by up to eight triangular elements, the approach is obviously more suited to research of fundamental behavioral characteristics than to the study of complete structures.

Innovative techniques are also being investigated. For example, in one case, a new type of no-tension fan-shaped finite element has been proposed (Braga and Liberatore 1990) to improve the computational efficiency over traditional meshing approaches. The element was specifically developed to analyze the seismic-response of masonry structures, but no results from this particular research endeavor have been reported at the time of this writing. The Boundary Element Method, a proposed alternative to the finite element method, is also currently being considered by some researchers (Brebbia and Niku 1991) for the study of historical structures, but the strength of the method resides largely in linear elastic analyses.

2.4.3. State-of-the-Art Hysteretic Models for URM Buildings:

A comprehensive hysteretic model capturing the seismic-behavior of masonry while considering its heterogeneous nature, with its inherent complex interaction of mortar, brick, layering patterns, and other distinctive features, remains elusive. As practising engineers have conventionally treated masonry as a linear elastic homogeneous isotropic material whose properties are obtained from standard static tests, most researchers are also comfortable with this simplified model. Yet, some attempts at the development of more advanced hysteretic models to capture the aforementioned experimentally observed non-linear behavior have been attempted.

Mengi and McNiven (1986) proposed an equivalent linear model that accounts for the non-linearity effect through variable secant shear modulus and secant damping coefficient. As one might expect, beyond first cracking, the shear modulus progressively decreases as a function of the shear strains whereas the damping coefficient increases on account of accrued friction-slip within the cracks. This is conceptually illustrated in Figure 2.5. Bi-linear relationships

between the values of these secant shear modulus and secant damping coefficient as a function of the absolute values of the shear strains and shear strain rates relatively, were found to be adequate. However, this model should be used with caution. Generally, computer programs capable of conducting seismic non-linear inelastic analyses of structures clearly differentiate damping from hysteresis; the damping coefficients relate to the elastic damping only. The notion of increased damping to simulate hysteretic behavior should not misused. In Mengi and McNiven, both G and ξ are evolving variables, a re-linearisation to new values being performed as new cracking occurs through-out given time history analyses; incorrectly adopting constant values for use in an equivalent linear elastic analysis would not provide a safe or realistic assessment of the non-linear inelastic seismic performance.

Further research is still needed to validate this model. Mengi and McNiven did not use their model to study the progression of damage from the uncracked state to the severely damaged condition, ensuing from a single severe earthquake excitation, nor have they considered earthquake records other than the El Centro 1940.. Moreover, for the analysis of a complete structure for which damage is not equally distributed to all URM structural elements, it is not known if the calculation of the secant damping coefficients of each components and subsequent assembly into a global structural damping matrix would yield the correct results. Nonetheless, some researchers (Prawel and Lee 1990a, 1990b) have already reported on the experimentally obtained values of these secant properties.

A true hysteretic model applicable to URM has been proposed by Benedetti and Benzoni (1984). Developed to replicate experimentally obtained shear stress-strain hysteretic curves, it is constructed from three superimposed bilinear hysteretic shear sub-elements, failing brittly at a prescribed strain intensity (Figure 2.6). Each sub-element is completely defined by its elastic shear modulus, G_i, limit elastic shear stress and strain, τ_i and γ_i respectively, and ultimate limit shear strain (γ_{iL}). The resulting shear-panel hysteretic curve is built from the direct summation of all individual sub-elements' strength, but sub-elements having exceeded their limit strain (γ_{iL}) are permanently removed from the model, as shown in Figure 2.6.

An estimate of the overall post-cracking "ductile" behavior is given by the ratio γ_{1L}/γ_3. The value of the maximum shear stress, τ_{max}, depends on the average applied normal stress, σ, and critical tensile strength, σ_t, by the relationship of Equation (3) presented earlier. The other parameters shaping this phenomenological hysteretic envelope are calibrated from available experimental results. While Benedetti and Benzoni did not provide a physical mechanism to obtain these other parameters without the need for experimental calibration, they demonstrated that the parameters α_1, α_2, (defined on Figure 2.6) and τ_{max} have the most dominant influence on the non-linear inelastic behavior. Also, other structural elements must be used jointly to provide axial load resistance as this hysteretic model only simulates a shear-panel response mechanism. Finally, as this model has been apparently derived from tests on stone masonry, its applicability to general URM structures is only inferred.

2.4.4. Seismic Resistance of Stone Masonry Construction:

A large part of the Eastern North American inventory of prestigious heritage buildings is of unreinforced stone masonry construction, including composite walls with stone wythes keyed into brick ones. Although differences in behavior are intuitively anticipated, a knowledge-base of their seismic performance is unfortunately nonexistent. In European and Middle-Eastern countries, where the collapse of stone masonry buildings during recent earthquakes produced many casualties, considerable efforts have been spent to develop expertise on this topic. Whereas the type of stone masonry construction used in those countries bears no resemblance to its North American counterpart, some of that existing knowledge could be used carefully. However, while this literature has also been reviewed, for the sake of brevity, a summary of these findings must be postponed.

2.4.5. Summary:

Information on the cyclic seismic performance of URM is comparatively scarce. With the

growing awareness that first cracking is not automatically equivalent to failure, many investigations are anticipated. This is particularly true of the in-plane response of URM walls, which, under certain conditions, can remain stable much beyond cracking, as demonstrated analytically. However, this stability is not infinite, and generates damage through-out its development; thus the problems inherent to the in-plane response of URM buildings should not be ignored or dismissed lightly. Similarly, only scant information exist on the dynamic damping properties of these types of construction. Awaiting more definitive knowledge, conservative values, preferably in the lower range of reported values, could be chosen for analytical studies. Alternatively, forced-vibration analyses would be one way to obtain this data for individual structures, as needed.

Dynamic stability is currently only indirectly considered through limits on wall slenderness which have been established experimentally. Although an alternative hand-calculation method based on energy-equivalence has been proposed to predict the out-of-plane dynamic stability of walls, an analytical computational approach to replicate this non-linear rocking behavior was not found to be available; such a model would obviously allow verification of the current empirical design criteria and permit non-linear time-history analyses of the influence of vertical ground accelerations on dynamic stability. Similarly, no computational-analytical model of the in-plane stability and/or ultimate strength of URM walls exists. Some finite element cracking models, the smeared-crack model in particular, are promising. In the meantime, linear elastic finite element analyses have found some use in spite of their obvious limitations.

Although masonry is a brittle material incapable of inelastic straining, there are energy dissipation mechanisms available in standard URM construction which can lead to the measurement of an hysteretic behavior and, thus, of effective "ductilities". The mechanisms responsible for this hysteresis are not well understood, but sliding friction on opened cracks and rigid-body rocking are known to be contributors. Unfortunately, there is currently no broadly accepted analytical models capable of replicating this behavior, nor is there agreement on what a reliable and acceptable value of this "ductility" is for URM elements.

Finally, the legal protection provided by seismic hazard mitigation ordinances endorsing these special evaluation procedures has been instrumental in their broad acceptance there. Elsewhere, no clear consensus emerges at to which of the many modelling schemes presented herein, to evaluate the in-plane and out-of-plane behaviour of URM walls, provides the most realistic appraisal of their true seismic resistance. Consequently, in this context and to protect against possible litigations following an earthquake, structural engineers have inevitably adopted conservative analytical models in their seismic evaluations of URM structures. As this has often translated into prohibitively expensive rehabilitation costs, and in light of the considerable savings that may ensue from the use of more realistic approaches, the reported and on-going research is expected to rapidly gain more acceptance.

2.4.6. Additional Research Needs:

Deficiencies in the current knowledge are numerous. Some of the research activities needed to improve the understanding of the seismic performance of URM buildings are suggested following.

The concepts of ductility and hysteretic behavior for URM buildings should be consolidated as these may have a considerable impact on the assessment of seismic-performance. Concurrently, reliable representative values of elastic damping coefficient should be established for the various types of masonry commonly encountered.

Promising finite element strategies should be aggressively pursued, first to enhance the fundamental understanding of the seismic performance the complete URM building systems, but thereafter to see how this technology could be integrated into a production environment, or lead to a simpler formulation usable by practising engineers.

The impact of various modelling procedures on the predicted performance of URM buildings predominantly constructed of pier/spandrel facades with numerous openings, and/or with

URM shear-walls having a smaller amount of openings, particularly in an ENA perspective, should be studied.

The seismic response of monumental, institutional or governmental high quality URM buildings should also be investigated to establish if their features (thicker walls, robust construction, etc.) can lead to superior performance, as often intuitively believed.

Finally, the effect of vertical ground accelerations should be reviewed considering the importance of stabilizing gravity forces for dynamic stability. Similarly, the more complex bi-directional earthquake effects that can lead to combined out-of-plane/in-plane failures have never been studied. Yet, as the out-of-plane dynamic stability of walls could be impaired by concurrent in-plane damage, this important failure mode should not be overlooked.

CHAPTER 3

Two-Dimensional Analysis of Montgomery Block Building: West Facade

3.1. Introduction:

The Montgomery Building is first studied by structural analysis of a 2-Dimensional model. By assuming an infinitely flexible diaphragm, each lateral-load-resistant structural element (LLRSE) must resist ground-induced dynamic motions of their tributary floor masses. By observations of the tributary areas and corresponding LLRSEs present in the building, the weakest component of the building, and that for which its lateral resistance is least understood, is the perforated URM facade. Hence, this chapter concentrates on the seismic performance of the west facade. This particular facade is also chosen on account of its

detrimental location, being the farthest away from the centre of rigidity in the direction undergoing the worst torsional response. The integrated 3-D structural response will be considered in the subsequent chapter.

The Structural Analysis Program SAP90 is used for this study. This facade of the building is modelled by using the beam elements of SAP90 for all piers and spandrels. The spandrels' axial deformations are assumed negligible. This will result in a reduction of the total number of degrees of freedom for this system. This is achieved in SAP90 by constraining all piers to have the same lateral displacement at each floor. The lumped floor masses and distribution of loads must be defined to be able to calculate the seismic resistance of this building. The details of this calculation follow.

3.2. Calculation of the Building's Lumped Floor Masses:

The building mass originates from the wood partition walls, wood floors and masonry spandrels, piers and walls. Some important assumptions are made for the calculation of the lumped wood and masonry floor masses (Table 3.1).

3.2.1. The Wood Partition Walls:

For partition walls, little was specified on the structural drawings other than their locations. Therefore, they are assumed in this study to be of the type most commonly found in buildings of that era, i.e. 76 x 102 mm^2 studs at 305 mm centre-to-centre continuous for the full story height with 76 x 102 mm^2 blockings at 305 mm centre-to-centre and a 13 mm thick plaster covering on each face. This type of partition weighs 763 N/m^2 of wall surface area.

After measuring the total length of these partition walls in each floor, the resulting lumped floor masses "M_{pwi}" can be calculated by:

$$M_{pwi} = (m_{pwi} + m_{pw(i-1)}) / 2 \quad (3.1)$$

where "m_{pwi}" is the total mass (kg) of the partition walls at the floor # i, and

$$m_{pwi} = (763 \times L_{wi} \times h_i) / 9.81 \quad (3.2)$$

where "L_{wi}" and "h_i" are respectively the total length and height (m) of the partition walls at floor # i.

3.2.2. The Wood Floors:

As shown on the drawings (Appendix A), the structure has 4 floors and a low ceiling attic. Thus, the roof can be assumed to be of 2 different parts; the lower part is a grid of 75 x 100 mm^2 beams and joists 406 mm centre-to-centre in each direction. Each face of the grid is covered by a 10 mm thick decking. The upper part of the roof is made of 250 x 125 mm^2 beams 625 mm centre-to-centre in the N-S direction covered by a 25 mm thick decking.

The resultant masses are 40,338 kg and 91,944 kg for the lower and the upper part of the roof respectively.

From the drawings, each floor is shown to have beams at 3.75 m centre-to-centre with a 100 mm thick decking and a 10 mm thick covering on the underside. Unfortunately, the beam's section is undefined. To determine the beam's section, a gravity-load re-design was accomplished by considering:

- the load per unit area on the floor and load per unit length on the joists.
- the load path along the floor system.
- the beams as simply supported.
- allowable stresses of 9.81 MPa for the wood beams (σ_{all}).

This procedure was repeated at each floor.

3.2.3. The Masonry Brick Piers and Walls:

The dimensions of these structural elements were read from the drawings. All walls have a thickness of 450 mm but different widths. Consequently a load of 7920 N/m^2 of masonry wall surface area is assumed.

The lumped masses "M_{mi}" due to masonry piers and walls are:

$$\mathbf{M_{mi} = (m_{mi} + m_{m(i-1)}) / 2} \qquad (3.3)$$

where "m_{mi}" is the total mass (kg) of the pier and walls at floor # i, and

$$\mathbf{m_{mi} = (7920 \times L_{mi} \times h_i) / 9.81} \qquad (3.4)$$

where "L_{mi}" and "h_i" are respectively the total length and height (m) of the masonry piers and walls at floor # i.

It is noteworthy that on the reconstructed drawings of the Montgomery building, done in 1958, piers were shown discontinuous at the first story. However, photographs of the building taken shortly after construction, reveal that all piers on the facade were originally continuous from roof to foundation with regular size opening of 3 ft wide throughout. Renovation work is believed and assumed to have taken place after the 1906 earthquake.

Finally, in view of the short distance between the lower and upper parts of the low-ceiling attic, the entire roof mass was lumped at an equivalent height, as shown on Figure 3.1. The distance between these 2 parts is 0.75 m. Their new centre of mass was defined and the building's roof became the sum of the 2 masses at a distance 3.1 m separating its new centre

of mass to floor # 3.

Resulting calculated lumped masses for the entire building are presented in Table 3.1. It is noteworthy that the contribution of wood to the total structural floor mass varies from 34% to 23 % from the upper to the lower floor. The larger number of masonry walls and piers on the first floor, and the low-ceiling attic on the last floor explain this variation.

3.3. Distribution of Gravity loadings:

After lumping the wood and masonry masses at each floor, the loads on every pier are determined :

- Wood dead loads: Assuming infinitely flexible diaphragms, the west facade, situated on Montgomery street, supports a tributary floor area of 226.2 m^2 (239" x 1467"). Thus, the wood weight at the floor # i, supported by the facade, is:

$$P_{wi} = (W_{wi} / A_{ti}) \times 226.2 \qquad (3.5)$$

where "W_{wi}" and "A_{ti}" are respectively the wood load (N) and the area (m^2) of the whole floor # i. According to Equation (3.6), every pier # j of floor # i will be withstanding a load "F_{wj}": where a_j is the sectional area of a pier and Σa_k is the total sectional area of all piers on the facade.

$$F_{wji} = \left(\frac{a_j}{\sum_{k=1}^{k=20} a_k} \right) \times P_{wi} \qquad (3.6)$$

- Masonry dead loads (piers and walls): This masonry dead load on the j^{th} pier at the floor # i is:

$$F_{Mji} = p_m \times h_i \times L_j \quad (3.7)$$

where: p_m is 7920 N/m^2 for 450 mm thick masonry wall or pier (as per section 3.1.2), "h_i" is the height between the i^{th} and the $(i+1)^{th}$ floor and "L_j" is the width of the pier "j". Self weights for each story pier are applied individually at the lower node of the element, the cumulative effect being automatically considered by SAP90 analyses.

- Loads from the masonry spandrel beams: These are considered simply supported and the sum of reactions from adjacent spandrels produces the masonry spandrel's load on that pier.

Wood and masonry dead loads are added to find the lumped masses "M_i" at each floor # i. The contribution of wood, masonry piers and spandrels are summarized in Table 3.2.

3.4. Earthquake load:

Equivalent earthquake static loads are distributed the usual way along the height of the facade, according to Equation (3.8):

$$F_x=(V-F_t)\times\left(\frac{W_x\times h_x}{\sum_{i=1}^{i=4} W_i\times h_i}\right) \quad (3.8)$$

where "h_i" is the height between floor # i and the 1st floor, "W_i" is the mass of the floor # i and F_t is neglected here. Recall that in this study, "V" is the unknown quantity to be found from the calculated material resistances.

3.5. Solid Pier/Cracked-Spandrel Model:

Here, each pier of the facade was modeled as a succession of 4 beam elements. Each beam element is representative of a pier segment between two floor diaphragms in SAP90 as shown in Figure 3.2. There are 20 piers and their widths are presented in Table 3.3. They are numbered from North to South (corresponding to left to right in Figure 3.2). The spandrels in this model are deliberately absent as they are assumed cracked.

In the analysis of this model, four types of failure modes are considered. These are the precompressed shear "Pr.S.", the pure shear "P.S.", the flexural compression "F.C." and the flexural tension "F.T.". A multi-step analysis is conducted for each failure type individually. When the capacity is reached at one level of a pier, the pier was eliminated from the model for the next analysis. This is logical since all piers were observed to fail at base. The results for these 4 possible modes are shown in Figure 3.3. It is observed that the dominant failure mode is flexural tension which is logical since the piers behave as tall cantilevers. The 1st crack is neither the general failure nor the point at which V_{max} occurs. In fact, the maximum base shear (V_{max}=77 KN) was attained at the 4th step when all the 17 identical piers cracked . This extra strength from the 1st to the 4th step is due to:

- the presence of 2 piers stiffer than all the others. These 2 stiff piers (10 & 11) which attract more force and, thus, crack first.
- the presence of 17 other identical piers which can not only absorb the loss of lateral strength due to cracking of piers 10 & 11, but even carry more load thereafter until their eventual simultaneous cracking.

If the flexural tension failure mode is assumed not to govern, the next failure mode becomes flexural compression and its corresponding capacity (V_{max}) will be 295 KN. It is noteworthy that shear failure is by far not a governing failure mode with a capacity equal to 1579 KN and 2453 KN for P.S. and Pr.S. respectively, as expected. The numerical values for the results in Figure 3.3 are summarized in Table 3.4 including the evaluation of the period

throughout response.

3.6. Frame Model without rigid Offsets:

The frame model without rigid offsets is a combination of piers and spandrels. Each beam element represents either a pier segment when situated between two floor diaphragms or a spandrel when located between 2 adjacent piers. Numbering is according to Figure 3.4 of SAP90. Spandrels have a length and width respectively equal to the distance centre-to-centre between 2 piers and to the thickness of a pier (0.45 m). Their height is equal to 4 ft for the floors # 1,2 and 3 and 5'6" for the floor # 3.

The multi-step analysis of this model was done by considering the same four failure modes as before with the exception that only the least capacity in each case is retained for the following presentation. Like in the previous model, through-out the analysis, flexural tensile failure consistently governs. When the capacity is reached at one element, the element's characteristics are changed and its sectional dimensions are replaced by arbitrarily small values of inertia and compressive and shear areas such that its lateral-load resistance is effectively eliminated without making the structure unstable locally under gravity loads. A maximum V_{max} of 171.5 KN was attained at 1st cracking but the general failure occurred when all piers of the last floor cracked, after 80 steps. Figure 3.5 illustrates the evolution of V_{max} with the number of damaged elements. The solid line is obtained by calculating the new capacity of the remaining structure immediately following removal of the element cracked at the previous step. By connecting all peak values with a curve of constantly decreasing strength, an assessment of the resulting progressive strength degradation is possible, as illustrated by the dotted line. The numerical values for the results of Figure 3.5 are summarized in Table B.1 which also includes the evolution of the period with the number of damaged elements. It is noteworthy that the facade's initial fundamental period was T = 0.5 s and was always increasing throughout the analysis. Indeed, Figure 3.6 illustrates this evolution with the number of damaged piers.

Because of the absence of the rigid offsets, the flexibility of the facade, and thus the lateral displacements of the floors might be overestimated. So, an attempt to study the facade in the presence of rigid offsets was done in order to get a more realistic 2-Dimensional model and investigate the offsets' influence on the results.

3.7. Frame model with rigid offsets:

The only difference between the previous model and the current one is the inclusion of the rigid offsets. These offsets are the distances from the joints to the faces of the supports. Their introduction in the model results in a shorter flexible length of the members since the actual elements' lengths are reduced by a quantity equal to the sum of its rigid-ends lengths. All the member forces are considered and outputted at the outer ends of the rigid offsets (faces of supports), as logically expected.

The same multi-step analysis described for the previous model was conducted. The maximum base shear response was also attained here at the 1st crack, with a V_{max} value of 297.8 KN. The general failure was attained at the 84th step of analysis when all the piers of the first floor failed. The resulting capacities and their corresponding number of damaged elements are presented in Figure 3.7 and Table B.2 which also includes the facade's fundamental period. In this case, the initial period was T = 0.35 s. (Figure 3.6). At the last step of the analysis, this value became T = 3.12 s which is more than T = 1.94 s, the last period of the previous model. Figure 3.7 can be interpreted the same way as Figure 3.5.

An investigation on the lateral floor displacement "Δ" was made for each floor of the facade. (see Table 3.5). When V_{max} was 297.8 KN, the floor displacements were 1.64 mm, 2.53 mm, 3.04 mm and 3.24 mm for the floor # 1 to the floor # 4 respectively. When the general failure occurred, these lateral floor displacements became 23.76 mm, 61.40 mm, 79.68 mm and 80.02 mm. The increase in Δ with the number of damaged piers was slow at the beginning and fast near failure. For example, referring to floor # 4 in Figure 3.8, the increase

was slow until 30 piers were damaged and became high after the failure of 40 piers. In this figure, two curves were drawn. The dotted line curve, is the calculated displacement that corresponds to the instantaneous capacity calculated immediately following cracking of the previous element. Since lateral displacements can only increase throughout analysis the displacement envelope curve connecting all peak values by a constantly increasing curve (solid line) is more realistic and meaningful.

3.8. Comparative observations and discussion:

In this chapter, the structural analysis of the west facade of the Montgomery building by two-dimensional models was investigated using 3 different approaches. By analyzing and comparing the results of these approaches, many conclusions can be made:

- From the solid pier/cracked-spandrel model to the frame model without offsets, an increase of 122% in the capacity is observed. A higher increase of 287 % is observed from the solid pier/cracked spandrel model to the frame with rigid offsets. Thus,the presence of the rigid offsets in the frame model has a positive impact to obtain a higher capacity. Consequently, the ratios V_{max}/W are increasing from the 1st model to the 3rd model; these ratios are 2.1 % , 4.7 % and 8.1 % for the 1st model (Piers only), the 2nd model (Frame without rigid offsets) and the 3rd model (Frame with rigid offsets) respectively (Table 3.7). The results of Figures 3.5 and 3.7 are superposed in Figure 3.9. The facade's instantaneous capacities and curves of capacity envelopes must be interpreted as described previously.
- For all models, the facade's fundamental period is always increasing (Figure 3.10) and proportional to the number of damaged piers. From the 1st step until almost 55 % of the total damage, the facade's period for the 2nd model is approximately 0.15 s higher than its period for the 3rd model. Since almost 75 % of the total damage occurred, the 3rd model's period becomes higher than in the 2nd model by 61 %. In addition, according to the 1st model, the initial period is very high (2.21 s) comparing to those in the other models and when all 17 piers are damaged together, the period jumped

from 2.55 s to 11.37 s.

- According to Figure 3.11, the number of damaged piers with the lateral floor displacement has an exponential shape. In fact, from step to step, the lateral floor displacements increase faster than the number of damaged elements. When the number of damaged elements increases, the structure will become less capable in impeding the lateral floor displacement. However, in the solid pier/cracked-spandrel model, the first lateral floor displacement for the floor # 4 is 75 mm, 77 mm at its maximum capacity and 64 mm when the general failure occurred. This almost constant value of Δ shows that the piers-only model can not give a real idea about the lateral floor displacement evolution.
- The shear-displacement curve of the facade from the frame models (rigid offsets case shown in Figure 3.12), shows a stiffness degrading behaviour. As Δ increases, progressively more structural elements get damaged; in turn for this damage to develop, a certain amount of energy, of quantity unknown at this time, must be dissipated in spite of the progressive drop in capacity. Therefore, as the resulting area under the strength-deformation curve of Figure 3.12 could be interpreted as a dissipated energy, the URM building could be said to have some ductility, at least under monotonically increasing static loading.
- By looking at the evolution of the damage (Figures 3.13 & 3.14) of elements in the frame models, it was clear that not all of the spandrels were damaged before the general failure of the facade. Therefore, to assume that all spandrels will crack first, as done in the solid pier/cracked-spandrel model is a wrong assumption.

If the maximum allowable flexural tensile stress in URM masonry elements became sufficiently large to preclude tensile failure as a governing mode, the maximum capacity of the facade becomes 1012.4 KN and 826.0 KN for the frame model with and without rigid offsets respectively instead of 171.5 KN and 297.8 KN. The new governing failure mode becomes pure shear failure. However, the strength degrading characteristics as obtained before would remain, as shown for the 3 first steps of the analysis in Table 3.6. Thus, a

bigger value of the allowable flexural tensile stress might lead to different capacities in presence of different failure modes for this building's facade.

CHAPTER 4

Three-Dimensional Analysis of Montgomery Block Building

4.1. Introduction:

The three-dimensional structural analysis of the Montgomery Block building was performed using two different models: (i) Solid pier/cracked-spandrel model and; (ii) Frame model with rigid offsets. A schematic representation of the typical floor plans and distribution of lateral load resisting elements considered is shown in Figure 4.1. It will be used thereafter to illustrate significant results. The original architectural plans are in appendix A. For both models, a rigid floor diaphragm was assumed at each floor. Thus, every LLRSE will resist ground-induced dynamic motions according to its relative stiffness, but furthermore, as the failure of weaker elements (such as facades) occurs, their loss of lateral strength can be picked up by stronger structural elements elsewhere throughout the building (i.e. in a different vertical plan). Transverse LLRSEs can also contribute in cases where large torsional motion

develops in this process.

Although special programs such as ETABS specifically designed to handle buildings with rigid diaphragms could have been used, SAP90 is equally capable of modelling rigid diaphragms using a master joint option. The concept is identical: all the joints' displacements at a given floor are geometrically related to the displacement of the master joint, resulting in a significant reduction in the number of degrees of freedom. In addition, any masses or loads assigned in the lateral directions and around an axis perpendicular to the diaphragm will be transferred to the master joint which is defined by its plan coordinates at every floor:

$$X_i^{MJ.} = \frac{\sum_{j=1}^{j=n} x_j \times m_{ji}}{M_i} \tag{4.1}$$

and

$$Y_j^{MJ.} = \frac{\sum_{j=1}^{j=n} y_j \times m_{ji}}{M_i} \tag{4.2}$$

where $X_i^{M.J.}$ and $Y_i^{M.J.}$ are the master joint's coordinates in the N-S and E-W directions respectively at floor # i. "y_i", "m_{ji}" and "M_i" are respectively the distance from the reference, the lumped mass of the pier or wall "j" and the total lumped floor mass at floor # i.

The floor masses and mass moments of inertia of the 3-D models to be lumped at the master joints, are in Table 4.1. These mass moments of inertia "MMI_i"(kg x m^2) are calculated by:

$$MMI_i = \sum_{j=1}^{n} m_{ji} \times d_{ji}^2 \tag{4.3}$$

where "m_{ji}" (kg), "d_{ji}" (m) and "n" are respectively the lumped mass of pier (or wall) "j", the

distance between the pier or wall to the master joint and the total number of piers and walls at each floor "i". The mass moment of inertias of individual elements around the vertical axis going through their centre of gravity is neglected. In addition, lumped masses are calculated by:

$$m_{ji}=\left(\frac{a_j}{\sum_{k=1}^{n} a_k}\right)\times M_i \tag{4.4}$$

where "a_j", "M_i" and "n" are respectively the sectional area (m^2) of the pier # j, the total lumped floor mass and the total number of piers and walls at floor # i.

The 3-D models' analyses consider:

- The lumped masses from wood partition walls, wood floors and masonry spandrels, piers and walls as calculated in the previous chapter (Table 3.1)
- The distribution of gravity loads at each floor due to masonry dead loads (piers and walls) and spandrels' reactions on piers and walls according to the procedures specific to these loads described in the previous chapter.

As the distribution of LLRSEs is rather uniform around the perimeter of the diaphragm (edge of building and interior court), results using this assumption resemble those which could have been obtained by a more stringent tributary area bookkeeping. Thus, for a given pier "j", the gravity load F_{wj} at floor # i from the wood dead loads due to partition wood walls and wood floor is:

$$F_{wji}=\left(\frac{a_j}{\sum_{k=1}^{k=n} a_k}\right)\times P_{wi} \tag{4.5}$$

where "a_j", "P_{wi}" and "n" are respectively the sectional area of the pier "j" (m^2), the total

lumped dead wood load (N) and the total number of piers and walls at floor # i.

The total lumped floor masses and their corresponding heights, defined in the previous chapter (Table 3.1 and Figure 3.1) will lead to the earthquake loads defined by Equation (3.8).

In this chapter, only the building's response under N-S earthquake excitation is considered. As the structure is fairly symmetric in the E-W direction, torsional response will be more significant for the case studied. Furthermore, this will compare the behaviours of 2D-models represented by the west facade in the N-S direction with that of the 3D-models.

4.2. Solid Pier/Cracked-Spandrel Model:

Only piers and walls are present in this model. Each one of them is modeled as a succession of 4 beam elements. In SAP90, each beam element represents a pier or wall segment between two rigid floor diaphragms. The complete building is modelled by 469 elements.

A multi-step analysis of this model was conducted by considering the four failure modes evoked in the previous chapter and retaining the least capacity in each case. From step to step, the change of elements' characteristics when cracked is achieved in such a way that the building's model integrity is conserved until general failure occurs, i.e. when all piers and walls at a given floor are cracked. Accordingly, when the capacity is attained at one element, its sectional dimensions are replaced by arbitrarily small values of inertia and compressive and shear areas, only over the floor height at which cracking occurred.

For all analyses conducted, flexural tensile failure governed. A maximum capacity of 1020 KN was obtained when 1st cracking occurred. The first element to be damaged was a very stiff pier (0.45 x 7.00 m^2 plan area) of the 2nd story at a small distance from the facade as shown on figure 4.2. The following 3 elements to crack are also stiff piers at the same

story and distance from the facade as the first cracked pier (Figure 4.2).

From the analysis results in table 4.2, many observations are possible. During the three first steps, the building's period increases by no more than .02 s. At the beginning of the 4th step, after damage to the four stiff piers, the structure has become extremely torsionally flexible in the N-S direction. At that point, the period increased by almost .70 s to reach 1.64 s (Figure 4.3) and the capacity dropped down to 401 KN. Still, the next element which failed was not in the west facade, but, instead, one of the more rigid walls/piers perpendicular to the direction of the applied load. Consequently, in spite of its low resistance, the west facade in this 3D-rigid floor diaphragm piers-only model is, as expected, too flexible to significantly contribute to the global lateral-load-resistance. As damage progresses, the capacity keeps decreasing as shown in Table 4.2 and Figure 4.4. The loss in rigidity is illustrated by the corresponding increase in period (Table 4.2 and Figure 4.3).

The N-S lateral displacement (X-displacement), the E-W displacement (Y-displacement) and the torsional rotation of the 3D-building models at the master joints are presented in Table 4.3 for each step of the analysis. Figure 4.5 shows that the inter-story displacement is almost the same for the 3 last stories, but very small for the 1st story which includes more rigid piers and walls than the other stories. This is typical of cantilever behaviour for which a more flexible segment occurs at the 2nd story. According to Figure 4.6, the calculated instantaneous displacement curve follows nearly always the actual displacement envelope. It is noteworthy that the torsional response "θ_z" of this 3D-model increased by almost 36 % for the 1st floor and more than 130 % for all other floors, after damage of the 4 rigid piers at the 2nd floor. In other words, the loss of the 4 rigid piers led to a radically more torsionally flexible structure.

4.3. Frame model with rigid offsets:

The difference between frame and piers-only models is the inclusion of horizontal spandrels between piers and the consideration of rigid offsets whenever a spandrel is present between

2 piers.

At the beginning of the analysis, 12 elements were found already cracked before the application of any lateral loads. Then, multi-step analyses proceeded with the capacity of the structure progressively increasing as elements located in the west facade ruptured sequentially. It is noteworthy that 9 of the 10 elements damaged during the 10 first steps under the action of the lateral loads were from the west facade and an "interim" maximum capacity was attained at the 6^{th} step with a value of 1453 KN (Table 4.4). For the 11^{th} step, failure of the entire facade was anticipated by removing it from the model; at that point, the maximum building's capacity of 1627 KN was attained. Failure occurred at the same rigid pier which failed in the first step of the previous model. Figure 4.7 shows the evolution of the capacity with the number of damaged elements.

The fundamental period of the building increased throughout analysis with an initial value of 0.34 s after the damage of 13 elements and 0.42 s after the damage of the entire facade and 14 elements (Figure 4.8). According to Figure 4.9, the interstory actual displacements of the master joints are almost the same for all the stories. By comparing Figures 4.7 and 4.10, the calculated V_{max} and Δ_x are observed to have the same shapes which means that there is a good proportionality between the 2 quantities. This is logical as the building has not been pushed beyond its strength threshold.

As seen in Table 4.5, an overall increase of the building's torsional response occurred. This is mainly attributable to an increase of the distance between the centre of mass and the centre of rigidity as damage to the facade occurs.

Based on observations of the evolution of the building's fundamental period and lateral displacements, at appears that assuming damage of the whole facade at the 11^{th} step was a reasonable assumption; increases in both these parameters at the 11^{th} step were relatively modest.

4.4. Observations and discussion:

In this chapter, lateral-load analysis of the Montgomery Block building was conducted using two 3D-models: Solid Pier/Cracked-Spandrel model (piers-only) and Frame model with rigid offsets. The following observations and interpretations are possible:

- The capacity of the frame model is 60 % higher than the piers-only model. Hence, the consideration of beams and offsets has a major impact on the predicted capacity of the building.
- In the piers-only model, cantilever flexural behavior dominates. The presence of beams which divide these piers into 4 different segments, and offsets which reduce the length of these segments,make the structure stiffer and stronger. Their consideration in the structural model is most beneficial for a more realistic assessment of structural behaviour.
- By the same logic, the capacity ratio V_{max}/W is higher for the frame model than for the piers-only model as shown in Table 4.6. However, by assuming a very high allowable flexural tension, to force a pure shear failure mode, V_{max}/W increased by about 3.7 for both models to reach 12.1 % for the 1st model (Piers-only) and 19.7 % for the 2nd model (Frame with rigid offsets). However, this ratio drops to 14.9 % for the 2nd model when the entire facade is assumed damaged. Apparently, this implies that, in both cases, the threshold of damage would be reached at failure of the first structural element if the shear failure mode governed. For the second model, at least, this would contradict what has been observed when tensile failures are dominant.
- The initial fundamental period of the 2nd model is close to what would be predicted using simple code equations recommended for moment-resisting space frames. In that respect, the 1st model would appear to be too flexible.
- The initial periods of piers-only and frame models when going from 2D to 3D analyses can be compared. It is found in both cases that this period is lower in the 3D model of the complete building than in the 2D model of the west facade. The greatest reduction of the period occurs for the more complex frame model. This is largely

attributable to the presence of multiple wide piers throughout the 3D model whose behaviour is not as significantly affected by the presence of spandrels when compared to a 2D facade with numerous openings.

- In the 3D piers-only model, it is assumed that all spandrels are already cracked and ineffective. Although 2D analyses of the facade have demonstrated that the sequence of element failures in the frame model does not totally support this assumption, the impact of this inaccuracy is far less significant in a full 3D model of this building assuming the rigid diaphragm assumption is valid. This is true even though the west facade is the first lateral load-load resisting system to fail in the frame model. It is noteworthy that as tall slender cantilevers as part of a group in the piers-only model, the facade's rigidity contributes very little to the lateral-load resistance of this system.
- The shear-displacement curve in Figure 4.11 of the piers-only model shows a stiffness degrading behaviour. Past the threshold of damage, V_{max} decreases with increases in Δ_x; eventually V_{max} stabilizes. Therefore, in this model, the building has a non-linear behaviour with some structural ductility to withstand further excitations. By contrast, the same curve in Figure 4.12 for the frame model shows a linear behaviour through the failure of all structural elements in the facade. Therefore, the loss of lateral-load resistance of the west facade is of little significance to the global stiffness of the structure. Beyond the last analysis step conducted for the frame model, it is reasonable to assume that the shear-displacement curve would be no worse, and may be better than that for the piers-only model for a slightly better "ductile" behaviour.

Although analysis of the 3D frame model was not pursued until global structural failure due to the complexities involved, the observed 3D structural behaviour and sequence of failure gives a reasonable confidence that the threshold of damage calculated at the 11^{th} step is a reliable maximum. If anything, compatibility of deformation suggests that capacity should be slightly higher since the residual strength of the facade, when first failure of an interior pier occurs, is not actually negligible as assumed in the above calculation.

Finally, free body diagrams of the shear forces at floor # 1 and # 2 are provided in

Figures 4.13, 4.14 and 4.14. This illustrates well that, for a structure with rigid diaphragms, as some structural elements fail and loose their lateral-load resistance, forces are redistributed in plan, even engaging orthogonal walls as necessary to withstand increased torsional forces.

CHAPTER 5

Uniform Code for Building Conservation (UCBC 1991): Special Procedure

5.1. Introduction:

In this chapter, the Montgomery Block building was studied using the special procedure of UCBC 1991 that originates from the ABK research. The west facade and interior walls are the selected LLRSE to be analyzed by this method. These are the same structural elements previously found to be most vulnerable under N-S earthquake excitation. The west facade was modelled as a combination of piers spanning between thick rigid spandrels, and the interior walls as a group of piers only.

The special procedure of the UCBC 91 is applicable here as flexible wood diaphragms present in the Montgomery building are in compliance with clause A109(d)4 and all other limitations of subsection A109(d)1 of the UCBC 1991. This leads to 2D-analyses of vertical planes of walls and LLRSE elements where ground-induced dynamic forces are transmitted to each plane as a function of tributary floor masses. It is noteworthy that the design equations expressed in ultimate strength in ABK methodology have been converted to working-stress based equations and allowable values when imported into the UCBC. These allowable values will be used in this chapter. Comparisons on an ultimate basis of all results obtained in this study will be performed in the following chapter.

5.2. Procedure of the analysis:

The UCBC methodology differentiates between the overburden dead load, i.e. applied at the top of a wall, and the self weight of the structural element being analyzed. These are separated in the analysis as they impact behaviour differently. Obviously, the self-weight of elements are lumped into the overburden weight acting on elements at lower floors.

5.2.1. Calculation of the lumped dead loads:

The total lumped dead load tributary to a diaphragm "W_{di}" at floor # i is that from the wood (partition walls and wood floors) and masonry (spandrels, piers and walls), excluding all walls spanning in the N-S direction. Thus, W_{di} is the sum of the lumped wood load "$W_{di,wd}$" and the lumped masonry load "$W_{di,ms}$":

$$W_{di} = W_{di,wd} + W_{di,ms} \qquad (5.1)$$

5.2.1.1. Contribution of the wood:

The lumped wood load (N) "$W_{di,wd}$" at each floor # i can be calculated by:

$$W_{di,wd} = \frac{(A_i / 2)}{A_{ti}} \times M_{di,wd} \times 9.81 \qquad (5.2)$$

where "A_i", "A_{ti}" and "$M_{di,wd}$" are respectively the tributary area between 2 adjacent walls, the total floor area and the total wood mass (kg) for the studied vertical element at floor # i.

5.2.1.2. Contribution of masonry:

The masonry dead load tributary to a diaphragm "$W_{di,ms}$" at each floor # i can be calculated by:

$$W_{di,ms} = (W_{di,sp} + W_{di,pr}) / 2 \qquad (5.3)$$

where:

$$W_{di,sp} = \sum_{j=1}^{j=s} d_{ji} \times tji \times 7920 \qquad (5.4)$$

and:

$$W_{di,pr} = \frac{\left(\sum_{m=1}^{m=p} L_{m,i} \times h_{m,i} + \sum_{n=1}^{n=q} L_{n,i-1} \times h_{n,i-1} \right)}{2} \times 7920 \qquad (5.5)$$

where "$W_{di,sp}$", "$W_{di,pr}$", "d_{ji}", "t_{ji}", "L_{ri}", "h_{ri}", "s" and "p" are respectively the total dead load of spandrels (N), total dead load of piers and walls (N), length of a spandrel (m), height of the spandrel (4'0" at floors #1, 2, 3 and 5'6" at floor # 4) (m), width and height (m) of a pier or wall "j" above floor # i, number of spandrels and number of piers and walls. According to

section 4.2.3 of chapter 4, a weight of 7920 N per m^2 area of masonry was adopted.

5.2.2. Calculation of the self dead load:

The self dead load "W_{wi}" of each wall or pier, its total weight to be used in the analysis according to the flow-chart of Figure 2.2 at floor # i, is used to obtain the lateral loads at each floor and the corresponding total base shear force. The calculated "W_{di}" and "W_{wi}" for the west facade and interior walls are summarized in Table 5.1. The UCBC 91 recommended allowable capacities and values necessary for the subsequent analysis are given in Table 5.2.

5.2.3. Calculation of the Demand-Capacity Ratio (DCR):

The Demand-Capacity Ratio (DCR) was calculated for the roof as:

$$DCR = \frac{0.83 \times Z \times \sum W_d}{\sum\sum (v_u \times D)} \tag{5.6}$$

and for the other walls as:

$$DCR = \frac{0.83 \times Z \times \sum W_d}{\left(\sum\sum v_u \times D + V_{cb}\right)} \tag{5.7}$$

where Z and υ_u are respectively the seismic zonal ratio and allowable shear value for a diaphragm.

The calculated DCR ratios for both the west facade and interior walls are presented in

Table 5.3. Since all DCRs fall within region 3 in Figure A-1-1 of UCBC 1991 (reproduced in Figure 2.1), no crosswalls are needed and the diaphragm spans are acceptable.

5.2.4. Verification of the dynamic stability:

The slenderness ratios h/t of the URM piers and walls are checked against the allowable ratios in Table A-1-B of the UCBC 1991 (reproduced in Table 5.4). The maximum calculated slenderness ratio for masonry is equal to the maximum pier or wall height which is 3.8 m over their common thickness of 0.45 m. This ratio is found to be 8.4. Thus, out-of-plane dynamic stability exists for the walls and piers of the Montgomery Block building.

5.2.5. Calculation of wall shears:

According to UCBC 1991, the wall shear strength at level x of an URM building is given by the following equation:

$$F_{wx} = Min \left\{ \begin{array}{l} 0.25 \times Z \times \left(W_{wx} + \dfrac{W_d}{2} \right) \\ 0.1 \times \left(W_{wx} + \sum W_d \times \dfrac{v_u \times D}{\sum \sum v_u \times D} \right) \\ 0.1 \times W_{wx} + v_u \times D \end{array} \right\} \qquad (5.8)$$

In this equation, Z is the zonal factor that identifies the Effective Peak Acceleration (EPA) received by the piers and walls. For San Francisco, situated in seismic zone 4, Z is equal to

0.4 and Equation (5.8) becomes:

$$F_{wx} = 0.1 \times W_{wx} + Min \left\{ \begin{array}{l} 0.1 \times \dfrac{W_d}{2} \\ 0.1 \times \sum W_d \times \dfrac{v_u \times D}{\sum\sum v_u \times D} \\ v_u \times D \end{array} \right\} \qquad (5.9)$$

The calculated bracketed value of Equation 5.9 are summarized in the last three columns of Table 5.1. The resulting wall shears are in Table 5.4 for both the vertical elements, i.e. west facade and interior wall.

5.2.6. Analysis of the URM walls for in-plane shear forces:

The analysis of the west facade and interior wall was realized by following the steps of the algorithm in Figure 2.2. According to the code V_a and V_R are calculated following:

$$V_a = D \times t \times v_a \qquad (5.10)$$

and

$$V_R = (0.50 \times P_D + 0.25 \times P_w) \times D/H \qquad (5.11)$$

where D, t, H, P_D and P_w are respectively the in-plane width, thickness and height dimension of a pier or wall, superimposed dead load at the top of the pier and its weight.

At each floor level, the shear forces (F_{wx}), the shear cracking strength (V_a) and the restoring shear (V_R) are calculated. The capacity at each level of the entire shear wall is obtained by following the flow-chart of Figure 2.2. Then, the capacity of the entire shear wall is equal to the base shear force times the smallest α_i, where α_i is equal to the capacity of the i^{th} storey

over the total shear force ΣF_{wx} at the floor of that storey.

5.2.6.1. Analysis of the west facade:

The rocking restoring shear strengths (V_R) and cracking shear strengths (V_a) of all piers in the west facade have been calculated (Table 5.5). It is found that:

- At each pier of a given floor, V_R is always less than V_a. Thus, individual piers can rock safely.
- The shear force ΣF_{wx} applied to the entire facade at each floor is less than the total restoring shear of all piers in the wall; rocking of pier system is safe in the west facade and according to Figure 2.2, the capacity of a storey is given by ΣV_R.
- The minimum ratio α is given at floor # 4. So, the west facade's capacity is reached at floor # 4 with a value of 1148 KN.

5.2.6.2. Analysis of the interior wall:

The calculated values of V_R and V_a for all walls and piers at each floor level are summarized in Table 5.6. They show that at floor # 4, individual piers can rock safely since V_R is smaller than V_a for all piers. At this level, the storey capacity is equal to the sum of the piers' restoring shears (ΣV_R). However, at the other floor levels, relative rigidity analysis was required since V_a is smaller than V_R for all piers and walls. The results of this analysis are given in Table 5.6. The minimum ratio α is obtained at floor # 1 with an entire wall's capacity of 2628 KN.

It is noteworthy that according to the UCBC analysis, neither the west facade nor the interior wall would require seismic rehabilitations. However, this not equivalent to predicting the total absence of structural damage during a major earthquake since the UCBC special procedure is only intended as a life safety measure.

CHAPTER 6

Interpretations of Results

6.1. Introduction:

Ultimately, all previous calculations find their meaning if they can successfully explain or demonstrate why the Montgomery Block building survived the 1906 San Francisco earthquake. In this chapter, the results of chapters 3, 4 and 5 will be reviewed as compared to the Pseudo Spectral acceleration "PSa" response of a Single-Degree-of-Freedom "SDOF" system with a damping ratio "ξ" of 10 % or 5 %.

6.2. Calculation of Elastic PSa:

No strong motion record exists of the 1906 San Francisco earthquake. Hence, quantitative analysis can only be approximate and speculative. The accuracy of the proposed following procedure is comparable to that of previous calculations.

A series of steps are necessary to obtain a plausible PSa for this historical earthquake. First, the moment magnitude "M_w" of the 1906 San Francisco earthquake has been estimated by others to be 7.9 (Naeim 1989). Second, the San-Andreas fault is known to be 15 km from the Montgomery Block building. Therefore, using Joyner and Boore's attenuation relationship from western U.S. records, the Peak Ground Acceleration "PGA" can be computed by:

$$\log(PGA) = -1.02 + 0.249 M_w - \log\left(R^2 + 7.3^2\right)^{1/2} - 0.00255\left(R^2 + 7.3^2\right)^{1/2} \qquad (6.1)$$

where R (km) is the distance from the causative fault.

This gives an estimated PGA of 0.48 g. According to proportionality rules of ground spectra proposed by Newmark-Hall, the corresponding Peak Ground velocity "PGV" and Peak Ground Displacement "PGD" are:

$$\mathbf{PGV = 48 \times (PGA/g)\ [in/sec]} \qquad (6.2)$$

$$\mathbf{PGD = 36 \times (PGA/g)\ [in]} \qquad (6.3)$$

This gives a PGV of 23.1 in/s and a PGD of 17.3 in.

Finally, the Pseudo Acceleration "PSa", Pseudo Velocity "PSV" and Displacement "S_d"

spectra can be obtained for various damping ratios "ξ" by multiplying the ground response spectrum by the Newmark-Hall amplification factors. These amplification factors are summarized in Table 6.1.

The resulting elastic Newmark-Hall design spectra are drawn in Figure 6.1. Numerical values as a function of selected fundamental periods "T" are in Table 6.2.

6.3. Ultimate capacities of Montgomery Block building:

In order to compare seismic demand (i.e. PSa) with structural strength supplied, a rough conversion of previous calculations is necessary. All material properties and structural strength in the previous chapters were at a working stress level. For masonry, a safety factor of 3.0 is generally assumed. Therefore, although not perfectly correct, approximate ultimate strengths can be taken as 3 times the previously calculated strengths.

Thereafter, to locate these strengths on the response spectra, they must be expressed as lateral capacities in percentage of gravity (g). For example, in chapter 3, the west facade piers-only model strength was calculated to be V/W equals to 0.02, i.e. the facade had an allowable base shear strength of 2 % its reactive tributary supported weight. This would correspond to an approximate ultimate strength of 3 times 2 % which equals 6 % of this weight. Hence, if V = 0.06 W = 0.06 mg , it can be treated as a SDOF system which would remain elastic up to a PSa value of 0.06 g, i.e. $V = (m \times PSa)_{equivalent}$. According to this procedure, ultimate strengths were calculated for the 2D, 3D and ABK models and results presented in Tables 6.3, 6.4 and 6.5.

6.4. Interpretation of results:

The Montgomery Block building survived the 1906 San-Francisco earthquake which most

probably had a PGA of nearly 0.5 g. This has been reported by Freeman as previously mentioned (Freeman 1932). An analytical method could predict survival if its ultimate strength exceeded the estimated seismic elastic demand as expressed by the response spectra. However, as shown in Figures 6.2 and 6.3, it appears that none of the analysis methods considered can predict survival except the "ABK" analysis method for 10 % damping. This might be attributable to one or more of the following points:

- Under-estimated value of the maximum allowable flexural tensile stress "f_t" (f_t = 0.19 MPa) used for the structural analysis of the models. However, this not probable as the selected f_t value is already a high estimate, but also because a value of nearly 4 times the allowable stress used in this study would be needed for the Montgomery Block building to survive this earthquake as shown in Figures 6.2 and 6.3. Shear failure would start to occur and govern seismic response. Indeed, in Tables 3.8 and 4.6, when f_t became ∞, the ultimate capacity ratios 3 x V_{max}/W became respectively 67.2 and 59.1 % for frame 2D and 3D models with offsets.
- Some models could be completely deficient. For example, the piers-only model assumes all beams are cracked before the analysis of the building, which is a wrong assumption as revealed by the damage propagation sequence observed in the frame models.
- Observations of no-damage could be wrong. It is true that no spectacular damage occurred; according to the dynamic stability principles, none of the piers or walls are likely to have out-of-plane failures because of their low slenderness ratio. However, tensile cracks could have opened and closed back after rocking.
- The mass of the building could be over-estimated. Smaller lateral loads and overburdens on structural elements would result from a smaller building mass. Yet, once all affected parameters are considered, a higher lateral load resistance would be obtained.
- There could have been, in 1906, additional structural or non-structural elements which could have added to the lateral load resistance. The incompleteness of structural and architectural drawings can unfortunately not be improved.
- Finally, the interaction between the frequency content of the earthquake and this

structure could have been more favourable than predicted by a smoothed design response spectra. Irregular largely variable peaks and valleys are more typical of single earthquake response spectra, and this building could have been fortunate to fall in one such valley. Alternatively, the spectra used for comparison herein could also be somewhat conservative.

Nonetheless, in spite of all these potential shortcomings, valuable observations have been possible regarding the adequacy of various analysis models.

CHAPTER 7

Conclusions

In this thesis, existing findings on the seismic performance, behavior concepts and masonry properties of URM masonry structures were collected , and an URM building which survived the 1906 San Francisco earthquake has been investigated by various existing analysis methods to determine the impact of engineering modelling assumptions on the seismic performance of unreinforced masonry structures. This impact is found to be major. Some important conclusions about the building analyses are summarized in the following paragraphs:

Behavior of the perforated facades:

- The simplistic 2D piers-only model has shown that under some circumstances, a large number of piers can accept the redistributed loss-of-capacity produced by cracking of a stiffer member. In this case, the 1st crack in the analysis does not correspond to the threshold of damage. The very high fundamental period of the facade in a 2D piers-only model further demonstrates that it is not a very realistic model. Thus, it

seems that assuming all beams of the facade cracked before its analysis is not correct and too conservative.

- In the 2D frame model without offsets, the 1st crack corresponds to the threshold of damage. The capacity increased by more than 100% compared to the piers-only model. After the initial damage of many beams, an alternating pattern of beam and pier damage was observed. The first fundamental period of this model was lower.
- The consideration of offsets in the 2D frame model has increased the capacity of the west facade and lowered its fundamental period. The 1st crack corresponds again to the threshold of damage. Thus, the added modelling complexity seems beneficial.
- The analysis of the building by the ABK method has shown that the facade can sustain a maximum base shear force 285 % greater than that predicted by the 2D frame model with offsets. This may be attributable to the fact that in the ABK procedure, the failure occurs in a rocking failure mode after a flexural tensile failure. However, the ABK method predicts failure at the 4th floor whereas in the 2D frame model with offsets, the failure occurs at the 1st floor. Differences can be partly explained by ABK's particular assumptions regarding the vertical distribution of the equivalent static seismic force, and the assumption that all piers crack and rock under rigid continuous spandrels. The last assumption, in particular, seems unlikely as revealed by 2D analysis of frames with offsets. The applicability of ABK to a perforated facade such as in the Montgomery Block building is not clear.

3D behavior of Montgomery Block building:

- In the 3D models, a rigid diaphragm was assumed to exist. This gives the building a totally different behavior. The perforated facade was assumed the weakest element in flexible diaphragm modelling. Here, instead, torsion allows transfer of the loss-of-capacity from damaged elements to other structural elements in the same plane, or even perpendicular to the direction of the lateral load.
- In the 3D piers-only model, the threshold of damage was reached at 1st cracking. In the 3D frame model with offsets, the threshold of damage occurred only after many structural elements cracked, particularly in the west facade. Total capacity was almost

60 % higher than that in the solid pier/cracked spandrel model. In both cases, maximum capacity occurred when the same rigid pier failed. In 3D rigid diaphragms model studies, the perforated facades had almost no influence on the ultimate behavior, as expected due to relative stiffnesses involved.

In many instances, the lateral load-displacement behavior of the 2D and 3D frame models with offsets showed what could be considered to be a semi-ductile behavior as expressed by the capacity to sustain large displacements and damage before complete structural failure.

Additional analytical and experimental research is desirable to resolve some of the outstanding issues regarding the credibility of some of the aforementioned models. However, from this study, it is clear that considerable differences in seismic performance assessments of URM buildings, of nearly an order of magnitude in some cases, exist depending on the structural model selected by the engineer.

References

ABK, A joint Venture, (1981a). *Methodology for mitigation of seismic hazards in existing unreinforced masonry buildings: Categorization of buildings,* ABK-TR-01, Agbabian Associates, El Segundo, California, USA.

ABK, A Joint Venture, (1981a), *Methodology for mitigation of seismic hazards in existing unreinforced masonry buildings: Diaphragm testing,* ABK-TR-03, Agbabian Associates, El Segundo, California, USA.

ABK, A Joint Venture, (1981b), *Methodology for mitigation of seismic hazards in existing unreinforced masonry buildings: Wall testing, out-of-plane,* ABK-TR-04, Agbabian Associates, El Segundo, California, USA.

ABK, A Joint Venture, (1984), *Methodology for mitigation of seismic hazards in existing unreinforced masonry buildings: The Methodology,* ABK-TR-08, Agbabian Associates, El Segundo, California, USA.

Abu-El-Magd, S.A. and Mac Leod, I.A. (1980), "Experimental tests on brick beams under in-plane bending conditions", *The Structural Engineer,* Vol. 58B, pp. 62-66.

ACI committee 530, (1988). *Joint committee report on Proposed Standards, Building Code*

Requirements for Masonry Structures and Specifications for Masonry Structures, ASCE Masonry Structures, Standards committee

Adham, S.A. (1985), "Out-of-plane response of masonry walls", *Proc. Third North American Masonry Conf.,* Arlington, Texas, USA, pp. (47-1)-(47-14).

Barberi, U., Borri, A., Sorace, S. (1991), "A Non-Linear 3-D F.E. Approach Analysis of Masonry Domes", *Proc. Second International Conf. on Repairs and Maintenance of Historical Buildings, Seville, Spain*, Computational Mechanics Publications, pp. 329-341.

Bariola, J., Ginocchio, J.F. and Quiun, D. (1990), "Out-of-plane response of brick walls", *Proc. Fifth North American Masonry Conf.,* Urbana-Champaign, USA, Vol.1, pp.429-439.

Benedetti, D. and Benzoni, G.M. (1984), "A numerical model for seismic analysis of masonry buildings: Experimental correlations", *Earthquake Engineering and Structural Dynamics*, Vol.12, pp.817-832.

Braga, F. and Liberatore, D.(1990), "A finite element for the analysis of the response of masonry buildings under seismic actions", *Proc. Fifth North American Masonry Conf.,* Urbana-Champaign, Illinois, USA, Vol.1, pp.201-212.

Brebbia, C.A., Niku, M. (1991), "The Boundary Element Method as an Analysis Tool for Repair of Historical Buildings", *Proc. Second International Conf. on Repairs and Maintenance of Historical Buildings, Seville, Spain*, Computational Mechanics, pp.343-354.

Bruneau, M., (1992), "State-of-the-art report on the seismic performance of unreinforced masonry buildings - Part I", *ASCE Structural Journal*, Vol.?, No.?, pp.?.

Chiostrini, S. and Vignoli, A. (1989), "An application of a numerical method to study

masonry panels with various geometry under seismic loads", *Proc. First International conference on structural studies, Repairs and maintenance of historical buildings*, Florence, Italy, pp. 309-534.

Chiostrini, S. and Vignoli, A. (1991), "Mechanical modelling of masonry walls with various openings", *Proc. Second International Conf. on Repairs and Maintenance of Historical Buildings, Seville, Spain*, Computational Mechanics Publications, pp.247-262.

Chiostrini, S., Foraboschi, P. and Sorace, S. (1989), "Problems connected with the application of a non-linear finite element method to the analysis of masonry structures", *Proc. First International conference on structural studies, repairs and maintenance of historical buildings*, Florence, Italy, pp. 525-534.

Davidson, E.B., Wang, L.R.L. (1985), "A study of the cyclic lateral resistance of low rise masonry wall panels", *Proc. Third North American Masonry Conf.*, Arlington, Texas, USA, pp.(48-1)-(48-15).

EERI, (1989). *Armenia Earthquake Reconnaissance Report*, Earthquake Spectra - Special Supplement , *Earthquake Engineering Research Institute*, El Cerrito, California, USA.

EERI, (1990). *Loma Prieta Earthquake Reconnaissance Report*, Earthquake Spectra - Supplement to Volume 6, May 1990, *Earthquake Engineering Research Institute*, El Cerrito, California, USA.

Elsesser, E., Naaseh, S., Walters, M., Sattary, V., Whittaker, A.S., (1991). "Repair of Five Historic Buildings Damaged by the Loma Prieta Earthquake", Proc. Seismic Historic Building Conf., Western Chapter Assoc. for Preservation Technology, San Francisco, pp.4-1, 4-39.

Englekirk, R.E. and Hart, G.C., (1984). *Earhquake design of concrete masonry Buildings,*

Vol.1: Strength Design of one-to-Four-Story Buildings, Printice-Hall, Englewood Cliffs, New Jersey, USA.

Englekirk, R.E. and Hart, G.C., (1984). *Earhquake design of concrete masonry Buildings, Vol.2: Strength Design of one-to-Four-Story Buildings,* Printice-Hall, Englewood Cliffs, New Jersey, USA.

Epperson, G.S. and Abrams, D.P. (1990), "Evaluating lateral strength of existing unreinforced brick piers in the laboratory", *Proc. Fifth North American Masonry Conference,* Urbana-Champaign, Illinois, USA, Vol. 2, pp. 735-746.

Gere, J.M., Timoshenko, S.P., (1984). "Mechanics of Materials", *Brooks/Cole Engineering Division*, California, USA, 762 pages.

Glanville, J.I. and Hatzinikolas, M.A., (1989). *Engineered masonry design,* Winston House Enterprises, Winnipeg, Mannitoba, Canada, 1st edition, 338 pages

Hendry, A.W., Sinha, B.P. and Davies S.R., (1987). *Load Bearing Brickwork Design,* Ellis Horwood Series in Engineering Science, 2nd edition

Ignatakis, C., Stavrakakis, E. and Penelis, G.(1989), "Analytical model for masonry using the finite element method". *Proc. First International conference on structural studies, Repairs and maintenance of historical buildings*, Florence, Italy, Vol. 1, pp. 511-524

International Conference of Building Officials, (1991). *Uniform Code for Building Conservation*, Whittier, California, USA.

Jiugqian, X. and Maogong, C. (1984), "Experimental study on aseismic behavior of brick buildings", *Proc. Eight World Conf. on Earthquake Engineering,* San Francisco, California,

USA, Vol.6, pp.831-838.

Kariotis, J.C., Johnson, A.W. and Ewing, R.D. (1985), "Predictions of stability of unreinforced masonry shaken by earthquake", *Proc. Third North American Masonry Conf.* Arlington, Texas, USA, pp. (49-1)-(49-11).

Konig, G., Mannand, W. and Otes, A. (1988), "Experimental investigations on the behaviour of unreinforced masonry walls under seismically induced loads and lessons derived", *Proc. Ninth world conf. of earthquake engineering*, Vol. 8, pp. 1117-1122

Mann, W., Muller, H. (1982), "Failure of the Shear-Stressed Masonry - An enlarged Theory, Tests and Application to Shear Walls", *Proc. British Ceramic Society*, No. 30, pp.223-235.

Mayes, R.L., Clough, R.W. (1975), "State-of-the-Art in Seismic Shear Strength of Masonry - An Evaluation and Review", *Earthquake Eng. Research Center, EERC 75-21*. University of California, Berkeley, USA.

Mengi, Y. and McNiven, H.D. (1986), "A mathematical model for predicting the non-linear response of unreinforced masonry walls to in-plane earthquake excitations", *Earthquake Eng. Research Center, UCB/EERC-86/07*, University of California, Berkeley, USA, 113 p.

Page, A.W., Samarasinghe, W., Hendry, A.W., (1982), "The in-plane failure of masonry - A review", *Proc. British Ceramic Society*, Load-Bearing Brickwork, No. 30, pp.90-100.

Pistone, G., Bono, D., Macchiorlatti, B., (1991), "Investigation and Simulation of the Static Behavior of S. Maria di Castello Church in Alessandria", *Proc. Second International Conf. on Repairs and Maintenance of Historical Buildings II, Seville, Spain*, Computational Mechanics Publications, pp.277-288.

Prawel, S.P. and Lee, H.H. (1990a), "The performance of upgraded brick masonry piers subjected to out-of-plane motion", *Proc. Fourth National Conference on Earthquake Engineering*, Palm Springs, California, USA, Vol.3, pp.273-281.

Prawel, S.P. and Lee, H.H. (1990b), "The performance of upgraded brick masonry piers subjected to out-of-plane motion", *Proc. Fifth North American Masonry Conference*, Urbana-Champaign, Illinois, USA, Vol.1, pp. 411-427.

Priestley, M.J.N (1985), "Seismic Behavior of Unreinforced Masonry Walls", *Bull. New Zealand Nat. for Earthquake Eng.*, Vol.18, No.2, pp.191-205, and Vol.19, No.1, pp.65-75.

Priestley, M.J.N., (1986), "Discussion : Seismic behaviour of Unreinforced Masonry Walls", *Bulletin of The New Zealand National Society for Earthquake Engineering*, Vol. 19, Nº1, pp. 65-75

Priestley, M.J.N., (1985), "Seismic Behaviour of Unreinforced Masonry Walls", *Bulletin of the New Zealand National Society for Earthquake Engineering*, Vol. 18, Nº2, pp. 191-205.

Quirós Lara, A.L., Gutiérrez, J.A. (1991), "Seismic Retrofit of the Historic National Theater San Jose, Costa Rica", *Proc. Seismic Historic Building Conf.*, Western Chapter Assoc. for Preservation Technology, San Francisco, USA, pp.17-1, 17-17.

Samarasinghe, W., Page, A.W. and Hendry, A.W. (1981), "Behaviour of brick masonry shear walls", *The Structural engineer*, Vol. 59B, pp. 42-48.

Sinha, B.P., (1980), "An ultimate load analysis of laterally loaded brickwork panels", *International Journal of Masonry Construction*, Vol. 1, No. 2, pp.57-61.

Sinha, B.P., and Hendry, A.W. (1969), "Racking Tests on Storey Height Shear-Wall

Structures with Openings, Subjected to Precompression", *Designing, Engineering and Constructing with Masonry Products*, Johnson, Gulf Publishing Co., Houston, Texas.

Sinha, B.P. (1978), "A simplified ultimate load analysis of laterally loaded model orthotropic brickwork panels of low tensile strength", *The Structural Engineer*, Vol. 56B, pp. 81-84.

Smith, R.C., Honkala, T.L. and Andres C.K., (1979). *Masonry: Materials, Design, Construction*, Reston Publishing Company, Inc., A Prentice-Hall Company, Reston, Virginia, U.S.A.

Tomazevic, M. and Weiss, P., (1978), "A rational, experimentally based method for the verification of earthquake resistance of masonry buildings", *Proceedings of the Fourth U.S. National Conference on Earthquake Engineering*, Vol.2, pp. 255-262.

Turnsek, V., Tercelj, S., Sheppard, P. (1978), "The Seismic Resistance of Stone-Masonry Walls and Buildings", *Proc. Sixth European Conf. on Earthquake engineering, Dubrovnic, Yugoslavia, Yugoslav Association for Earthquake Engineering*, Vol. 3, pp. 255-262.

Vestroni, F., Giannini, R., Grillo, F., (1991), "Seismic Analysis of an Ancient Church and a Proposal of Strengthening Repairs", *Proc. Second International Conf. Repairs and Maintenance of Historical Buildings, Seville, Spain*, Computational Mechanics, pp.77-88.

Zingali, A.E. (1984), "Tests on Specimen Walls in St. Gregorio Magno", *Proc.: Joint USA/Italy Workshop on Seismic Repair and Retrofit of Existing Buildings, Rome Italy, Center for Environmental Design Research, University of California*, Berkeley, pp. 207-217.

EQ Name	Coalinga May 2, 1983	Borah Peak Idaho Oct. 28, 1983	Morgan Hill April 24,1984	Michoacan Sept. 19,1985	Whittier Narrows Oct. 1, 1987	Armenia Dec. 7,1988	Saguenay Dec. 7, 1988	Loma Prieta Oct. 17,1989
Magnitude	6.7	7.3	6.2	8.1	5.9	6.8	6.0	7.1
City near the epicentre State Distance PGA	Coalinga (California) 15 km 0.54 g	Mackay (Idaho) 21 km 0.10 g*	Morgan Hill (California) 21 km 0.45 g	Mexico (Mexico) 360 km 0.17 g	Whittier Narrows (California) 3 km 0.50 g**	Spitak (Armenia) 80 km 0.21 g	Chicoutimi (Quebec) 36Km 0.11g	Santa Cruz (California) 16Km 0.65g
# deaths	0	2	----	10000	3	>25000	0	62
# injuries	180	1	----	----	1349	31000	0	3757
# homeless	----	17 families	5 families	50000	----	514000	0	>12000
Typical URM Buildings	1 to 5 story (2 to 3 wythe walls)	1 story (2 to 3 wythe or megablock walls)	1 to 2 story	---- (infill-masonry)	----	4 to 5 story (2 stone wythe, 600mm thick walls)	2 to 5 story	3 to 4 story
Damage degree***	Very high	Medium	Low	Very high	Medium	Very high	Very low	Medium
Out-of-plane failures	Many	Many	Few	Many	Few	Many	Few(nonstructural)	Many
In-plane failures	Very few	Very few	Many	Many	Many	Few	Few	Many
Anchorage	Inadequate and defective	defective and improper	Defective	Not applicable	improper	defective	----	Inadequate
Other problems	Dynamic instability, mortar: poor quality and its absence between wythes	Fallen parapets and veneers	Fallen parapets and ceiling panels	soil amplification effect	----	mortar: Poor quality and its absence between wythes	----	Diaphragm flexibility ,Pounding, Low quality of mortar and masonry

* Estimated ** Average *** Subjective evaluation

Table 2.1: Overview of the seismic performance of URM buildings during some selected earthquakes.

Source	Value	Notes
Hendry, Sinha and Davies	For brick masonry : 700 f'_m	According to Drysdale and Suter, E_m= 1000 f'_m for concrete block masonry. However, E_m= 700 f'_m is better for brick masonry
Supplement Nb. 4, NBCC 1975	1000 $f'_m \leq$ 20,000 MPa	
CAN3-S304-M84	1000 $f_m' \leq$ 20,000 MPa	
ABK (1984)	689 MPa	
ACI committee 530	1000 $f'_m \leq$ 20,000 MPa	It depends on the compressive strength of the units and the mortar type

Table 2.2: Modulus of elasticity of URM in compression.

Source	Value	Notes
Hendry, Sinha and Davies	0.4 MPa	This value is for URM brick walls. It depends on the moisture content of bricks. Typically, this value is applied for a moisture content of 8% . The mortar type has also an influence
Suter (Personal communication)	0.1 → 0.2 MPa	According to Suter, it's difficult to find out experimentally the exact value

Table 2.3: Maximum allowable tensile stress in URM.

Source	Value	Notes
Hendry, Sinha and Davies	0.8 MPa → 2MPa	parallel to bed joint
	1/3*(0.8MPa→2MPa)	normal to bed joint
Supplement Nb. 4, NBCC 1975 (2)	M or S mortar: 0.50 MPa	parallel to bed joint
	N mortar: 0.39 MPa	
	M or S mortar: 0.25 MPa	normal to bed joint
	N mortar: 0.19 MPa	
CAN3-S304-M84	Same as (2)	same as (2)
ACI committee 530	M or S mortar: 0.50 MPa	parallel to bed joint Portland cement-lime
	N mortar: 0.37 MPa	
	M or S mortar: 0.25 MPa	parallel to bed joint lime mortar
	N mortar: 0.19 MPa	
	M or S mortar: 0.25 MPa	normal to bed joint Portland cement-lime
	N mortar: 0.19 MPa	
	M or S mortar: 0.12 MPa	normal to bed joint lime mortar
	N mortar: 0.09 MPa	

Table 2.4: Maximum allowable flexural tensile stress in URM.

Source	Value	Notes
Supplement Nb. 4, NBCC 1975 (2)	walls : 0.32 f'_m	
	columns : 0.26 f'_m	
CAN-S304-M84	same as (2)	
ACI committee 530	(1/3) f'_m	

Table 2.5: Maximum allowable flexural compressive strength in URM.

Source	Value	Notes
Hendry, Sinha and Davies		It depends on the brick and mortar strengths
Supplement Nb. 4, NBCC 1975 (2)	walls : 0.25 f'_m	
	columns : 0.20 f'_m	
CAN3-S304-M84	same as (2)	
ACI committee 530	0.15 f'_m	

Table 2.6: Maximum allowable axial compressive strength in URM.

Source	Value	Notes
Hendry, Sinha and Davies	The test results give : $v_m = v_o + \mu * \sigma_c$	For $f'_{br} = 20 \rightarrow 50$ MPa : $v_o = 0.3$ MPa: strong mortar (1:1/4:3) $= 0.2$ MPa: medium mortar(1:1:6) μ (average) $= 0.4$ & $\sigma_c \leq 2$ MPa
Supplement Nb. 4, NBCC 1975 (2)	M or S mortar:	$0.083\sqrt{f'_m} \leq 0.35$ *MPa*
	N mortar:	$0.083\sqrt{f'_m} \leq 0.24$ *MPa*
CAN3-S304-M84	same as (2)	same as (2)
ABK	$v_m = 3/4*(3/4*v_t+P/A)$	This value is for walls and piers (see appendix "D" in report Nb. 8)
ACI committee 530	v_m =min(0.83 MPa, $1.5\sqrt{f'_m}$, 0.26+0.45P/A)	P : Axial Load (in N) A : Shear surface (in mm^2)

Table 2.7: Maximum allowable shear stress in URM.

Designation	Value	Notes
f'_m	4 → 10 MPa	
E_m	400 → 1000 MPa	This value will apply up to about 75% of f'_m
Direct : f_t	0.15 MPa	
Flexural : f_t	N mortar : 0.39 MPa	Parallel to bed joint
	N mortar : 0.19 MPa	normal to bed joint
Axial : f_m	Walls : 1.00 → 1.50 MPa	
	Columns : 0.80 → 1.20 MPa	
Flexural : f_m	Walls : 1.28 → 1.92 MPa	
	Columns : 1.04 → 1.56 MPa	
Shear : v_m	$v_m = v_o + \mu^* \sigma_c$	see Table 3.7

Table 2.8: Suggested allowable brick masonry characteristics.

Lumped Masses					
Floor #	Wood (kg)		Masonry (kg)		Total (kg)
	Partition walls	Floor	Spandrels	Piers and Walls	
4	42856 (8%)	132282 (26%)	111381 (22%)	220000 (44%)	506519 (100%)
3	90145 (12%)	148549 (19%)	81005 (10%)	463009 (59%)	782708 (100%)
2	99011 (12%)	155371 (18%)	81005 (10%)	508624 (60%)	844011 (100%)
1	70933 (7%)	162495 (16%)	108005 (10%)	703348 (67%)	1044781 (100%)

Table 3.1: Lumped masses from wood and masonry components for the entire building.

Floor #	Pier #					Floor Mass (kg)
	1	2→9 & 12→19	10	11	20	
Load due to all Wood components (N)						
4	12054	12054	16177	15860	11419	25318
3	18454	18454	24767	24281	17482	38761
2	19661	19661	26387	25870	18626	41297
1	18047	18047	24222	23747	17098	37907
Load due to Masonry piers (self weight) (N)						
4	0	0	0	0	0	0
3	23698	23698	31805	31181	22450	49776
2	24462	24462	32831	32187	23175	51381
1	26755	26755	35908	35204	25347	56197
Load due to Masonry Spandrels (N)						
4	6070	12140	12140	12140	6070	23513
3	4415	8830	8830	8830	4415	17102
2	4415	8830	8830	8830	4415	17102
1	4415	8830	8830	8830	4415	17102

Table 3.2: Gravity loads' distribution at each floor for all piers of the facade.

Pier width (m)				Notes
1→9 & 12→19	10	11	20	All the piers are 0.45 m thick
0.97	1.30	1.27	0.91	

Table 3.3: Sectional widths of the piers of the facade.

	Precompressed Shear		Pure Shear		Flexural Compression		Flexural Tension		
Step	Pier #	V_{max}(KN)	Pier #	V_{max}(KN)	Pier #	V_{max}(KN)	Pier #	V_{max}(KN)	F. Period: T(s)
1	10	1824	10	1154	10	285	10	75	2.20902
2	11	1695	11	1071	11	259	11	68	2.33739
3	1	2453	1→9 & 12→19	1579	2→9 & 12→19	295	1	75	2.48147
4	2→9 & 12→19	2398	20	84	1	32	2→9 & 12→19	77	2.55404
5	20	130	---	---	20	15	20	4	11.36659

Table 3.4: Lateral load capacities for all modes of failure and fundamental period of the solid pier/cracked-spandrel model.

V_{max} (KN)	Δ(Floor#1) (mm)	Δ(Floor#2) (mm)	Δ(Floor#3) (mm)	Δ(Floor#4) (mm)
297.8	1.638	2.532	3.037	3.241
217.4	1.241	1.929	2.299	2.448
192.6	1.171	1.825	2.155	2.288
246.2	1.581	2.468	2.890	3.061
112.9	1.602	2.681	2.910	3.000
123.6	2.207	3.729	3.981	4.073
137.9	2.179	3.672	3.956	4.061
184.3	1.573	2.525	2.862	3.000
206.7	4.239	7.173	7.591	7.736
148.4	3.162	5.401	5.691	5.794
184.2	4.015	7.027	7.497	7.629
113.3	2.651	4.620	4.953	5.034
12.4	0.296	0.525	0.566	0.570
164.4	3.838	6.664	7.161	7.335
180.0	4.229	7.401	7.944	8.110
171.9	4.082	7.226	7.792	7.954
137.1 (Step 30)	3.290	5.884	6.368	6.500
137.1 (Step 32)	3.290	5.884	6.360	6.489
176.8	2.373	7.611	8.262	8.509
78.8	4.249	5.143	6.028	6.179
95.1	3.007	6.730	7.984	8.170
84.1	2.840	6.614	7.929	8.091
120.0	4.398	10.700	12.957	13.171
74.4	3.197	8.375	10.622	10.786
35.0	1.930	5.517	7.837	7.852
97.1	5.755	16.767	25.000	25.144
109.4	7.163	20.854	30.689	30.863
71.5	7.602	21.259	29.982	30.084
34.1	8.418	21.147	28.399	28.603
88.1	23.764	61.400	79.682	80.019

Table 3.5: Lateral displacement at each floor for the frame model with rigid offsets.

Step #	Frame with offsets V_{max} (KN)		Frame without offsets V_{max} (KN)
	f_t = 0.19 MPa	$f_t = \infty$	$f_t = \infty$
1	297.8	826.0	1012.4
2	217.4	742.1	---
3	192.6	808.4	---
Failure Mode	F. T.	P. S.	P. S.

Table 3.6: Comparison of the facade's capacities in presence of high and code's value of f_t.

Model	V_{max} (KN)	V_{max}/W (%)
Piers only	77	2.1
Frame without rigid offsets	171.5	4.7
Frame with rigid offsets	297.8	8.1

Table 3.7: Comparison of the capacities and their ratios with the model.

Floor #	M_i (kg)	MMI_i (kgxm^2)	Notes
4	506519	181364497	The lumped floor masses "M_i" are calculated in chapter 4.
3	782708	280256896	
2	844011	302207085	
1	1044781	307543616	

Table 4.1: Lumped floor masses and mass moments of inertia at each floor.

Step #	# Damag. Piers	V_{max}(KN)	T(s)
1	1	1020	0.913309
2	2	773	0.921203
3	4	570	0.955101
4	5	401	1.639953
5	6	370	1.695335
6	7	326	1.767036
7	8	368	1.845701
8	9	357	1.906709
9	10	375	1.917525
10	11	385	1.944214
11	12	383	1.952909
12	13	421	1.996969
13	14	448	2.003739
14	15	422	2.074874
15	16	416	2.113084
16	17	408	2.151586
17	18	382	2.204917
18	19	442	2.211458
19	20	386	2.229011
20	21	420	2.251434

Table 4.2: Capacities, periods and lateral displacements of the 3-D Solid Pier/Cracked-Spandrel Model.

Step #	Floor # 1			Floor # 2			Floor # 3			Floor # 4		
	Δ_X (mm)	Δ_Y (mm)	$\theta_Z x10^5$ (rad)	Δ_X (mm)	Δ_Y (mm)	$\theta_Z x10^5$ (rad)	Δ_X (mm)	Δ_Y (mm)	$\theta_Z x10^5$ (rad)	Δ_X (mm)	Δ_Y (mm)	$\theta_Z x10^5$ (rad)
1	.430	-.021	1.471	1.320	-.112	4.886	2.461	-.303	9.578	3.574	-.517	14.402
2	.339	-.019	1.202	1.220	-.118	4.711	2.382	-.321	9.632	3.523	-.546	14.695
3	.267	-.017	1.007	1.205	-.137	4.887	2.490	-.371	10.494	3.766	-.632	16.268
4	.284	-.029	1.371	2.543	-.355	11.304	5.923	-.980	26.602	9.295	-1.680	42.346
5	.270	-.031	1.321	2.476	-.427	11.093	5.765	-1.144	26.044	9.043	-1.926	41.366
6	.247	-.033	1.228	2.330	-.495	10.553	5.425	1.295	24.672	8.502	-2.145	39.120
7	.292	-.044	1.472	2.823	-.709	12.887	6.565	-1.815	30.062	10.286	-2.972	47.546
8	.291	-.049	1.487	2.875	-.824	13.195	6.679	-2.081	30.723	10.460	-3.379	48.552
9	.309	-.052	1.580	3.059	-.878	14.048	7.099	-2.214	32.666	11.115	-3.593	51.563
10	.322	-.056	1.656	3.216	-.962	14.807	7.454	-2.407	34.361	11.662	-3.892	54.208
11	.322	-.056	1.661	3.232	-.967	14.887	7.484	-2.419	34.512	11.704	-3.910	54.424
12	.360	-.068	1.868	3.650	-1.209	16.865	8.454	-2.998	39.073	13.224	-4.820	61.592
13	.384	-.072	1.997	3.906	-1.294	18.054	9.038	-3.208	41.786	14.134	-5.158	65.843
14	.365	-.061	1.875	3.875	-1.356	17.948	9.031	-3.417	41.888	14.145	-5.503	66.085
15	.357	-.061	1.833	3.940	-1.389	18.271	9.231	-3.506	42.848	14.468	-5.649	67.642
16	.346	-.061	1.783	3.985	-1.415	18.495	9.380	-3.576	43.615	14.721	-5.765	68.911
17	.349	-.042	1.844	4.168	-.816	19.509	9.787	-2.010	45.764	15.349	-3.199	72.198
18	.406	-.048	2.146	4.853	-.952	22.728	11.395	-2.344	53.305	17.861	-3.729	84.024
19	.362	-.037	1.932	4.377	-.661	20.543	10.252	-1.641	48.057	16.061	-2.619	75.656
20	.405	-.031	2.180	4.952	-.442	23.302	11.571	-1.129	54.306	18.110	-1.822	85.428

Table 4.3: Master joints' displacements and rotations at each floor of the piers-only model.

Step #	# Damag. Elts	V_{max}(KN)	T(s)
1	13	774	0.340197
2	14	926	0.340713
3	15	716	0.341767
4	16	1110	0.343737
5	17	1138	0.345739
6	18	1453	0.345999
7	19	1084	0.346914
8	20	1090	0.348946
9	21	396	0.350095
10	22	1000	0.351197
11*	170	1627	0.419839

* Step at which the facade is assumed damaged.

Table 4.4: Capacities, periods and lateral displacements of the 3-D Frame model with rigid offsets.

Step #	Floor # 1			Floor # 2			Floor # 3			Floor # 4		
	Δ_X (mm)	Δ_Y (mm)	$\theta_Z x10^5$ (rad)	Δ_X (mm)	Δ_Y (mm)	$\theta_Z x10^5$ (rad)	Δ_X (mm)	Δ_Y (mm)	$\theta_Z x10^5$ (rad)	Δ_X (mm)	Δ_Y (mm)	$\theta_Z x10^5$ (rad)
1	.230	-.008	.686	.473	-.004	1.190	.710	-.004	1.637	.891	.001	1.935
2	.273	-.006	.811	.563	.004	1.409	.845	-.000	1.937	1.060	.001	2.290
3	.211	-.004	.629	.438	.004	1.103	.666	.001	1.555	.843	.002	1.873
4	.327	-.008	.972	.684	.003	1.737	1.043	-.002	2.463	1.275	-.001	2.948
5	.339	-.009	1.020	.712	.002	1.840	1.083	-.003	2.599	1.366	-.002	3.104
6	.432	-.012	1.299	.906	.001	2.331	1.377	-.005	3.286	1.738	-.005	3.930
7	.323	-.008	.973	.680	.003	1.759	1.035	-.003	2.491	1.307	-.002	2.984
8	.325	-.008	.979	.683	.003	1.767	1.040	-.003	2.502	1.314	-.002	2.997
9	.120	-.001	.366	.255	.005	.676	.390	.003	.972	.492	.005	1.169
10	.298	-.007	.899	.627	.003	1.623	.952	-.002	2.288	1.195	-.001	2.709
11	.551	-.019	1.850	1.252	-.005	3.842	2.048	-.019	6.126	2.731	-.022	8.021

Table 4.5: Master joint's displacements and rotation at each floor of the frame model with rigid offsets.

Step #	f_t = 0.19 MPa		$f_t = \infty$	
	V_{max} (KN)	V_{max} / W (%)	V_{max} (KN)	V_{max} / W (%)
Solid Pier/Cracked-Spandrel Model				
1	1020	3.3	3762	12.1
Frame Model with rigid offsets				
1	774	2.5	6130	19.7
2	926	3.0	6129	19.7
11	1627	5.2	4653	14.9
Failure Mode	F.T.		P.S.	

Table 4.6: Comparison of the maximum capacities and capacity ratios.

Floor #	W_w	ΣW_w	W_d	ΣW_d	$0.1W_d/2$	$0.1\Sigma W_d \cdot \rho^*$	$v_u \cdot D$
West Facade (KN)							
4	474.8	474.8	835.7	835.7	41.8	41.8	135.9
3	663.9	1138.8	1221.0	2056.7	61.0	145.2	326.2
2	695.4	1834.2	1290.9	3347.5	64.5	138.5	326.2
1	742.7	2576.9	1526.2	4873.7	76.3	142.6	326.2
Interior Wall (KN)							
4	320.5	320.5	1997.5	1997.5	99.9	141.0	135.9
3	651.4	972.0	2850.6	4848.1	142.5	342.2	326.2
2	692.8	1664.7	2891.8	7739.9	144.6	320.3	326.2
1	678.0	2342.7	3695.4	11435.3	184.8	334.7	326.2

* $\rho = v_u D / \Sigma\Sigma v_u D$

Table 5.1: Calculated weights by the special procedure of UCBC 91.

Variable	Designation	Value
v_u	Roof shear capacity	3648 N/m
v_u	Floor shear capacity	8756 N/m
v_a	Shear wall shear capacity	240,000 N/m
v_c	Crosswall shear capacity	5837 N/m
D	In-plane width dimension of pier or wall	For the whole wall: 37.25 m
L	Diaphragm span west → interior wall	21.00 m
L	Tributary diaphragm span of Interior wall	16.60 m

Table 5.2: Allowable shear capacities and some wall lengths.

Floor #	DCR(West Facade)	DCR(Interior Wall)
4	1.02	2.44
3	0.47	1.74
2	0.53	1.63
1	0.67	1.70

Table 5.3: DCR ratios for the west facade and interior wall.

Wall types	Seismic Zone No. 2B Buildings	Seismic Zone No. 3 Buildings	Seismic Zone No. 4 Buildings with crosswalls	Seismic Zone No. 4 All other Buildings
Walls of one-story buildings	20	16	16[2,3]	13
First story wall of multistory buildings	20	18	16	15
Walls in top story of multistory buildings	14	14	14[2,3]	9
All other walls	20	16	16	13

[1]Applies to the special procedure of Section A109 (d) only. See Section A109 (d) for other restrictions.

[2]This value of height-to-thickness ratio may be used only where mortar shear tests in accordance with Section A106 establish a tested mortar shear strength, υ_t, of not less than 100 psi or where the tested mortar shear strength, υ_t, is not less than 60 psi and a visual examinationof the collar joint indicates not less than 50 % mortar coverage.

[3]Where a visual examination of the collar joint indicates not less than 50 % mortar coverage and the tested mortar shear strength, υ_t, when established in accordance with Section A106 is greater than 30 psi but less than 60 psi, tha allowable height-to-thickness ratio may be determined by linear interpolation between the larger and smaller ratios in direct proportion to the tested mortar shear strength, υ_t.

Table 5.4: Allowable slenderness ratios.

Floor #	V_R (Pier #*) (N)				West Facade (KN)			
	1→9&12→19	10	11	20	ΣF_{wx}	ΣV_R	ΣV_a	α
4	9675	15798	15276	8860	89	204	2182	2.29
3	49403	71879	69220	37239	217	1018	2182	4.69
2	56028	98025	94381	50600	351	1195	2182	3.40
1	76974	135333	130264	69445	501	1644	2182	3.28
Va (N)	105909	142142	139355	100335	**Facade's Capacity** = 1148 KN			

* For piers' numbering, refer to Figure 4.2.

Table 5.5: Calculated wall shear capacities of the west facade.

Floor #	V_R (Pier #*) (N)			Interior Wall (KN)			
	1	2	3 & 4	ΣF_{wx}	ΣV_R	ΣV_a	α
4	744255	742359	513217	132	2513	2865	19.04
3	1816530	1811903	1252625	340	Relative rigidity analysis		8.43
2	3217457	3209259	2218661	553			5.18
V_a (N)	758089	769237	668902				
V_R (Piers of Floor # 1) (N)							
5	6	7	8 & 9	ΣF_{wx}	ΣV_R	ΣV_a	α
15,846,143	707449	370969	494678	806	Relative Rigidity Analysis		3.26
1,530,113	323303	234116	270348	**Wall's Capacity** = 2628 KN			

* For piers' numbering, refer to Figure 5.1.

Table 5.6: Calculated wall shear capacities of the interior wall.

	Amplification Factors		
	ξ = 10 %	ξ = 5 %	ξ = 2 %
For PGA	1.5	2.6	4.3
For PGV	1.3	1.9	2.8
For PGD	1.1	1.4	1.8

Table 6.1: Newmark-Hall amplification factors for design response spectra.

T (s)	Psa (g) (ξ=10%)	Psa (g) (ξ=5%)	Psa (g) (ξ=2%)
0.033	0.48	0.48	0.48
0.038	0.50	0.54	0.55
0.040	0.51	0.55	0.57
0.044	0.55	0.57	0.62
0.050	0.56	0.61	0.70
0.055	0.56	0.65	0.75
0.06	0.57	0.70	0.80
0.08	0.60	0.80	1.02
0.10	0.64	0.95	1.25
0.12	0.65	0.99	1.40
0.15	0.69	1.15	1.75
0.17	→ 0.65 s 0.72	→ 0.55 s 1.25	→ 0.50 s 2.07
0.7	0.70	1.00	1.41
0.8	0.61	0.85	1.25
1.0	0.49	0.71	1.05
1.2	0.40	0.58	0.85
1.5	0.33	0.48	0.68
2.0	0.24	0.34	0.52
2.4	0.22	0.30	0.44

Table 6.2: PSa values for each damping ratio at each structure's fundamental period.

"Piers only"		"Frame without offsets"		"Frame with offsets"	
T (s)	(V/W)x3 (g)	T (s)	(V/W)x3 (g)	T (s)	(V/W)x3 (g)
2.209	0.061	0.500	0.140	0.35	0.243
2.337	0.055	0.526	0.136	0.37	0.201
2.481	0.061	0.782	0.105	0.59	0.112
2.554	0.063	0.810	0.110	0.67	0.168
11.367	0.003	1.119	0.101	0.70	0.150
		1.14	0.105	0.72	0.133
		1.19	0.089	0.73	0.147
		1.24	0.074	0.75	0.144
		1.33	0.063	1.10	0.098
		1.34	0.065	1.63	0.079
		1.40	0.066	1.70	0.089
		1.52→1.59	0.048	2.04	0.063
		1.90	0.036	2.63	0.035
				3.12	0.072

Table 6.3: Ultimate Capacity ratios versus structure's fundamental period for each 2D model.

"Piers only"		"Frame with rigid offsets"	
T (s)	(V/W)x3 (g)	T (s)	(V/W)x3 (g)
0.91	0.098	0.340	0.074
0.92	0.074	0.341	0.089
0.96	0.055	0.342	0.069
1.64	0.039	0.344	0.107
1.70	0.036	0.346	0.109
1.85	0.035	0.346	0.140
1.92	0.036	0.347	0.104
1.94	0.037	0.349	0.105
2.00	0.041	0.350	0.038
2.00	0.043	0.351	0.096
2.07	0.041	0.420	0.157
2.15	0.039		
2.21	0.043		
2.25	0.040		

Table 6.4: Ultimate Capacity ratios versus structure's fundamental period for each 3D-model.

West Facade		Interior Wall	
T (s)	(V/W)x3 (g)	T (s)	(V/W)x3 (g)
0.347	0.707	0.416	0.689

Table 6.5: Ultimate Capacity ratios versus structure's fundamental period for ABK models.

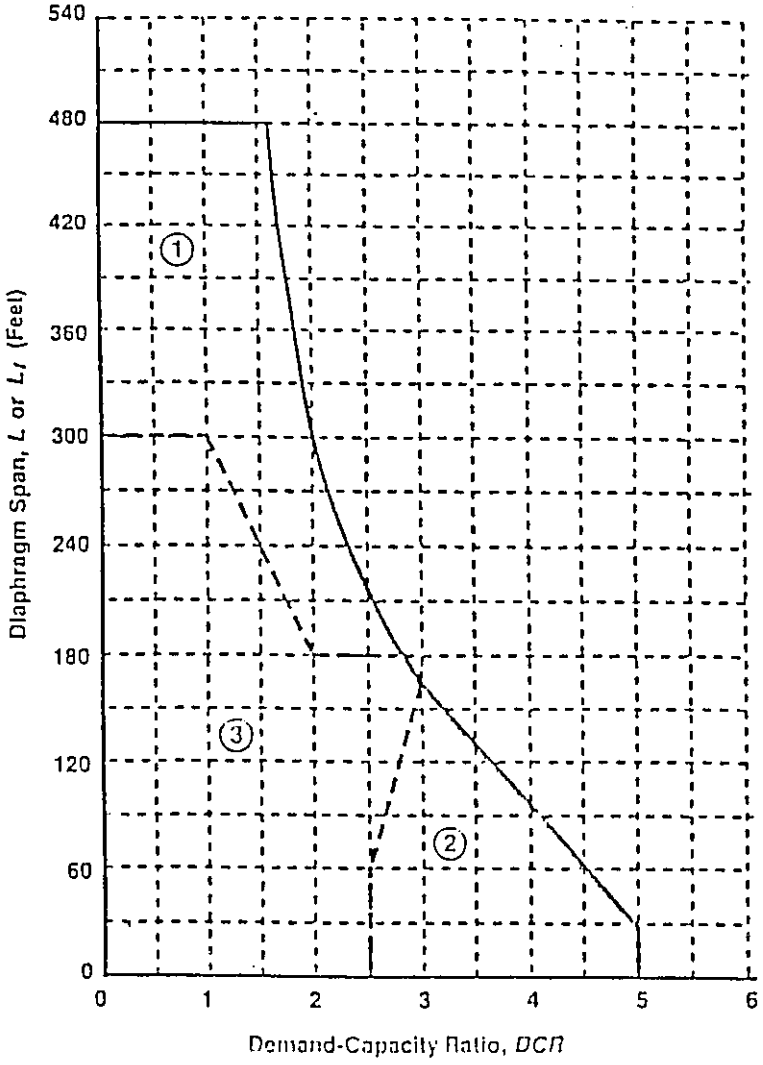

Figure 2.1: Acceptable diaphragm span by ABK procedure.

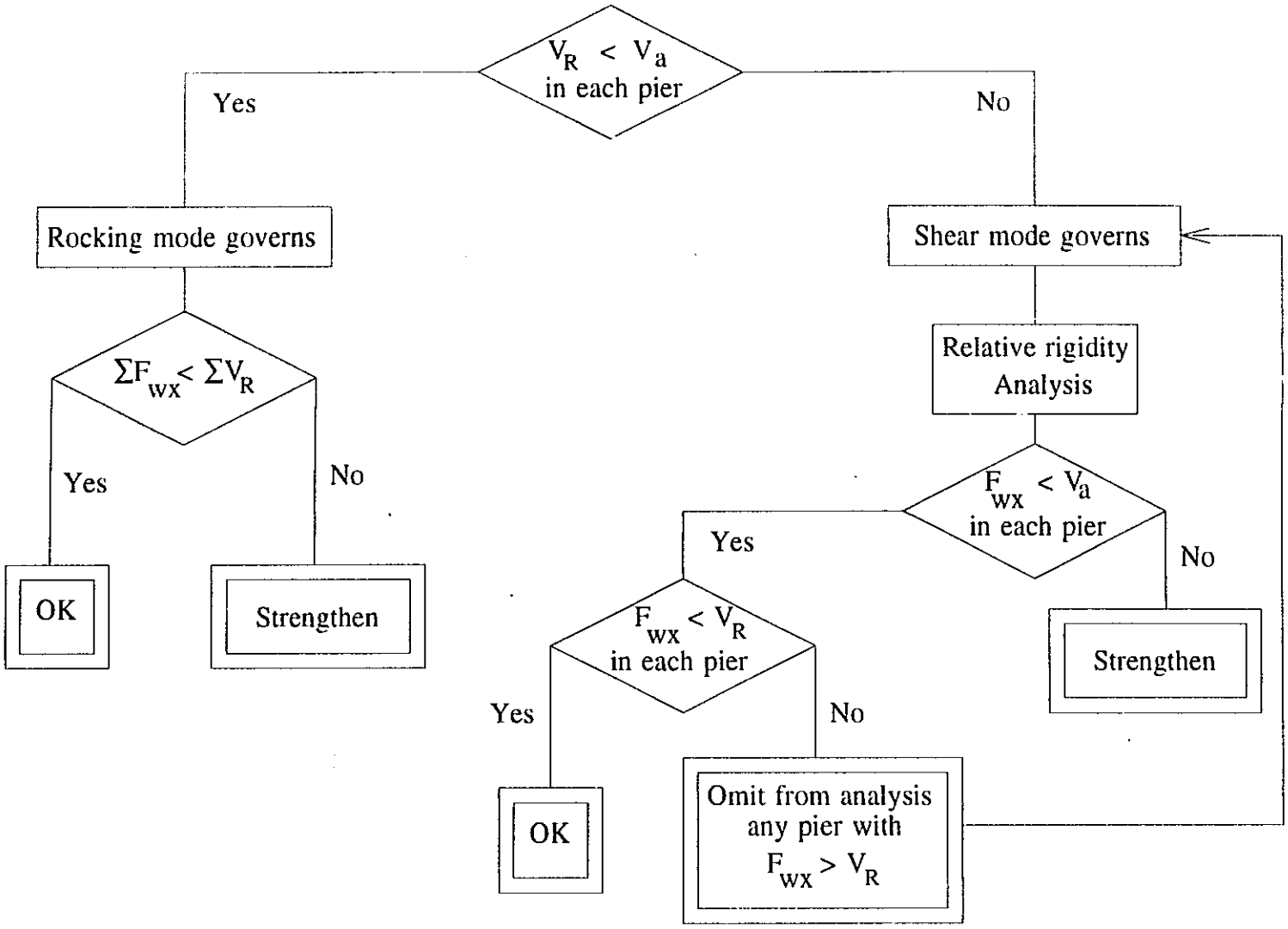

Figure 2.2: Flow chart for the analysis of URM walls for in-plane shear by ABK procedure.

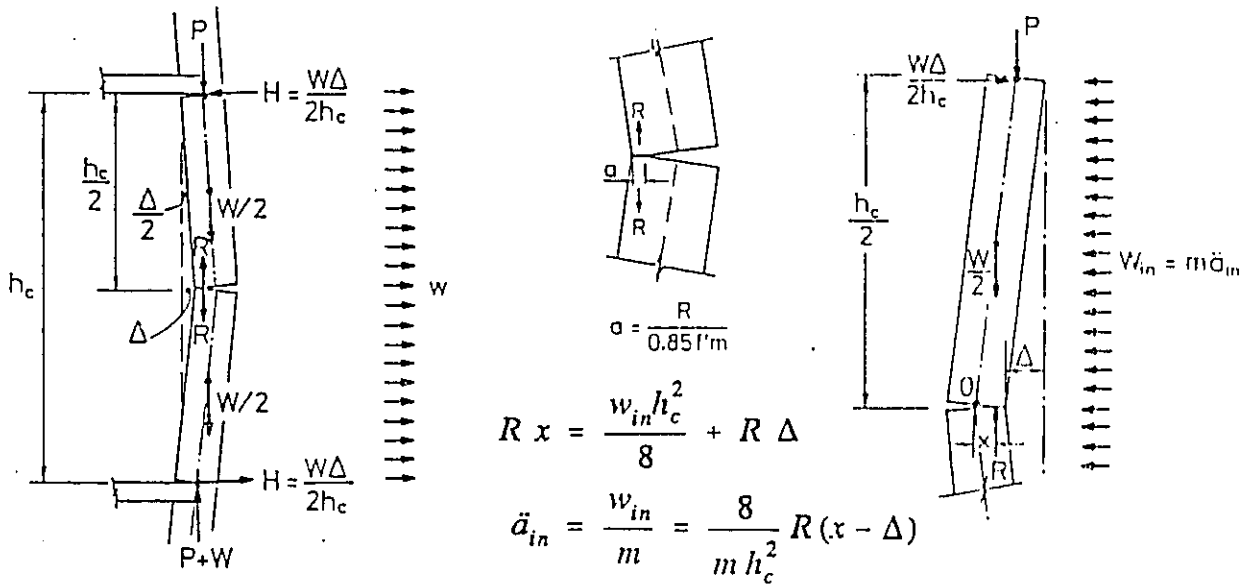

$$R\,x = \frac{w_{in} h_c^2}{8} + R\,\Delta$$

$$\ddot{a}_{in} = \frac{w_{in}}{m} = \frac{8}{m\,h_c^2} R\,(x - \Delta)$$

Figure 2.3: Out-of-plane dynamic stability concept (Adapted from Priestley).

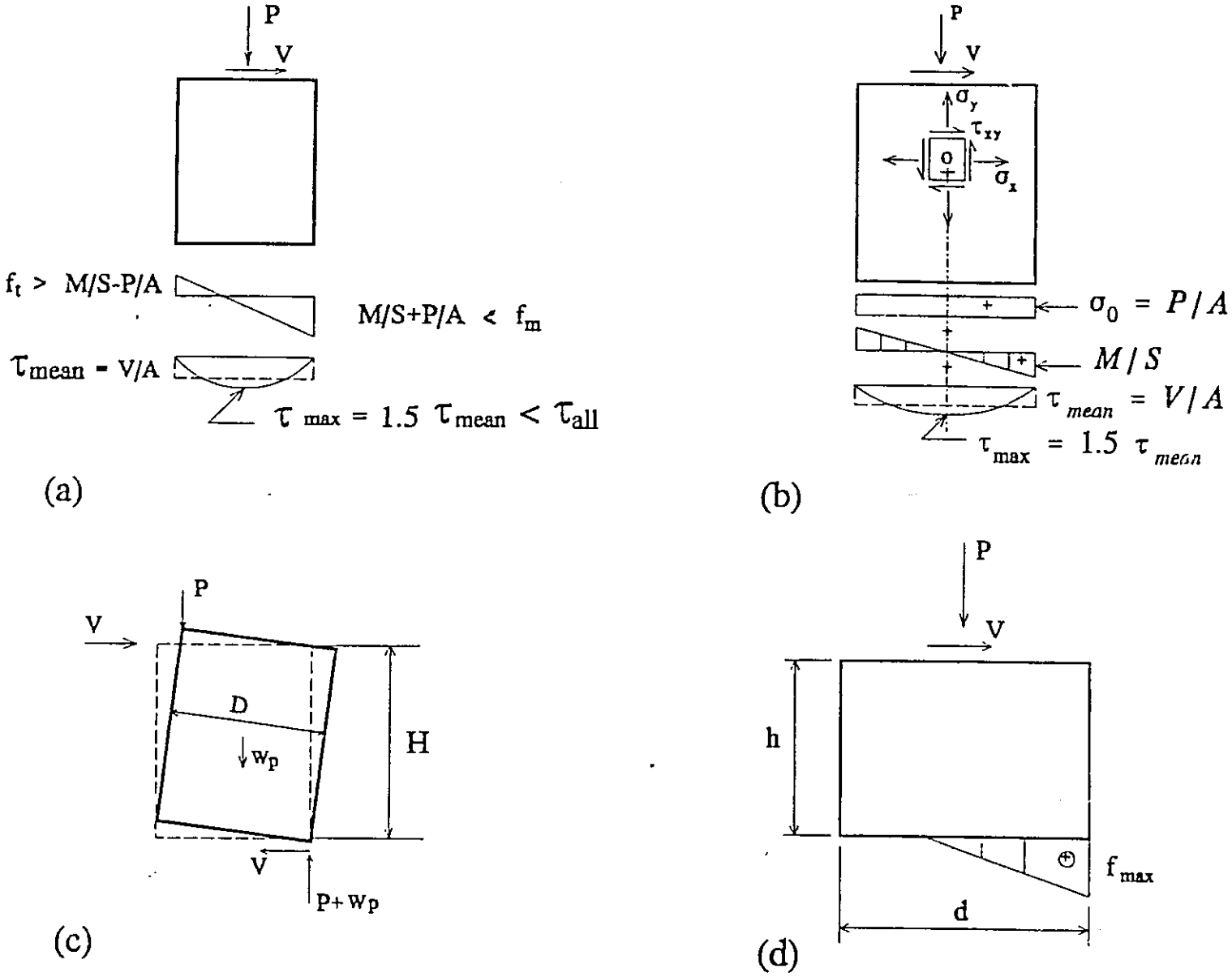

Figure 2.4: Hand-calculation oriented models of the in-plane response of URM walls.

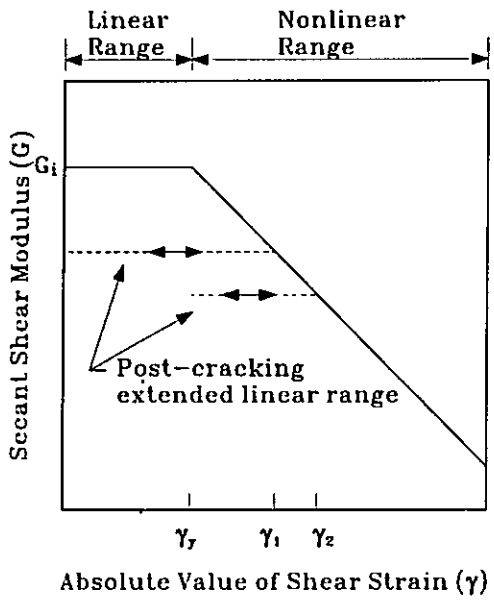

Figure 2.5a: Secant shear modulus model (Adapted from Mengi and McNiven)

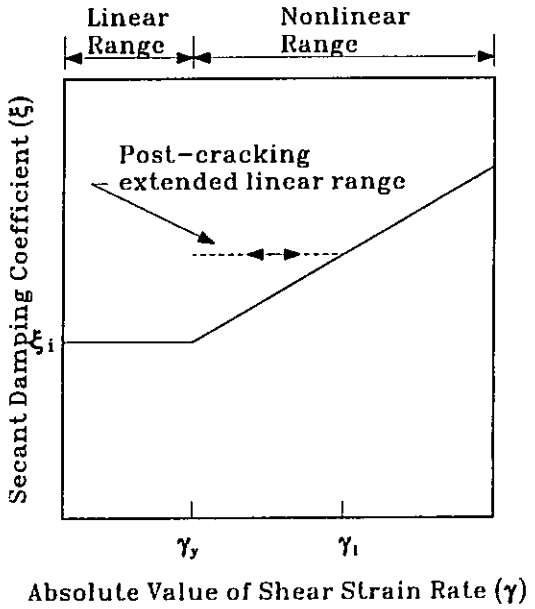

Figure 2.5b: Secant damping model (Adapted from Mengi and McNiven)

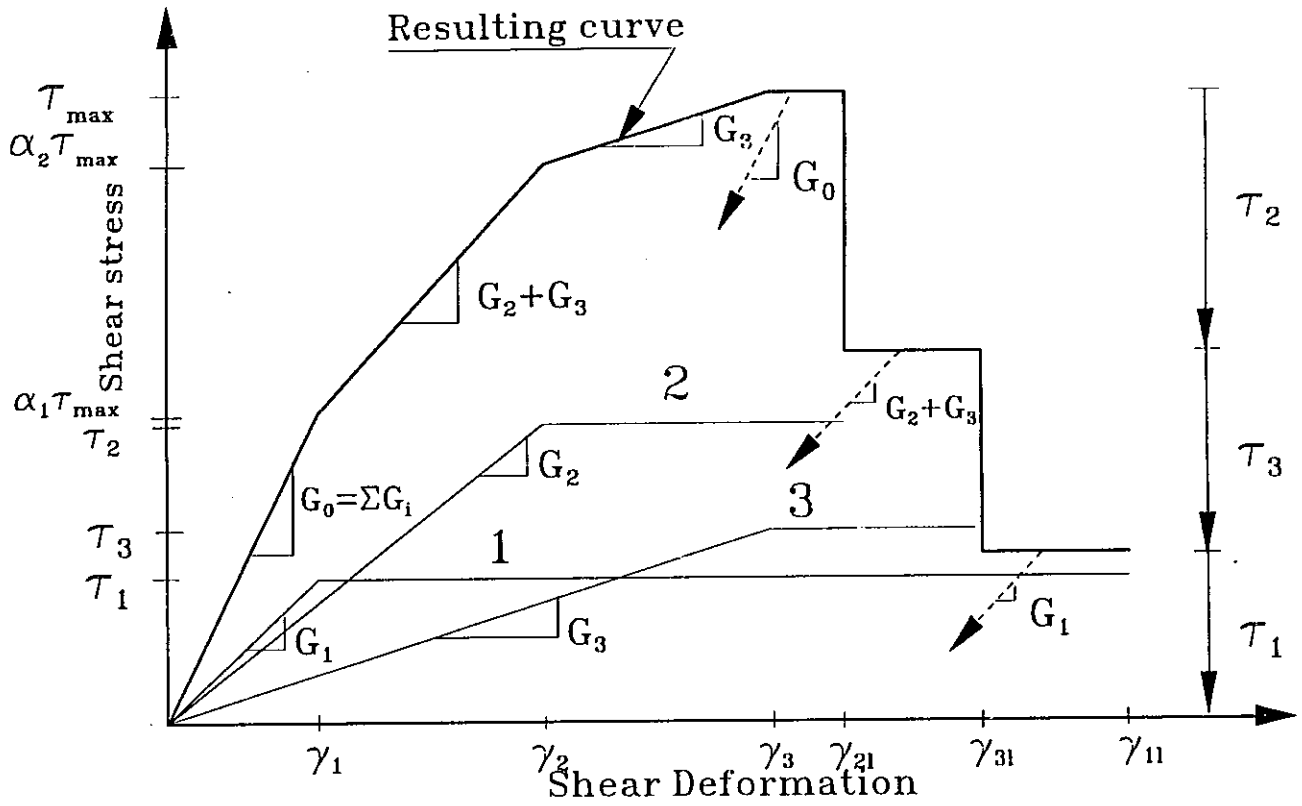

Figure 2.6: Hysteretic shear-strain model proposed for URM (Adapted from Benedetti and Benzoni 1984)

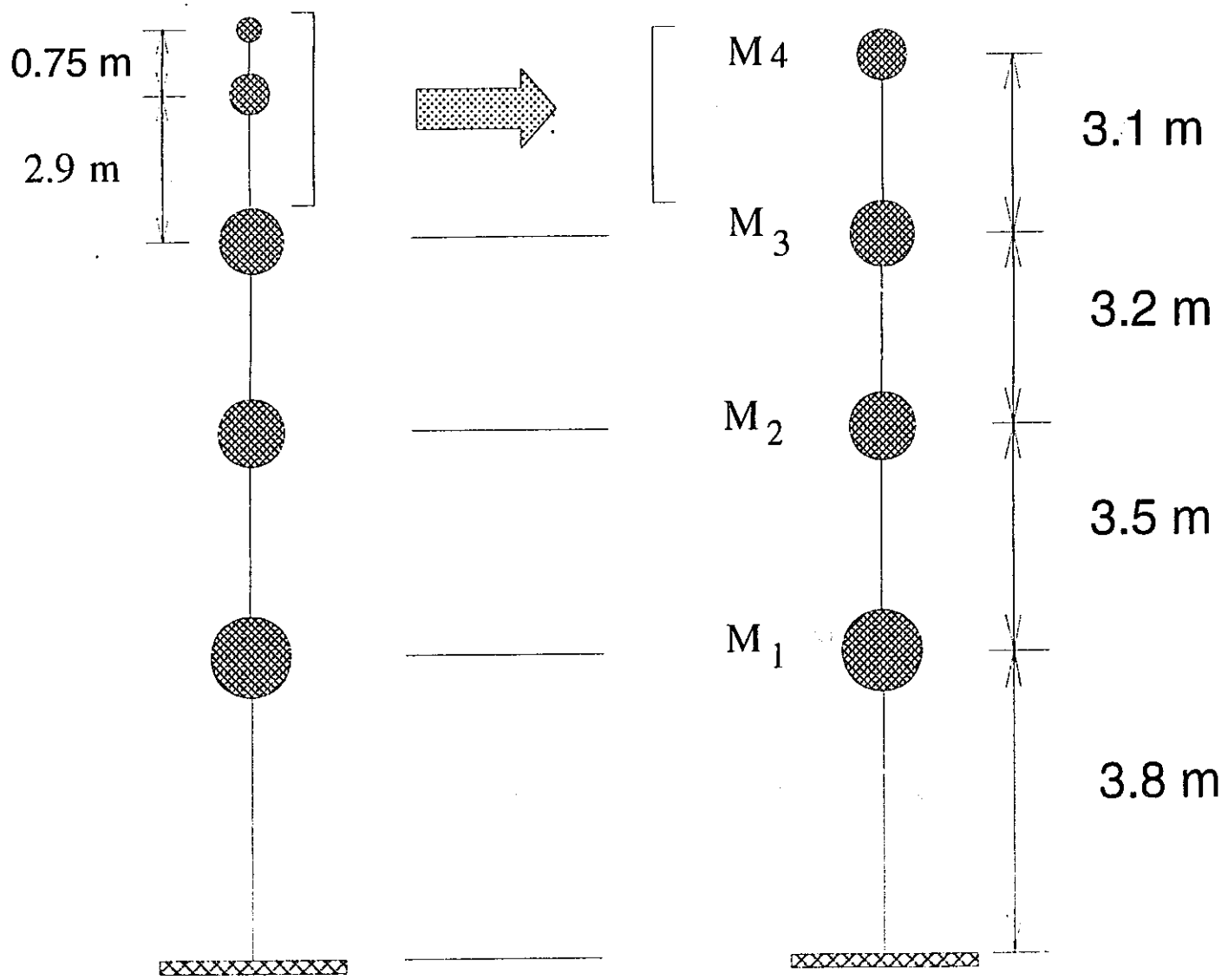

Figure 3.1: Transformation of the building from five to four dof system.

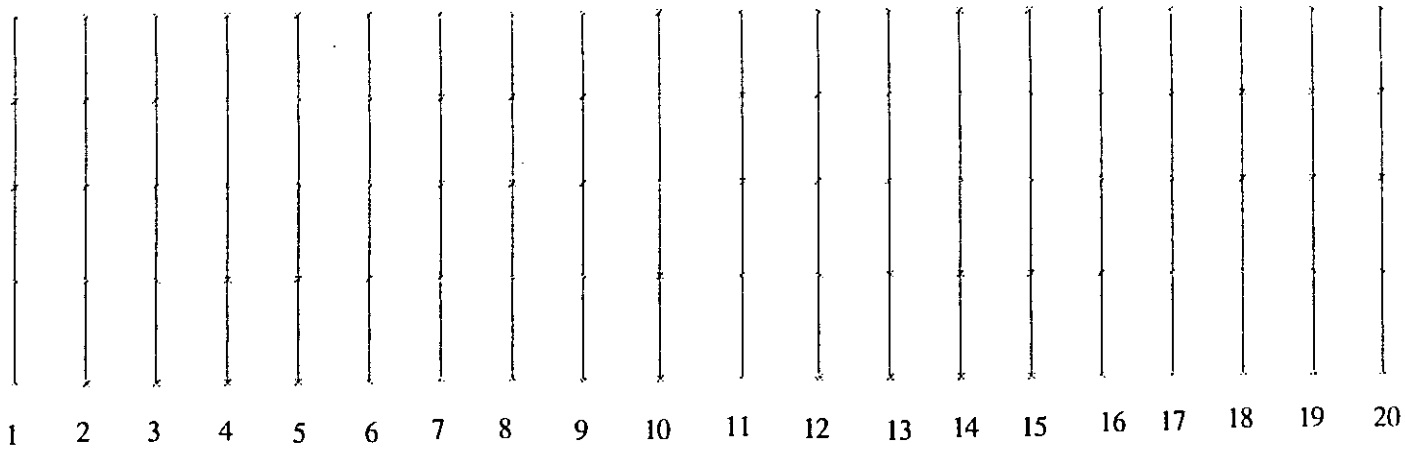

Figure 3.2: Elements' identifications of the solid pier/cracked-spandrel model.

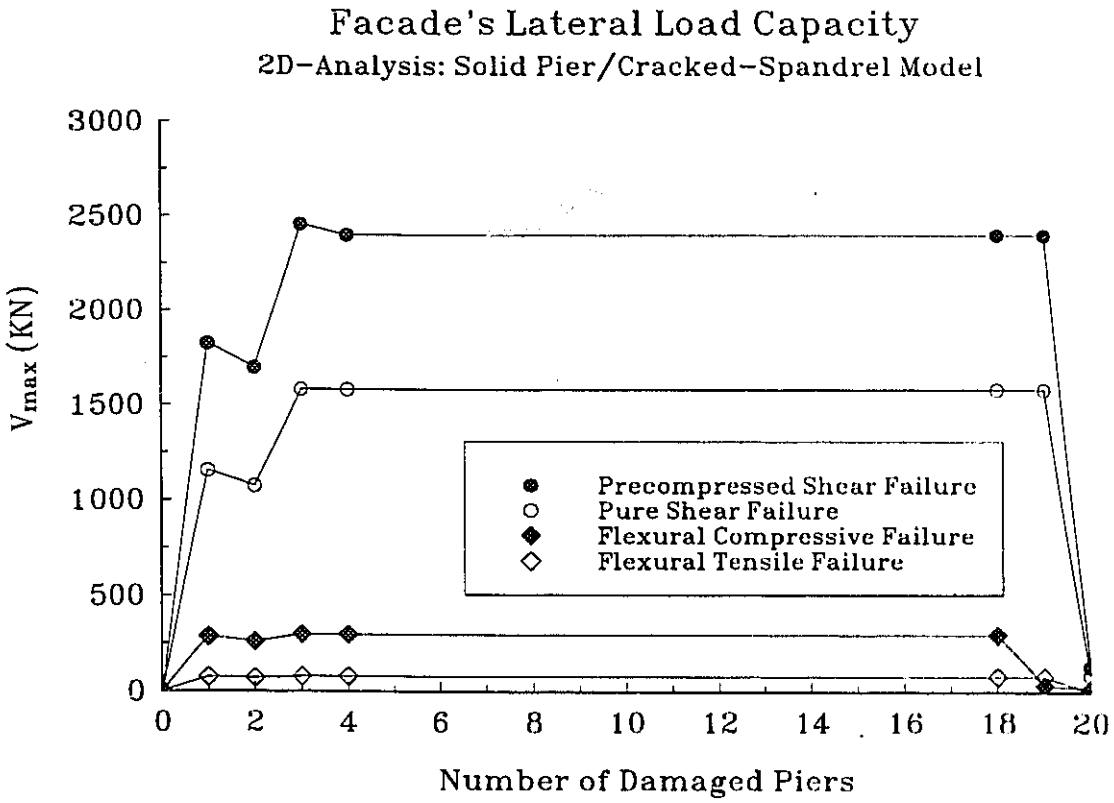

Figure 3.3: Facade's lateral load capacity (solid pier/cracked-spandrel model).

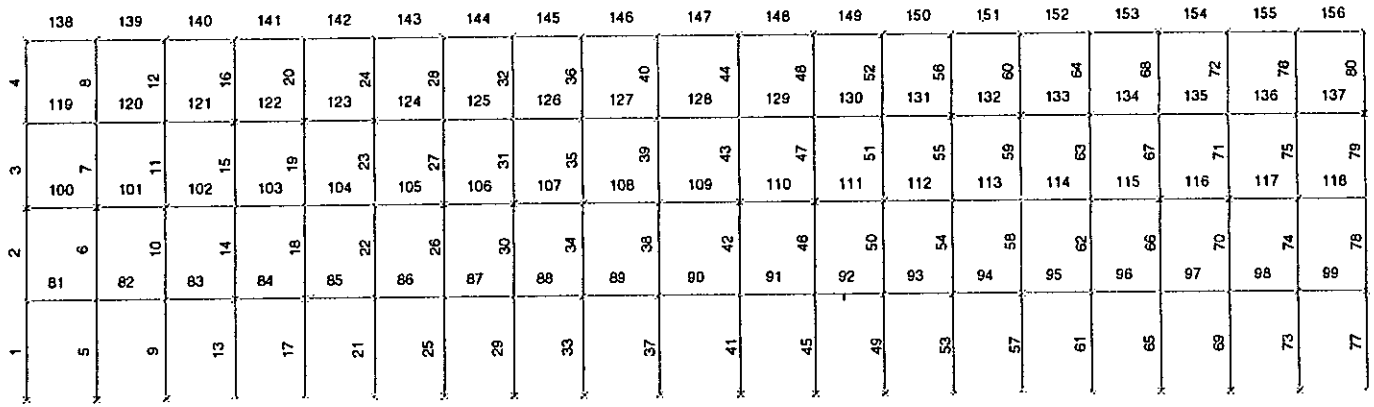

Figure 3.4: Elements' identifications for the frame model (with and without offsets).

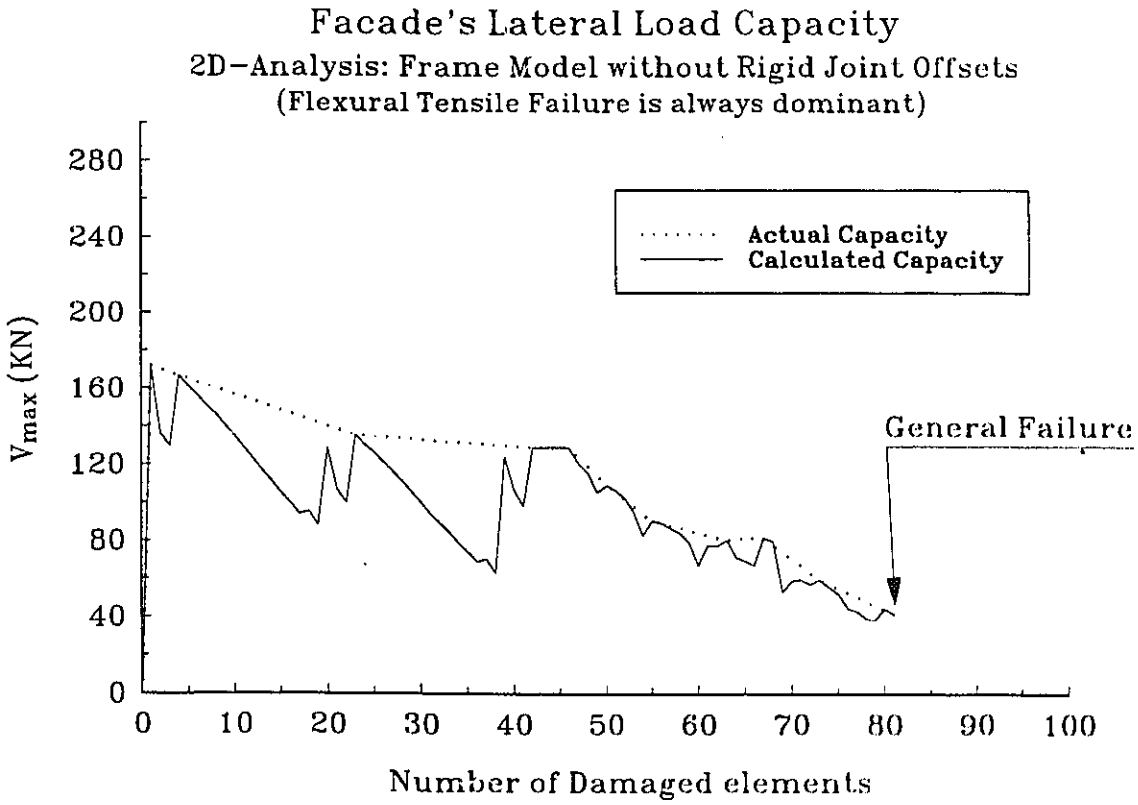

Figure 3.5: Facade's lateral load capacity (Frame model without offsets).

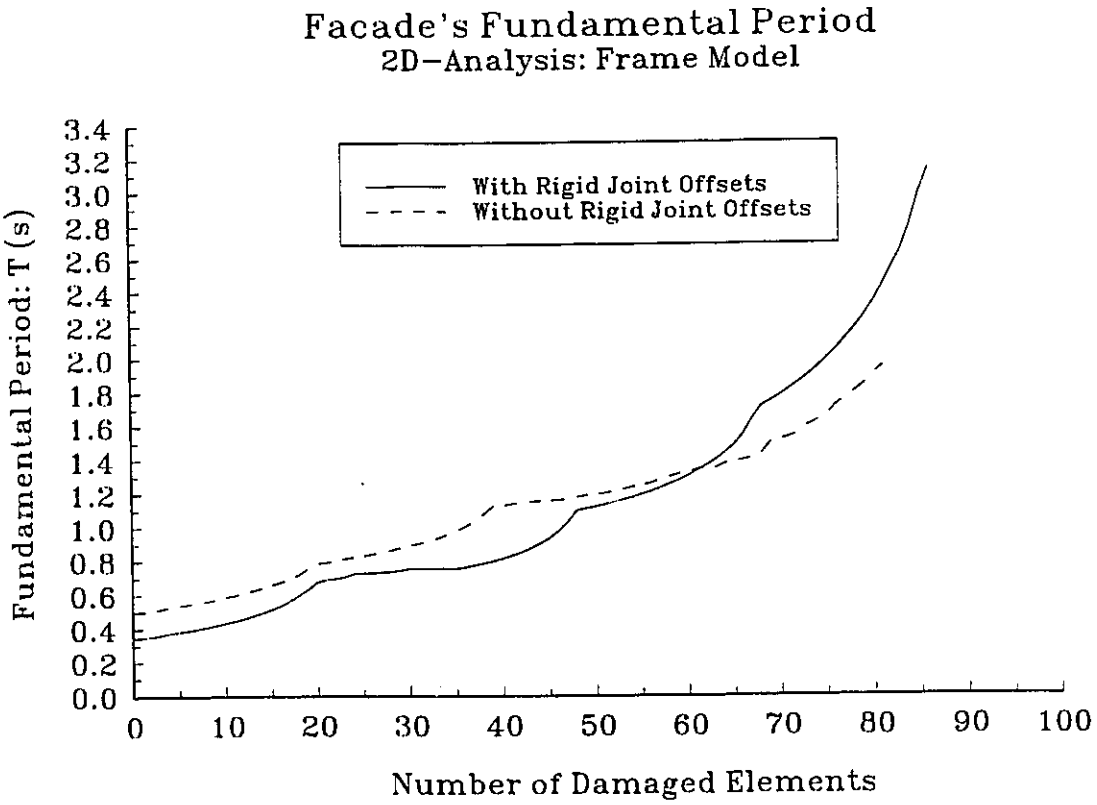

Figure 3.6: Facade's fundamental period (Frame models).

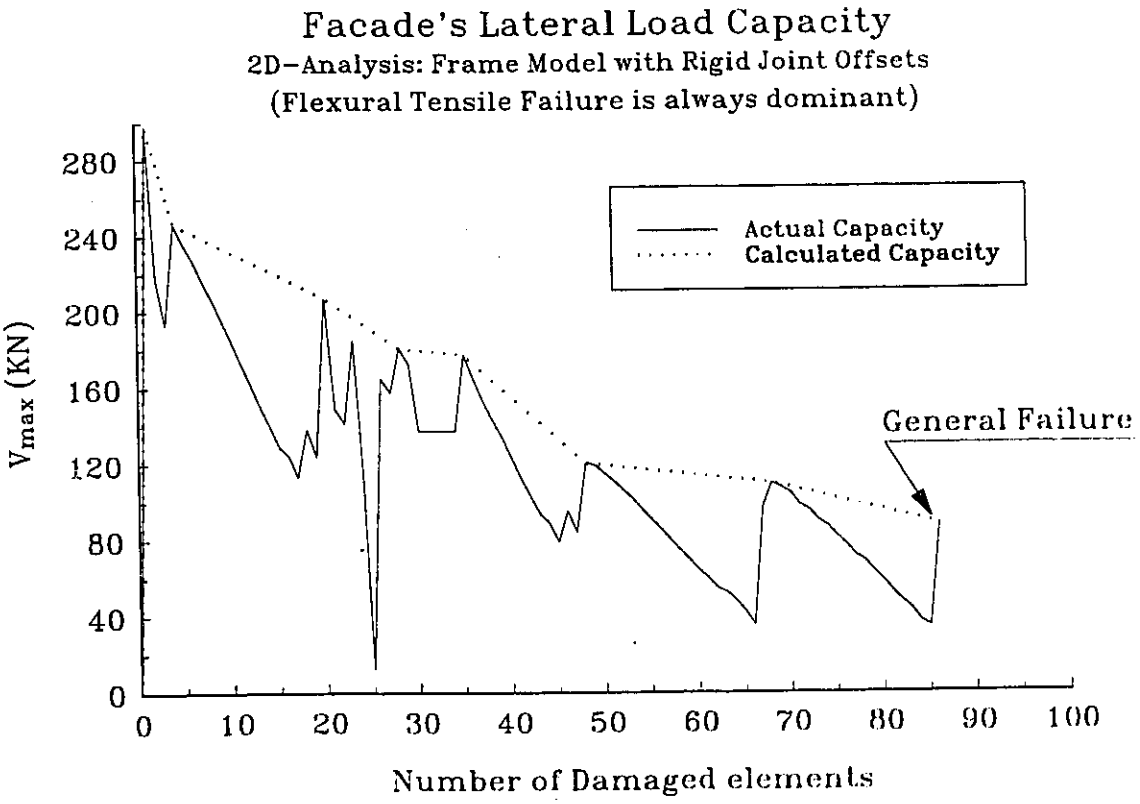

Figure 3.7: Facade's lateral load capacity (Frame model with offsets).

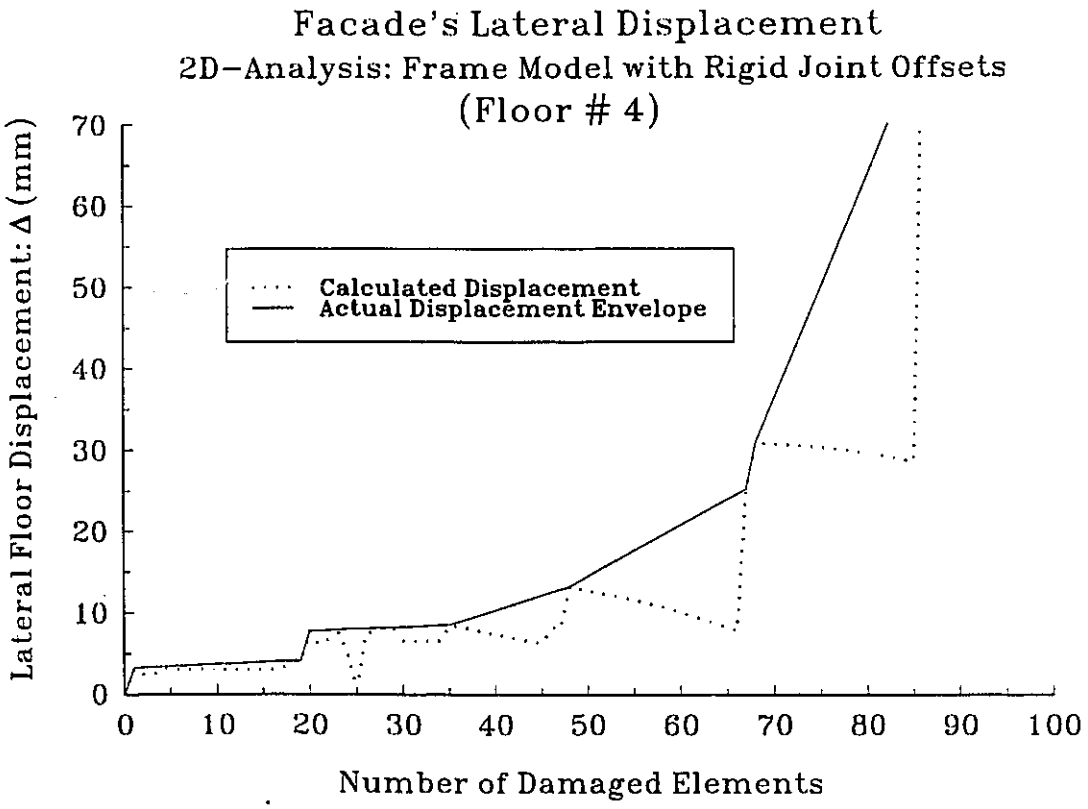

Figure 3.8: Facade's lateral displacement (Floor # 4 of frame model with offsets).

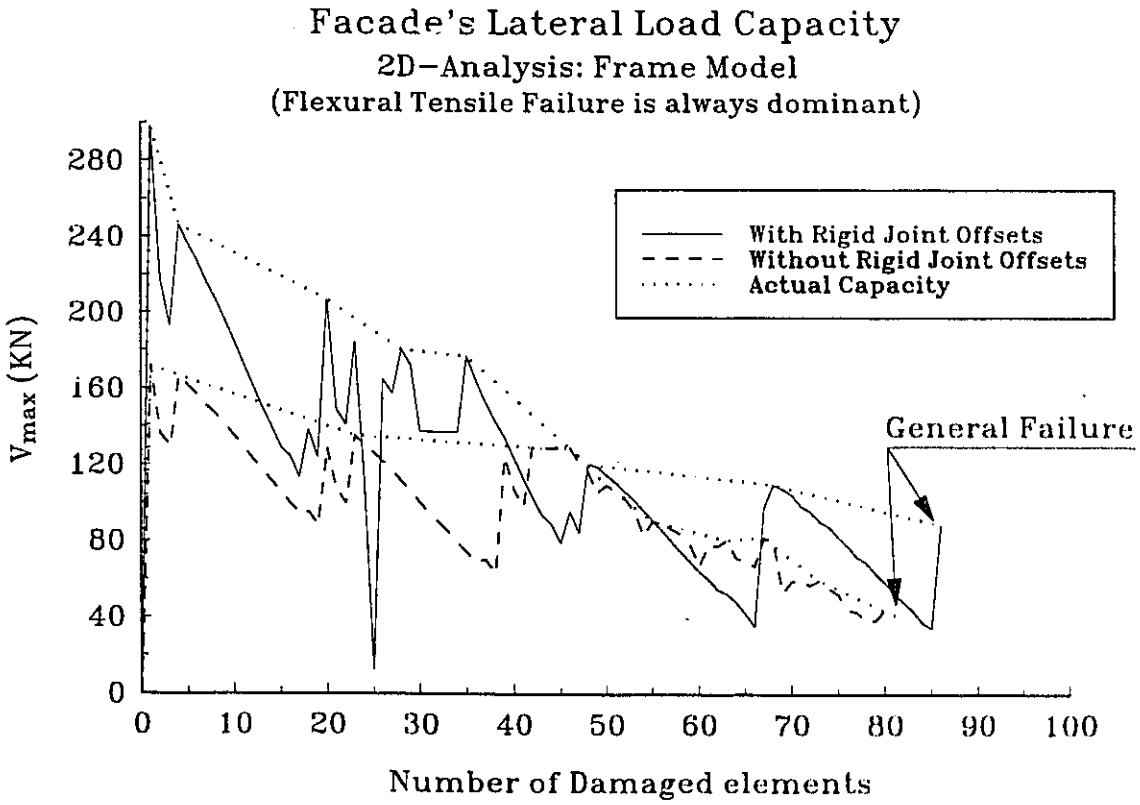

Figure 3.9: Facade's lateral load capacity (Frame models).

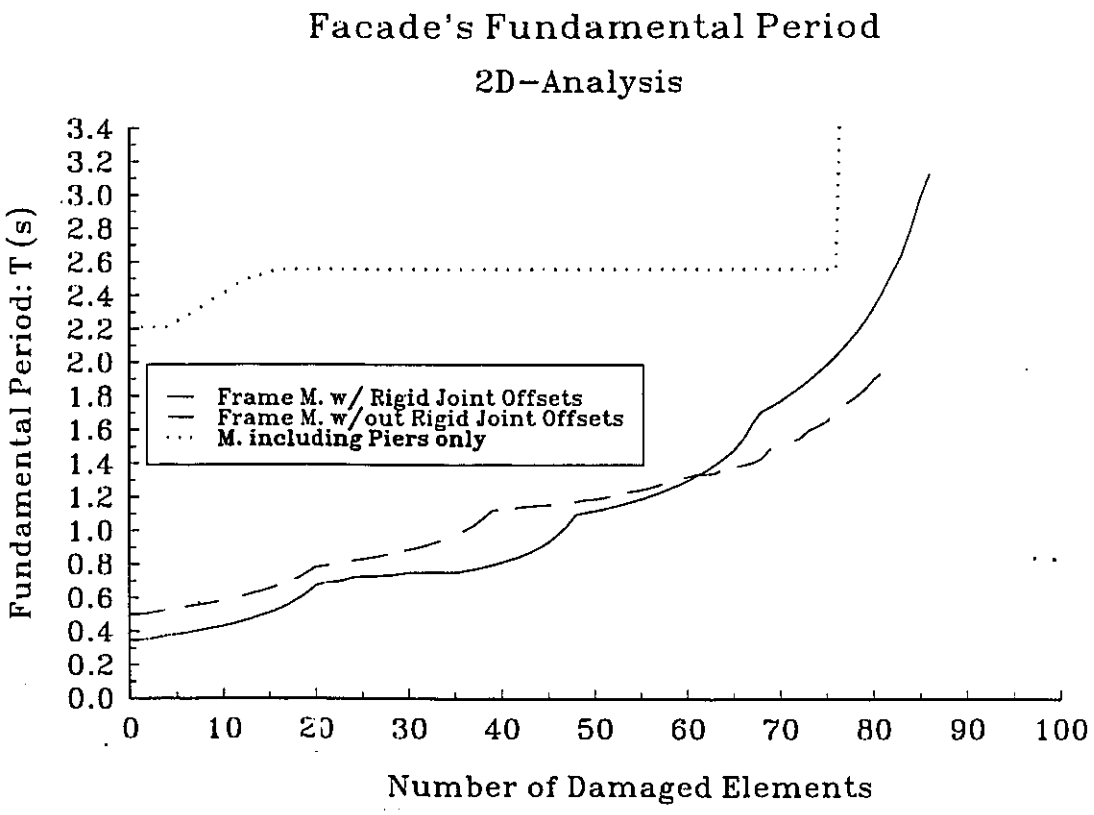

Figure 3.10: Facade's fundamental period (All models).

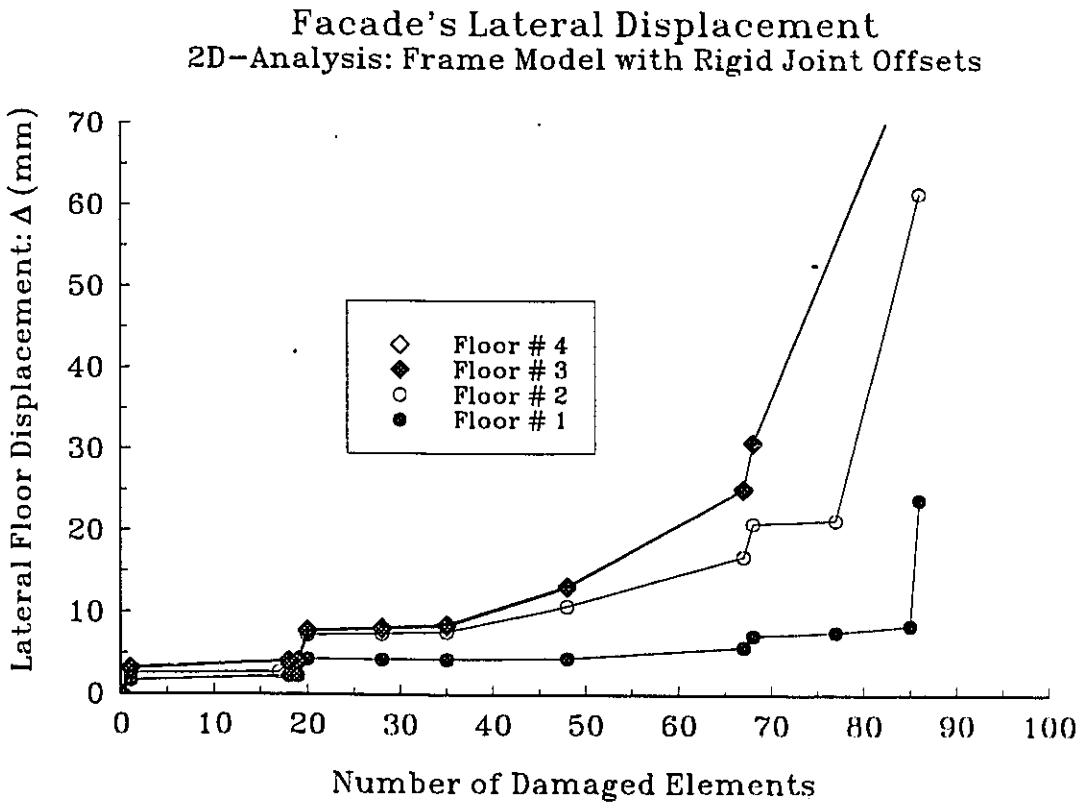

Figure 3.11: Facade's lateral displacement (All 4 floors of the frame model with offsets).

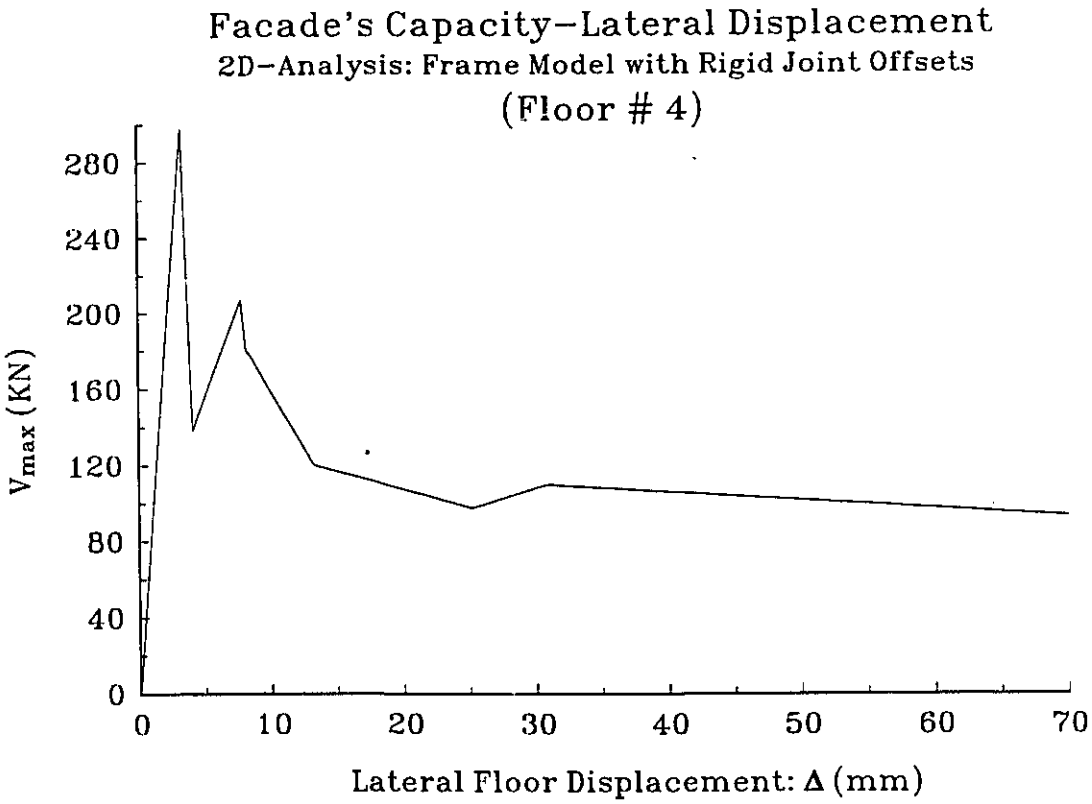

Figure 3.12: Shear-Displacement behaviour of the floor #4 (Frame model with rigid offsets).

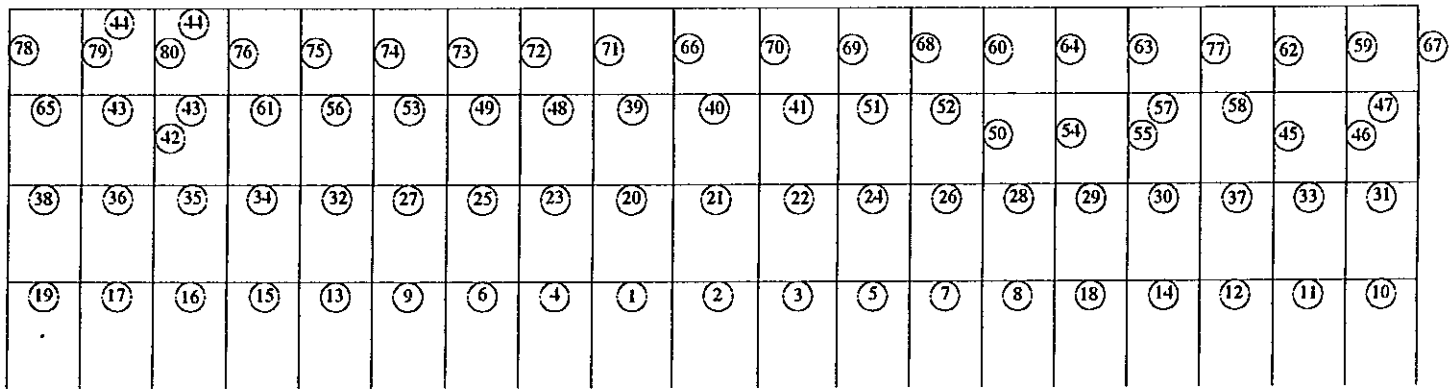

Figure 3.13: Damage evolution of the frame model without rigid offsets.

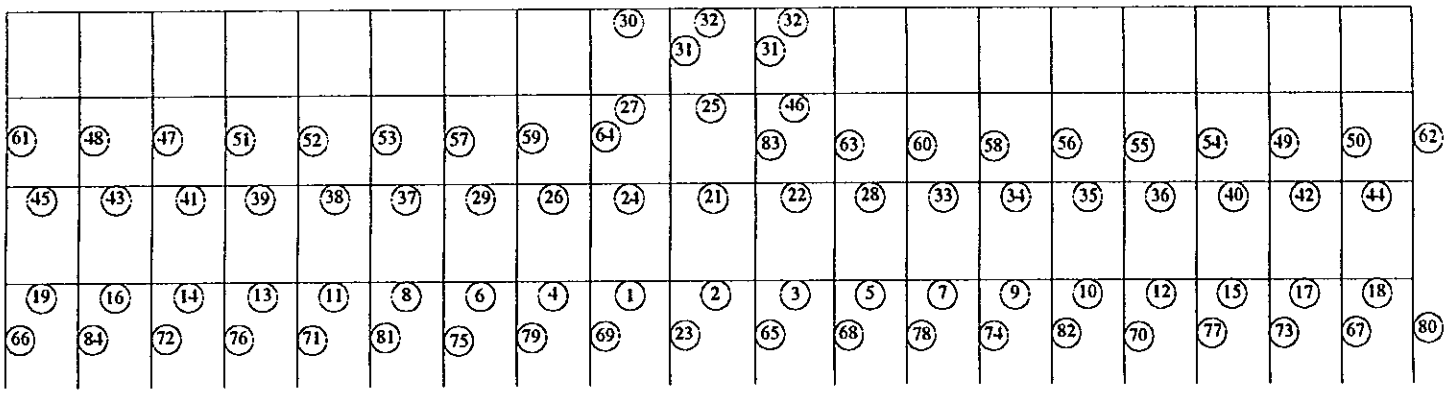

Figure 3.14: Damage evolution of the frame model with rigid offsets.

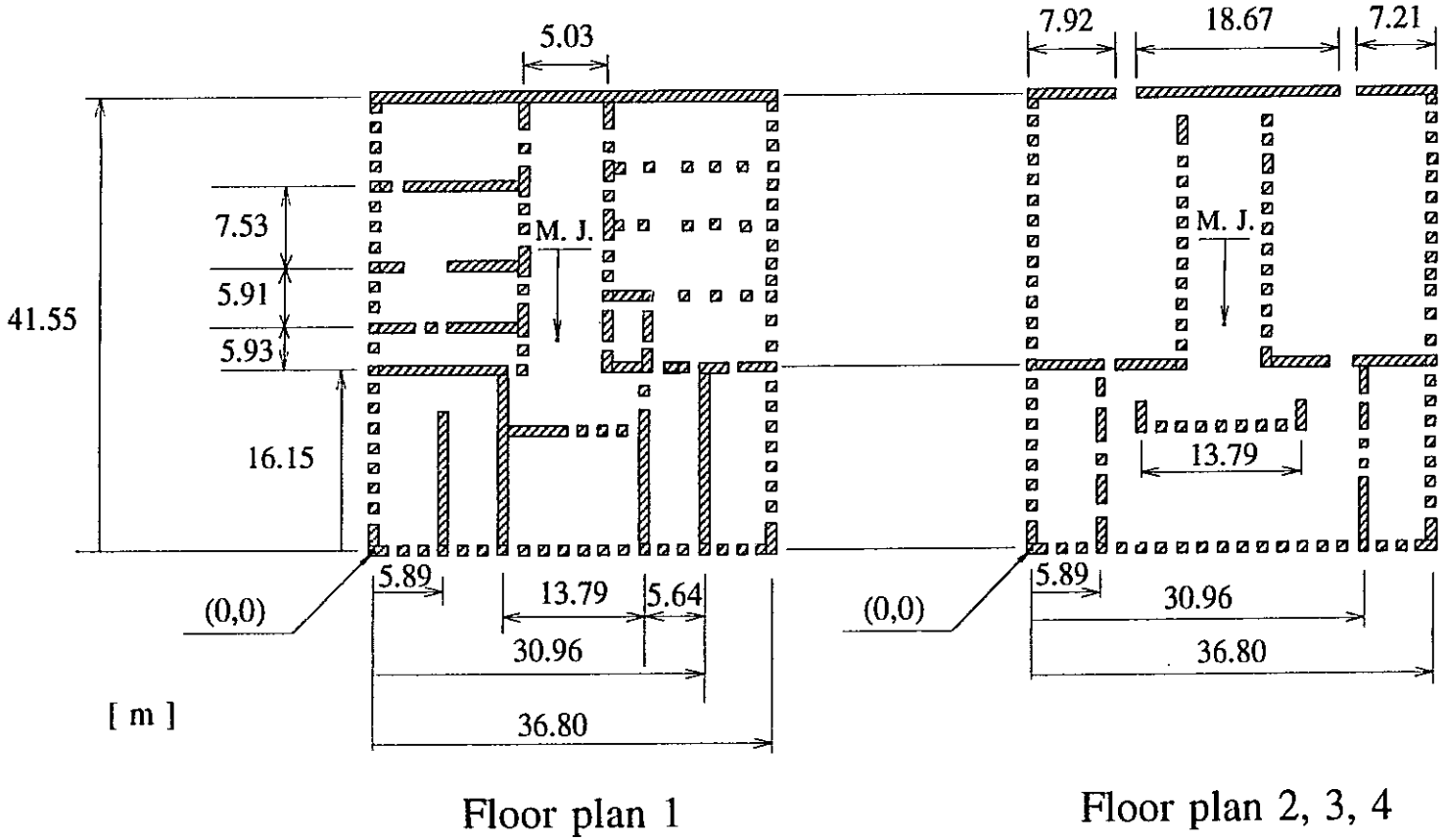

Figure 4.1: Floor plan dimensions for all stories.

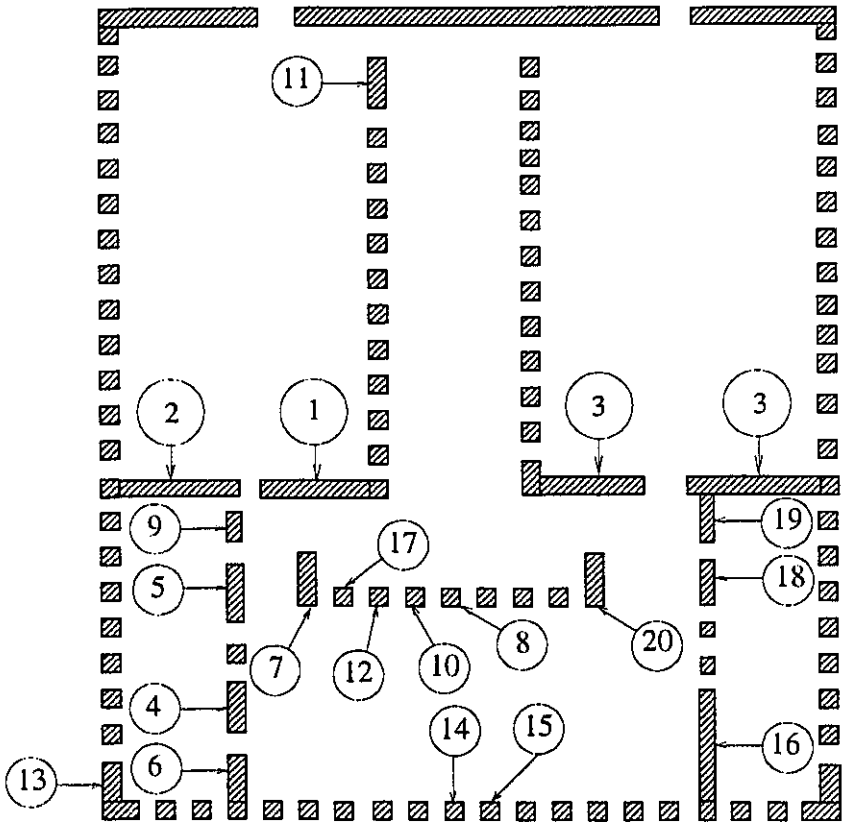

Figure 4.2: 3D-Analysis: Evolution of piers' damage in the piers-only model at the 2nd floor.

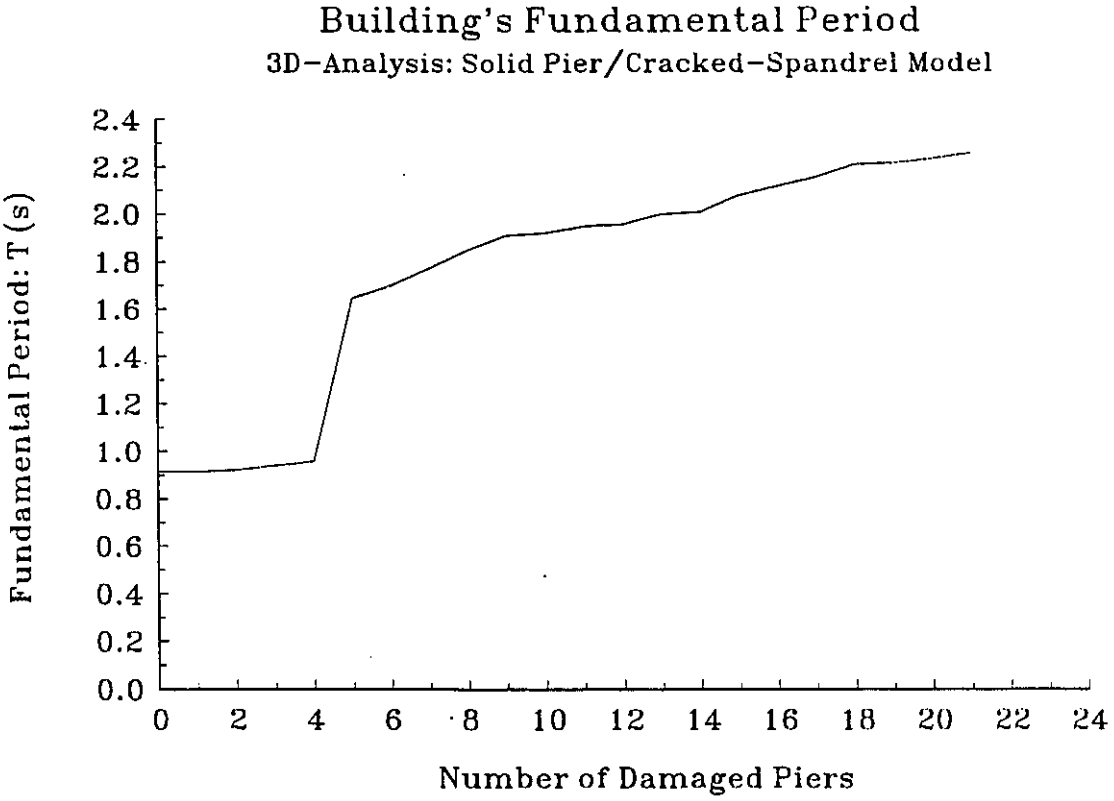

Figure 4.3: 3D-Analysis: Building's fundamental period for piers-only model.

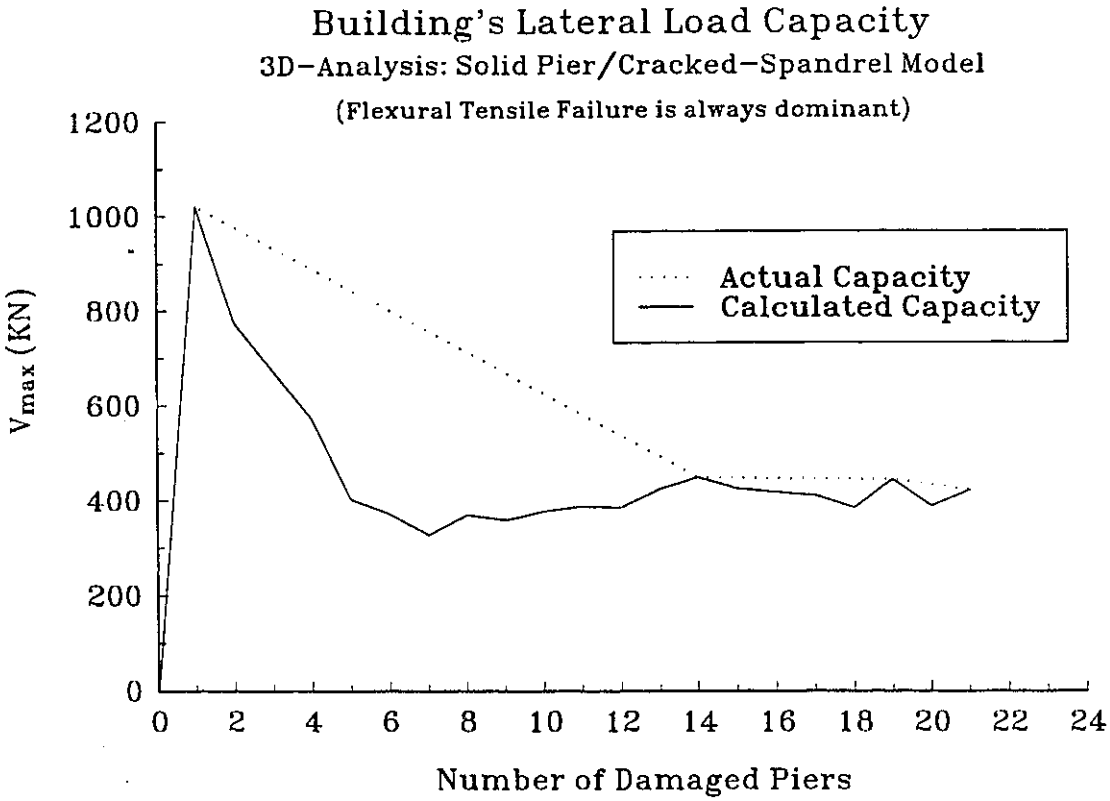

Figure 4.4: 3D-Analysis: Building's lateral load capacity for piers-only model.

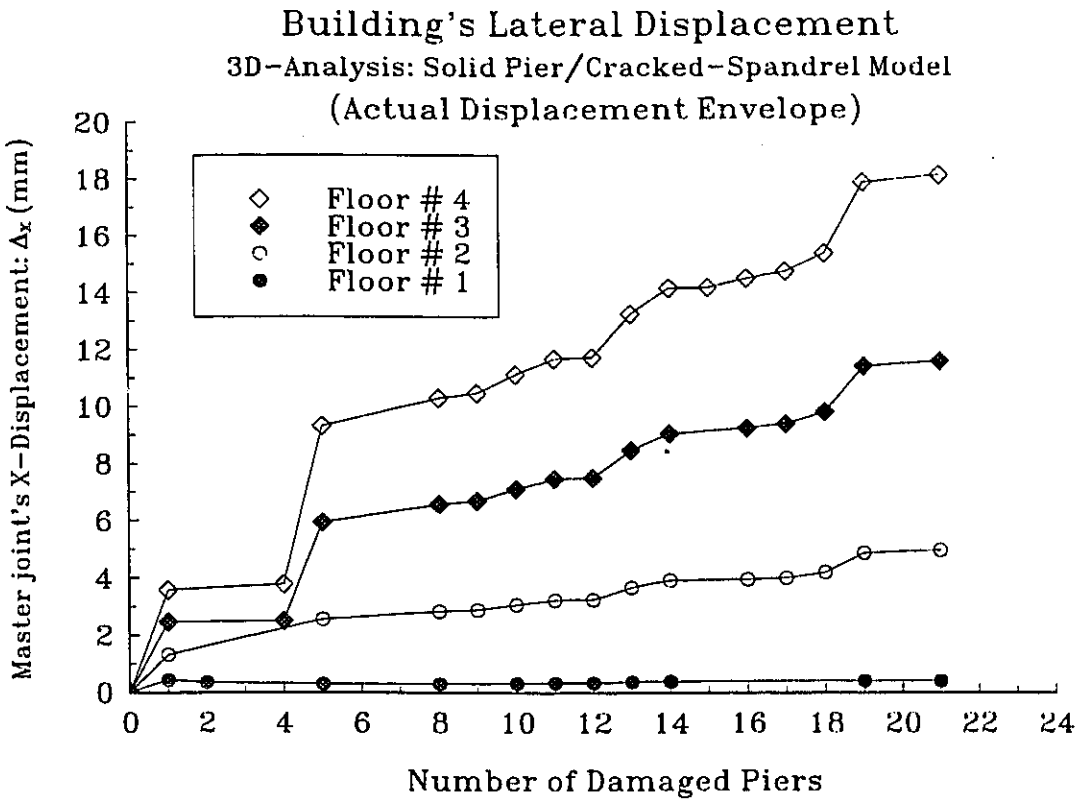

Figure 4.5: 3D-Analysis: Building's lateral displacement for piers-only model.

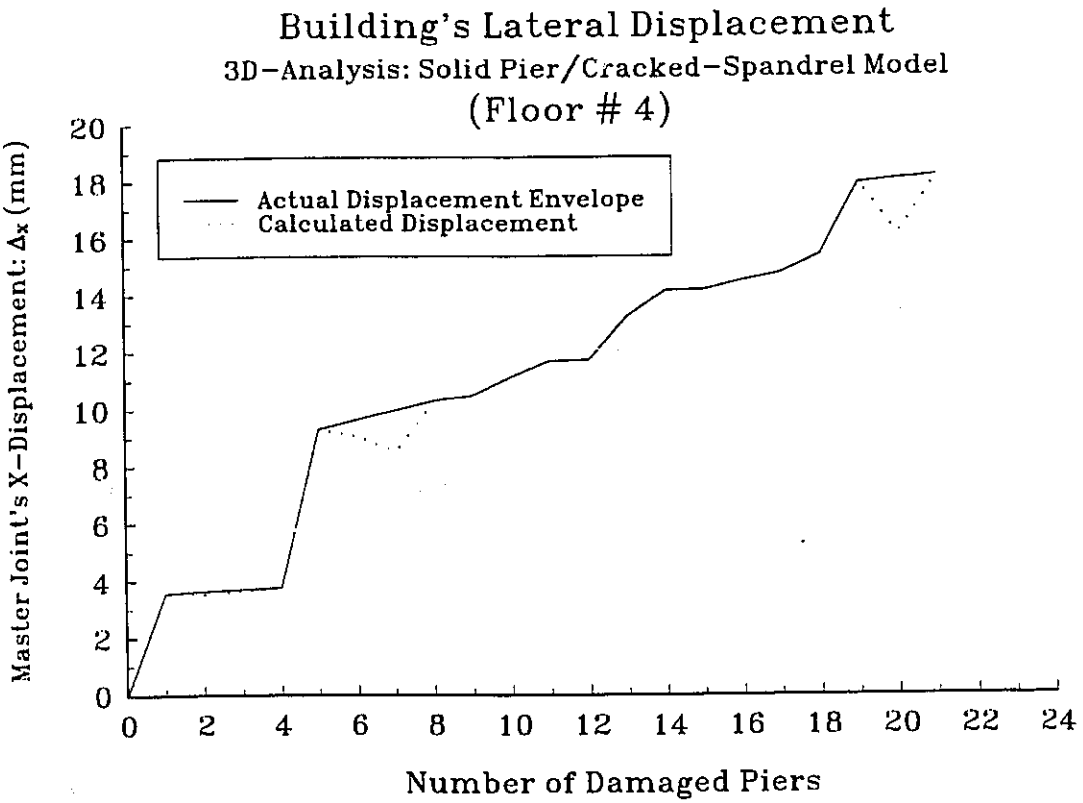

Figure 4.6: 3D-Analysis: Building's 4th floor lateral displacement for piers-only model.

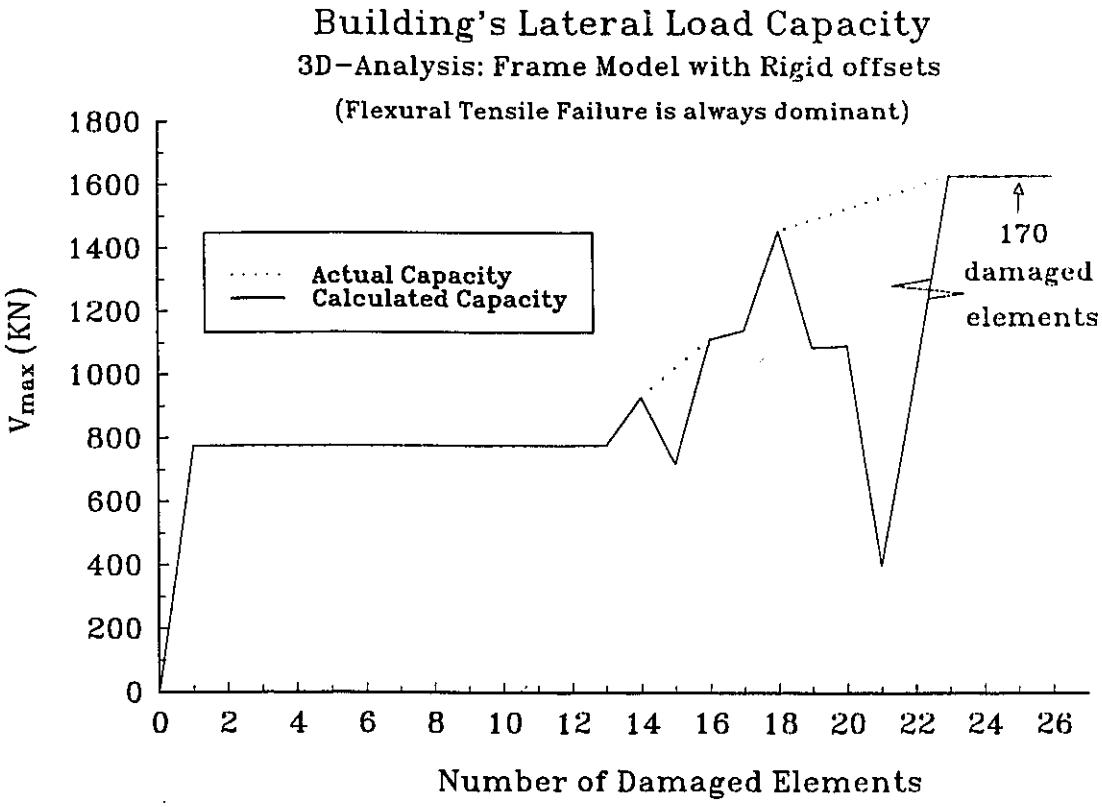

Figure 4.7: 3D-Analysis: Building's lateral load capacity for frame model with rigid offsets.

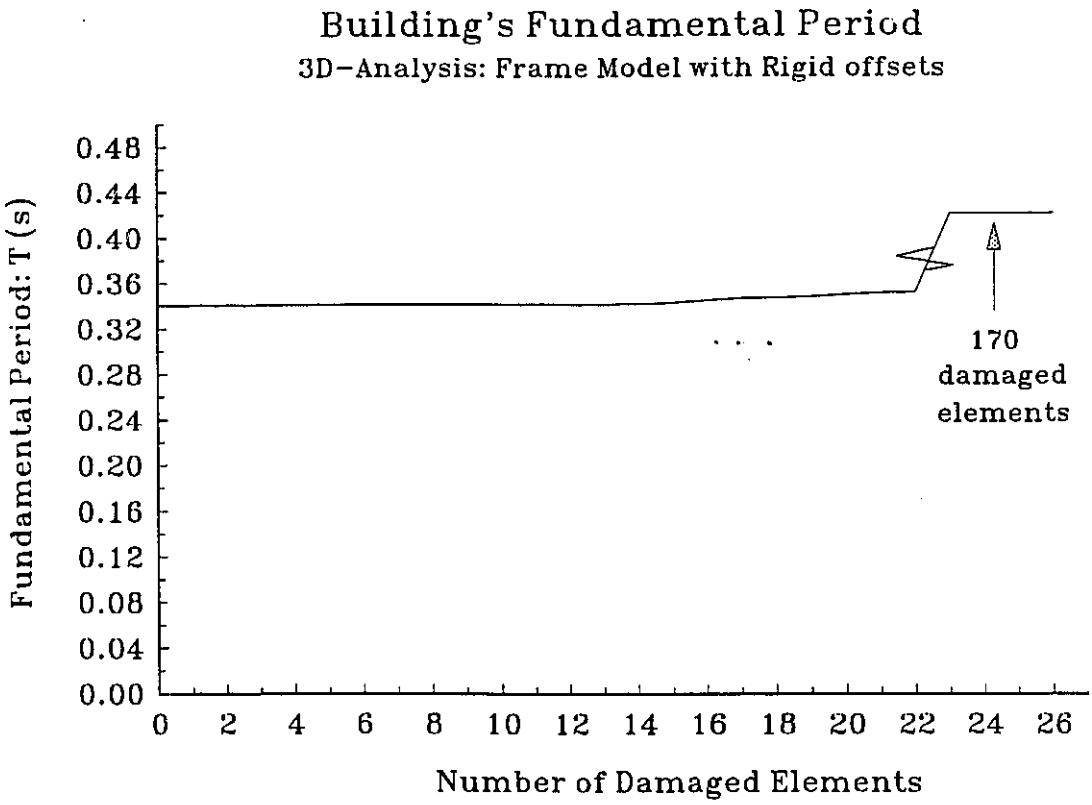

Figure 4.8: 3D-Analysis: Building's fundamental period for frame model with rigid offsets.

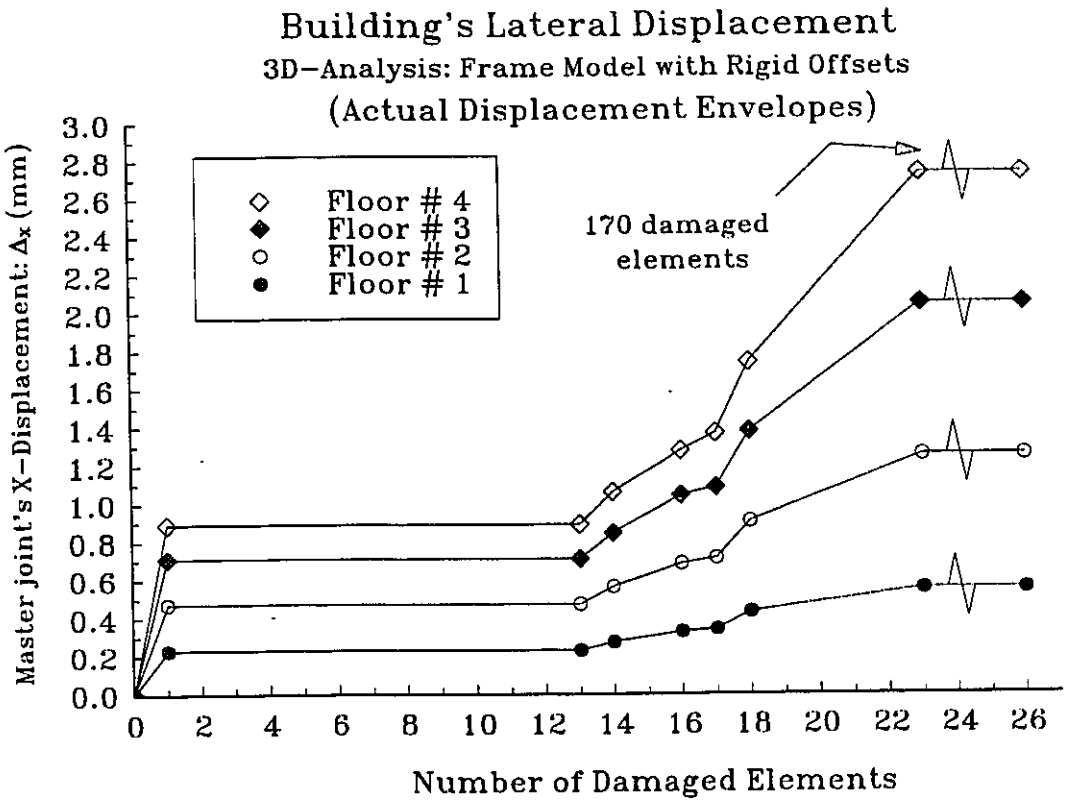

Figure 4.9: 3D-Analysis: Building's lateral displacements for frame model with rigid offsets.

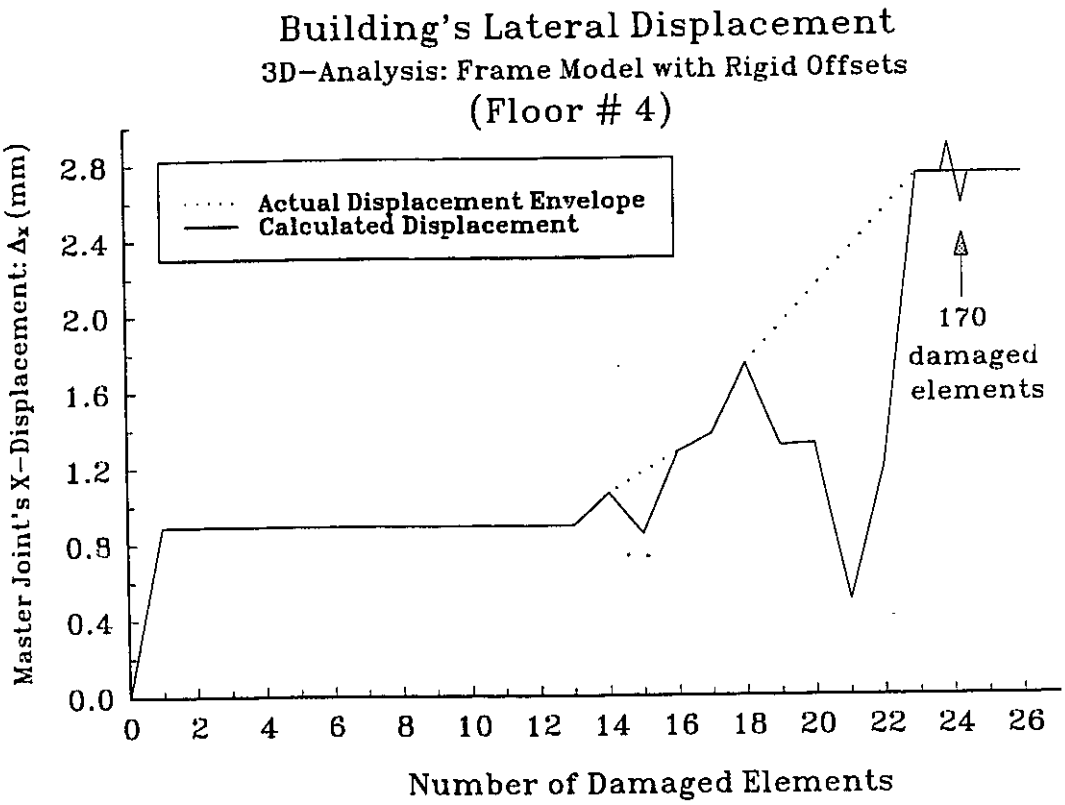

Figure 4.10: Building's 4th floor lateral displacement for frame model with rigid offsets.

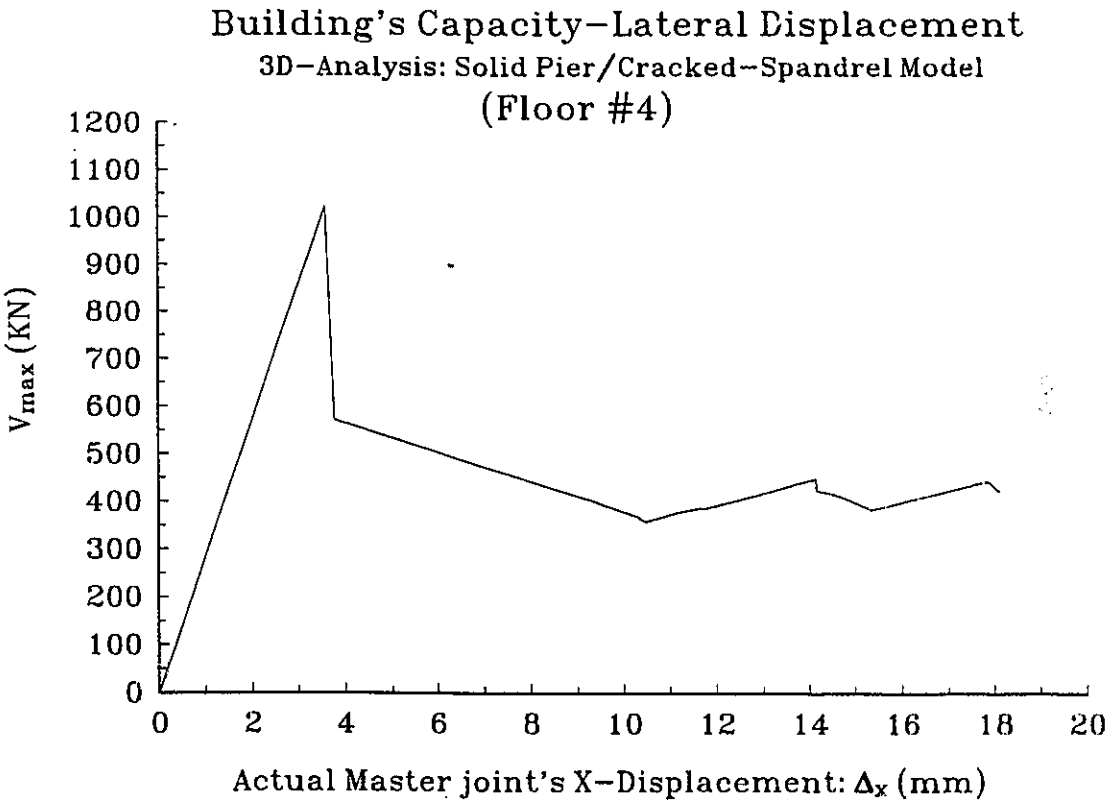

Figure 4.11: 3D-Analysis: 4th floor shear-displacement behaviour of piers-only model.

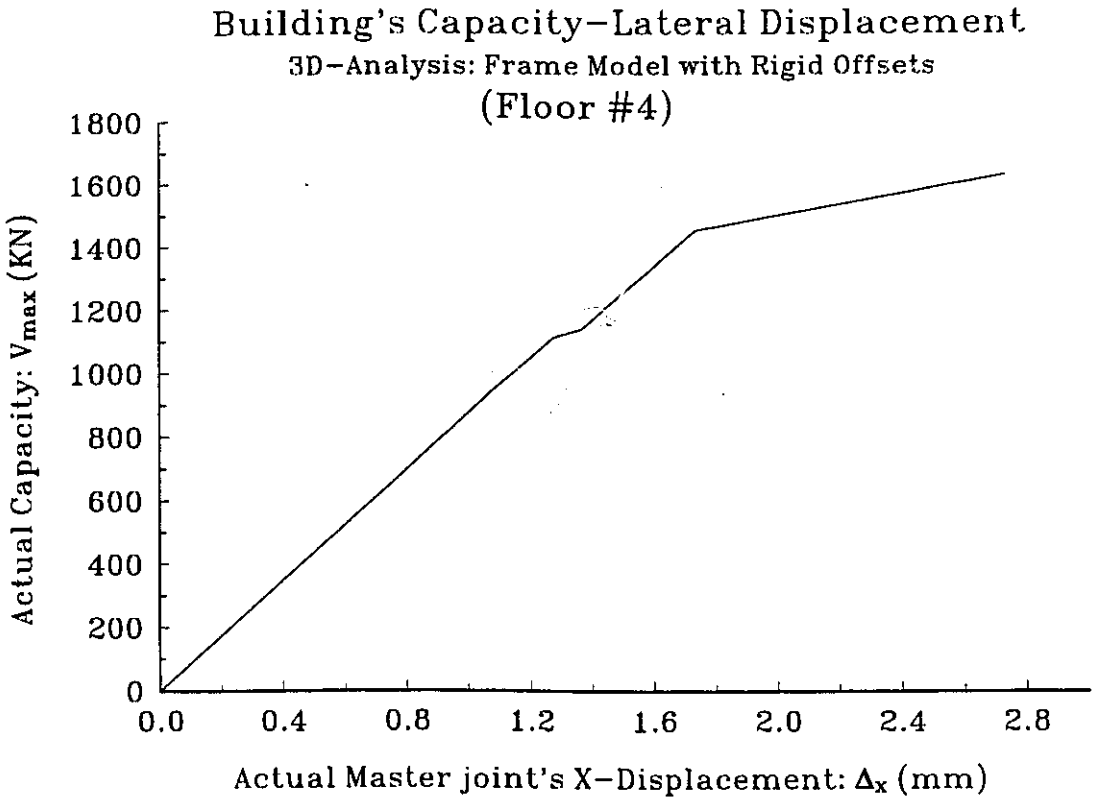

Figure 4.12: 3D-Analysis: 4th floor shear-displacement behaviour of frame model with rigid offsets.

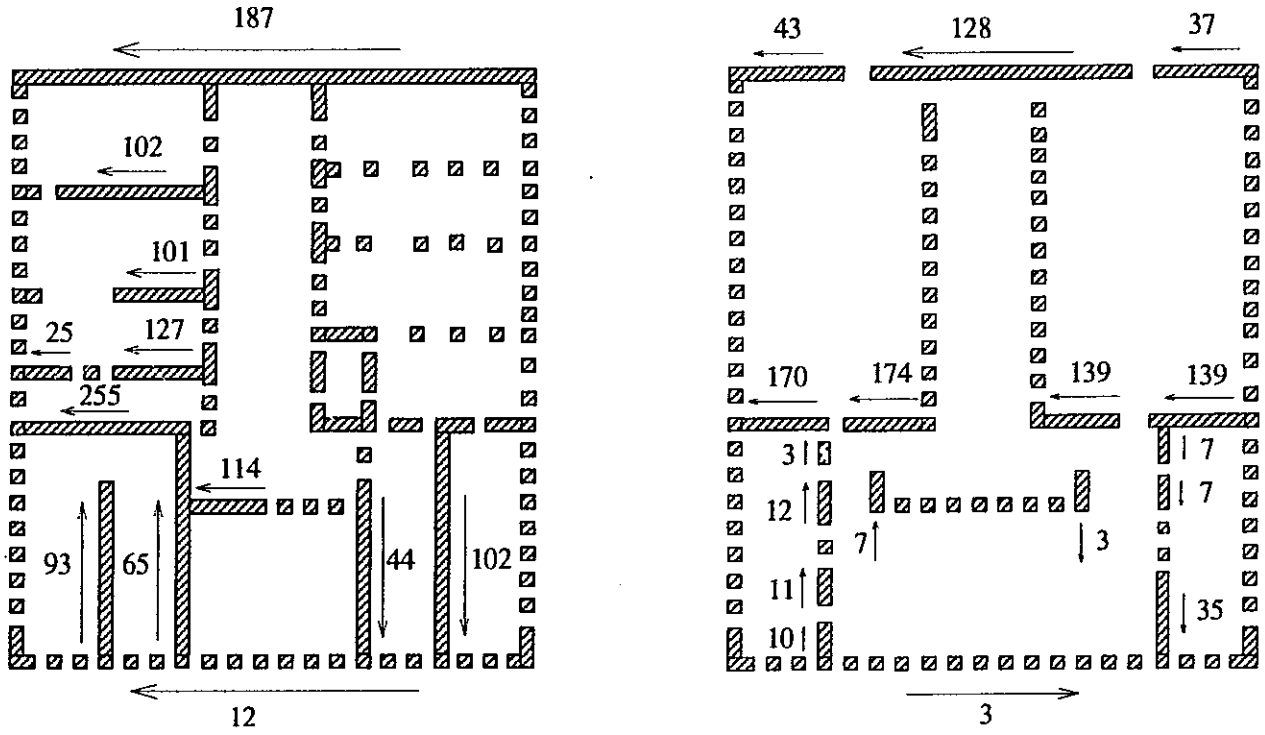

Figure 4.13: 3D-Analysis: Free body diagram of piers-only model at threshold of damage.

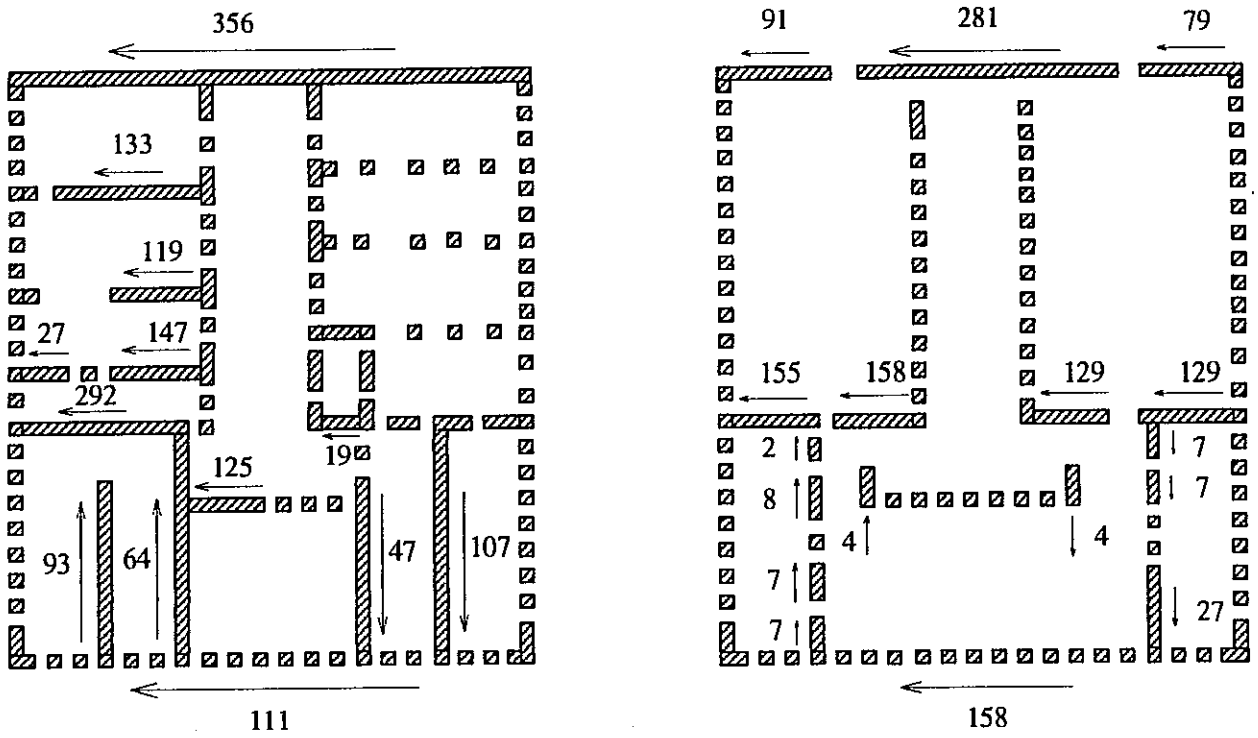

Figure 4.14: 3D-Analysis: Free body diagram of frame model with rigid offsets at 6th step.

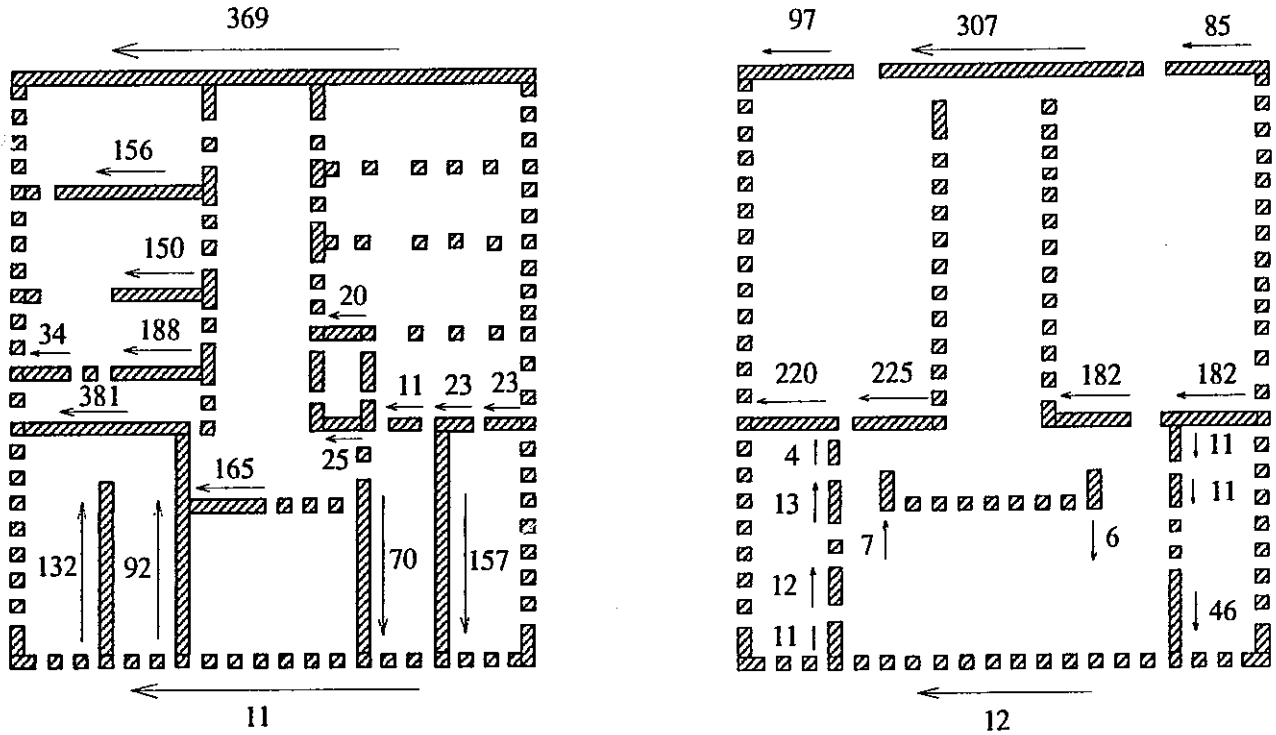

Figure 4.15: 3D-Analysis: Free body diagram of frame model with rigid offsets at 11th step (West facade damaged).

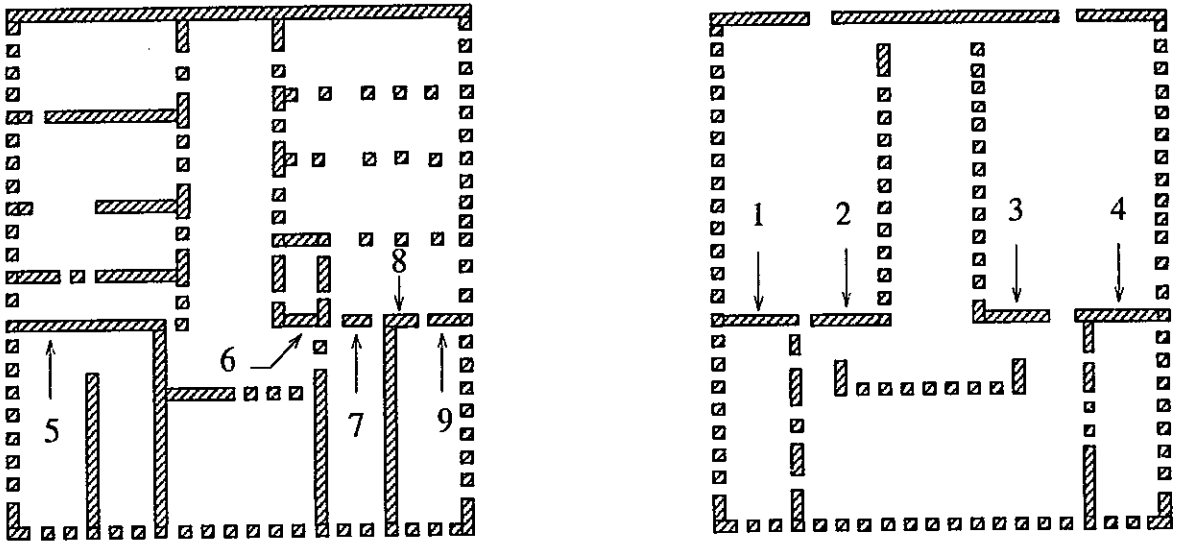

Figure 5.1: Piers' numbering of the interior wall.

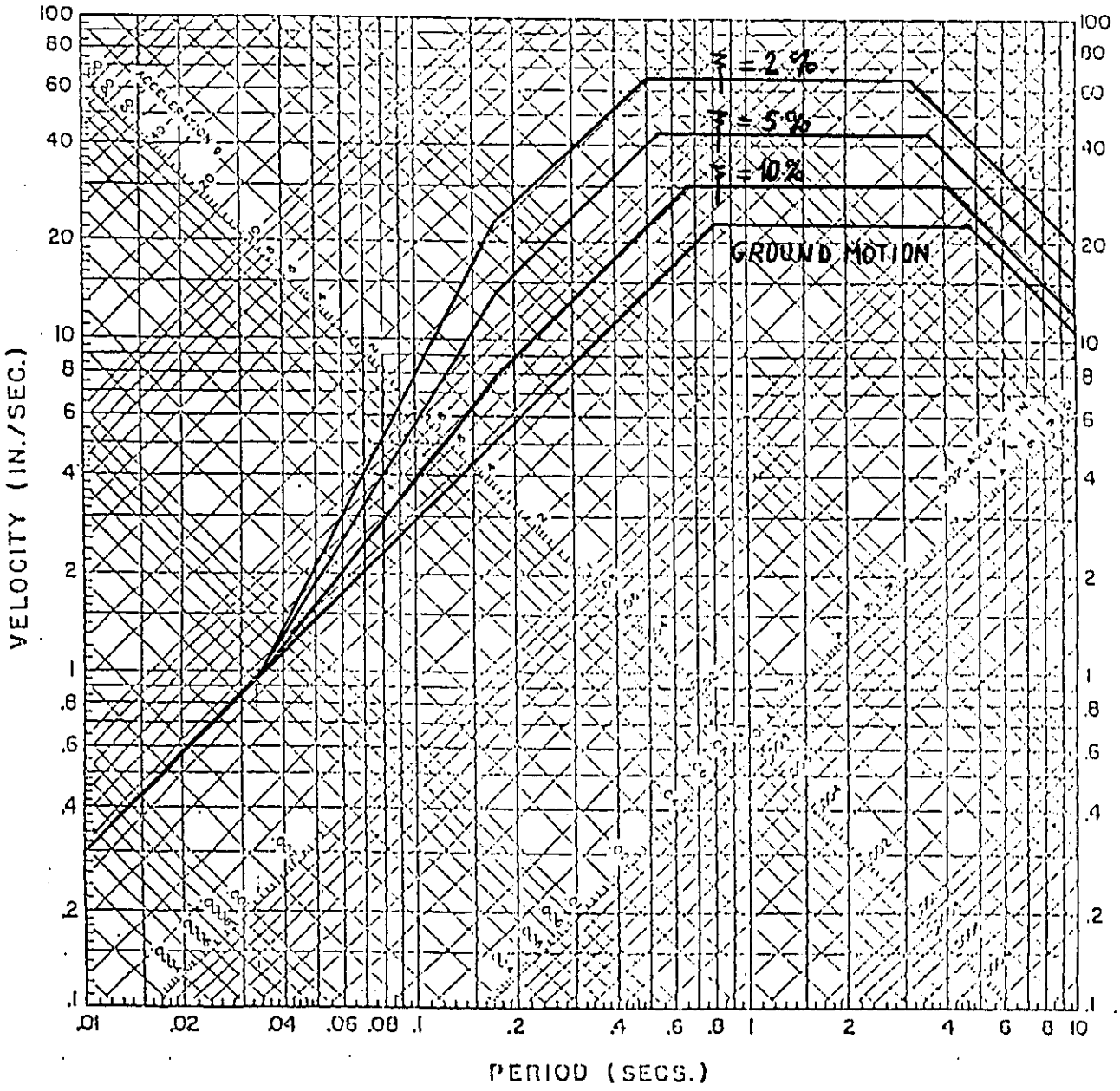

Figure 6.1: Newmark-Hall design spectra.

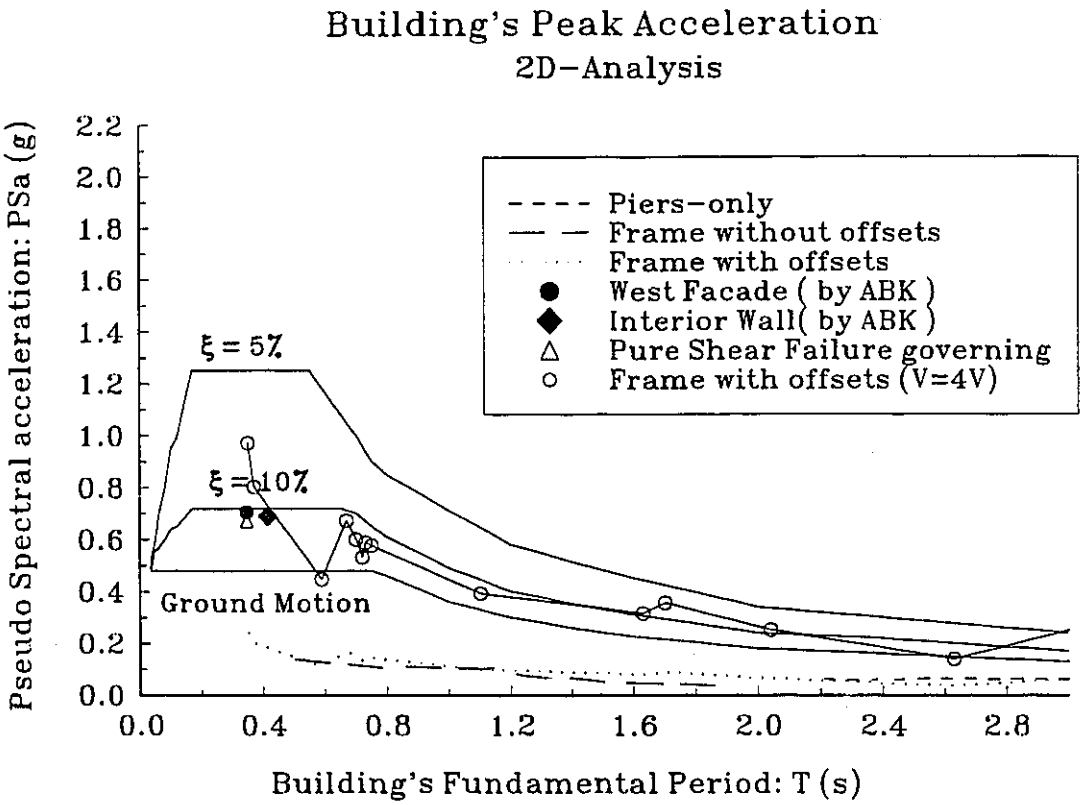

Figure 6.2: Pseudo Spectral accelerations and ultimate capacity ratios of the 2D models.

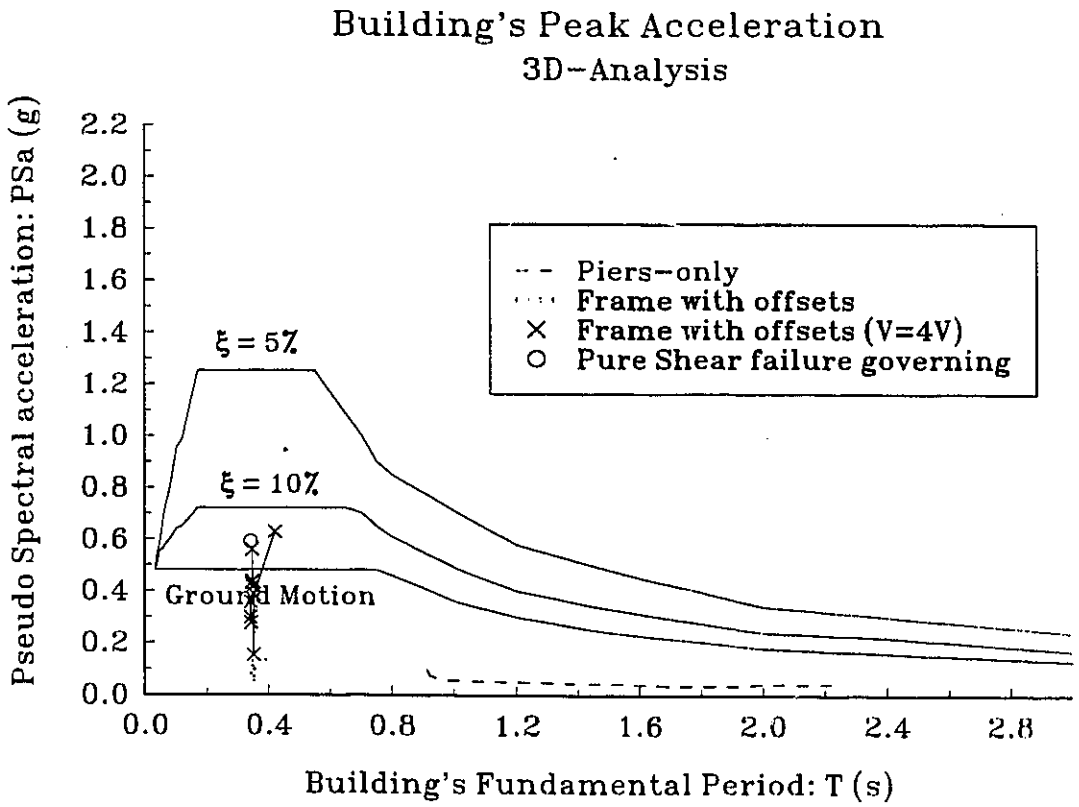

Figure 6.3: Pseudo Spectral accelerations and ultimate capacity ratios of the 3D models.

Appendix A

MONTGOMERY BLOCK

628 MONTGOMERY STREET

SAN FRANCISCO • CALIFORNIA

COMPLETED DECEMBER 1853 BY HENRY W. HALLECK

ARCHITECT . GORDON P. CUMMINGS

BUILDERS

MASONRY COOK AND COFFIN

CARPENTRY LAROACHE, KING AND CHITTENDEN

SCULPTOR JAMES SHELTON

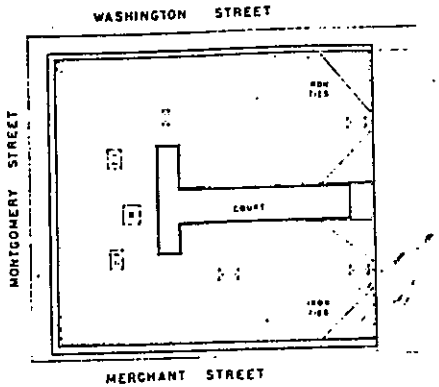

ROOF PLAN
SCALE A

CONRAD L. WIRTH
THE DIRECTOR, NATIONAL PARK SERVICE

THOMAS C. VINT
CHIEF OF DESIGN AND CONSTRUCTION

DICK SUTTON
CHIEF ARCHITECT, DESIGN AND CONSTRUCTION

SANFORD HILL
CHIEF OF WESTERN OFFICE, DESIGN AND CONSTRUCTION

CHARLES ST. GEORGE POPE
SUPERVISING ARCHITECT

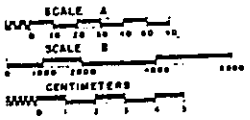

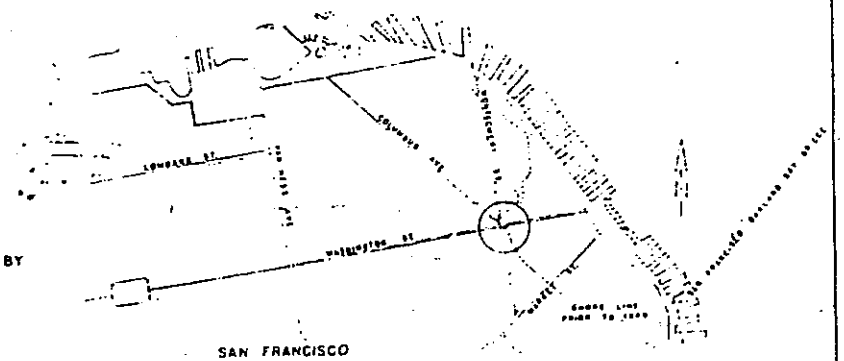

MEASURED AND DRAWN AUGUST 1958 UNDER SUPERVISION OF KENNETH CAROWELL, ARCHITECT, UNIVERSITY OF CALIFORNIA, BY
DAVID W. BELL, UNIVERSITY OF CALIFORNIA
W. L. WEBER, UNIVERSITY OF CALIFORNIA
JAMES R. GARTY, UNIVERSITY OF CALIFORNIA
MYRLE HUGHES, UNIVERSITY OF CALIFORNIA

W. L. WEBER, MYRLE HUGHES - DELS

THIS PROJECT WAS FINANCED FROM FUNDS OF THE "MISSION 66" PROGRAM

NAME OF STRUCTURE
MONTGOMERY BLOCK
628 MONTGOMERY STREET - SAN FRANCISCO - SAN FRANCISCO COUNTY - CALIFORNIA

HISTORIC AMERICAN BUILDINGS SURVEY

Plan 1
135

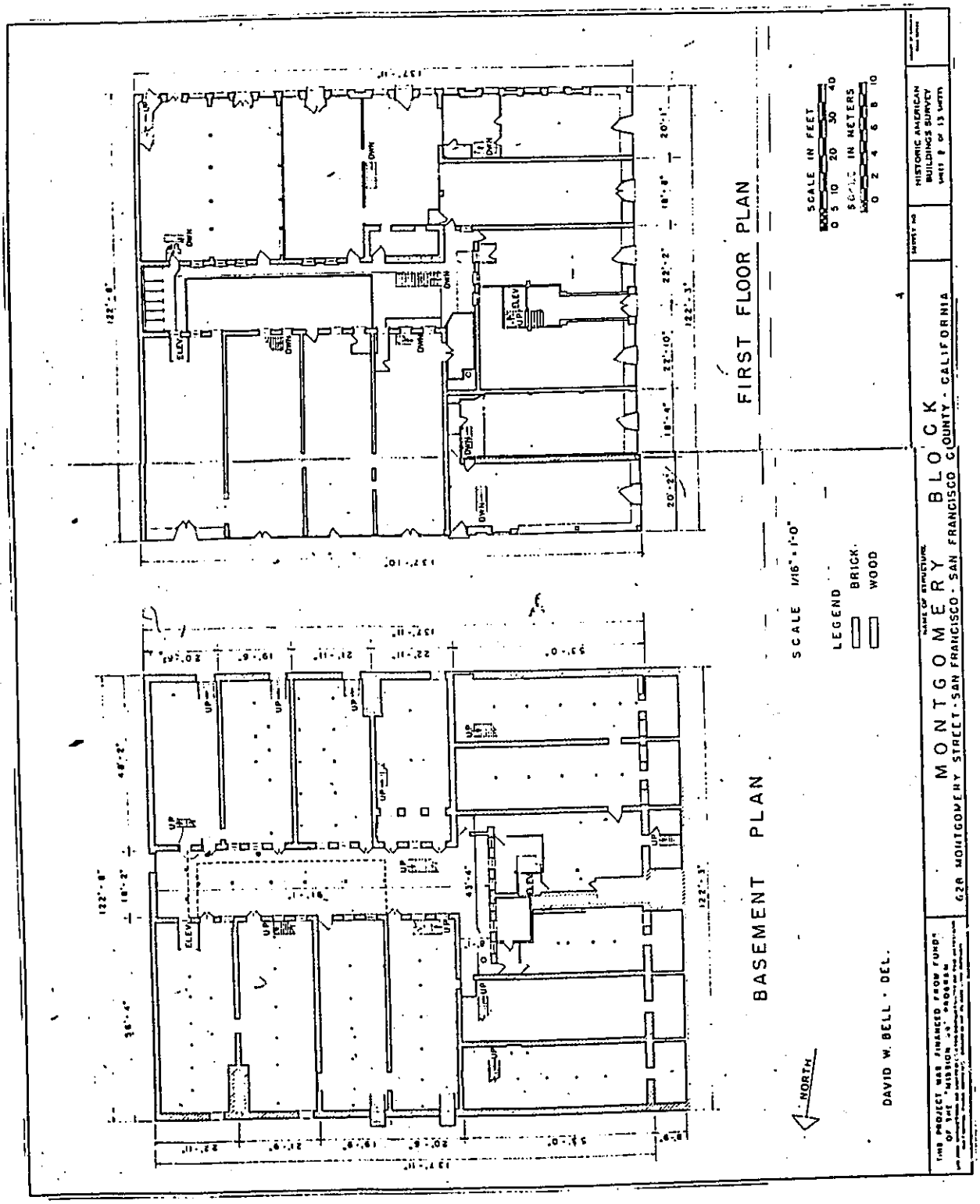
FIRST FLOOR PLAN
BASEMENT PLAN
SCALE 1/16" = 1'-0"
LEGEND
BRICK
WOOD
SCALE IN FEET
SCALE IN METERS
NORTH
DAVID W. BELL - DEL.
MONTGOMERY BLOCK
628 MONTGOMERY STREET - SAN FRANCISCO - SAN FRANCISCO COUNTY - CALIFORNIA
HISTORIC AMERICAN BUILDINGS SURVEY

Plan 2
136

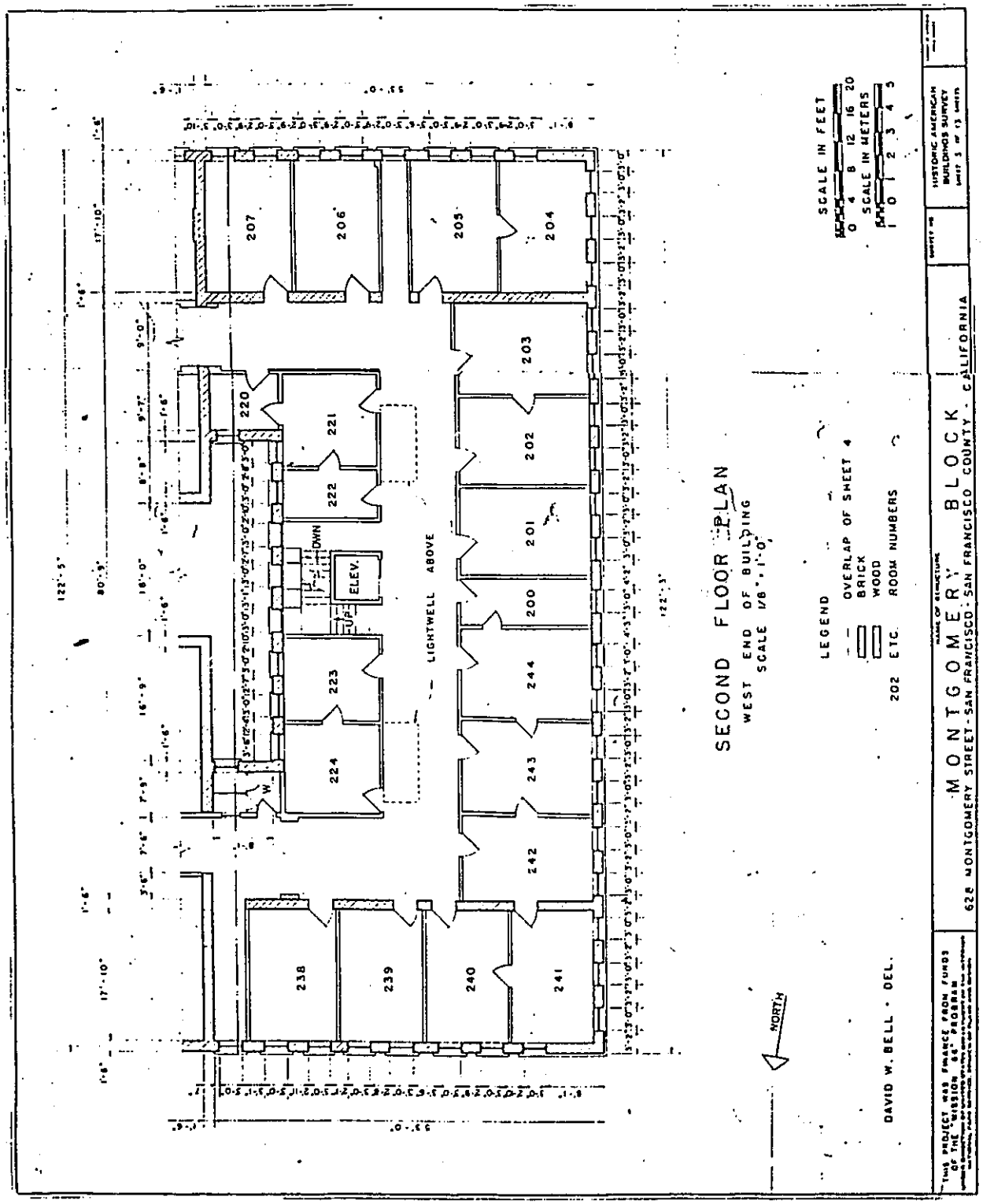
SECOND FLOOR PLAN
WEST END OF BUILDING
SCALE 1/8" = 1'-0"
LEGEND
OVERLAP OF SHEET 4
BRICK
WOOD
202 ETC. ROOM NUMBERS
SCALE IN FEET
SCALE IN METERS
NORTH
LIGHTWELL ABOVE
ELEV.
DOWN
MONTGOMERY BLOCK
628 MONTGOMERY STREET - SAN FRANCISCO - SAN FRANCISCO COUNTY - CALIFORNIA
DAVID W. BELL - DEL.
HISTORIC AMERICAN BUILDINGS SURVEY

Plan 3
137

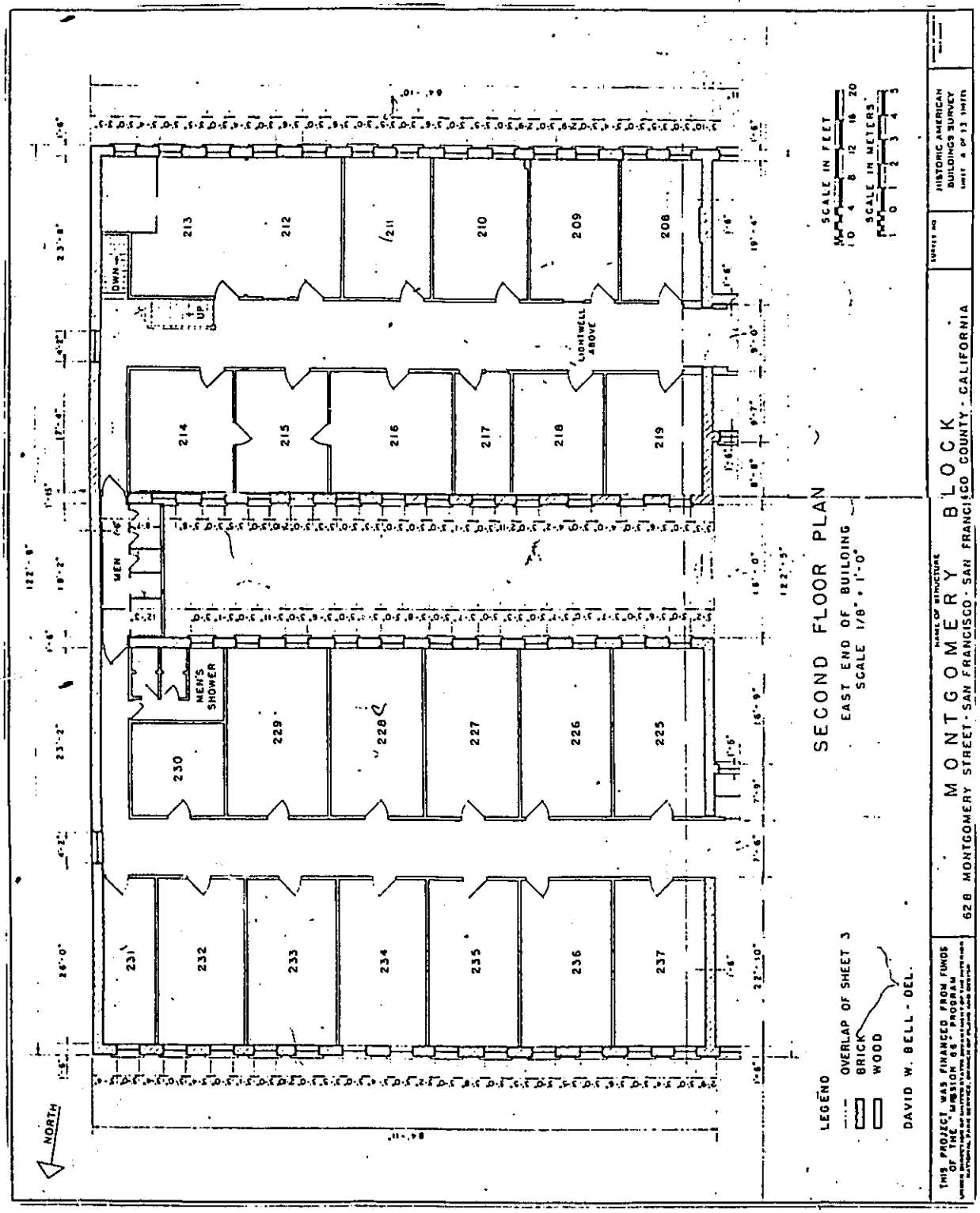
SECOND FLOOR PLAN
EAST END OF BUILDING
SCALE 1/8" = 1'-0"
MONTGOMERY BLOCK
628 MONTGOMERY STREET - SAN FRANCISCO - SAN FRANCISCO COUNTY - CALIFORNIA
NAME OF STRUCTURE
HISTORIC AMERICAN BUILDINGS SURVEY
SCALE IN FEET
SCALE IN METERS
LEGEND
OVERLAP OF SHEET 3
BRICK
WOOD
DAVID W. BELL - DEL.
NORTH
MEN
NEN'S SHOWER
DWN
UP
LIGHTWELL ABOVE
213
212
211
210
209
208
214
215
216
217
218
219
230
229
228
227
226
225
231
232
233
234
235
236
237

Plan 4
138

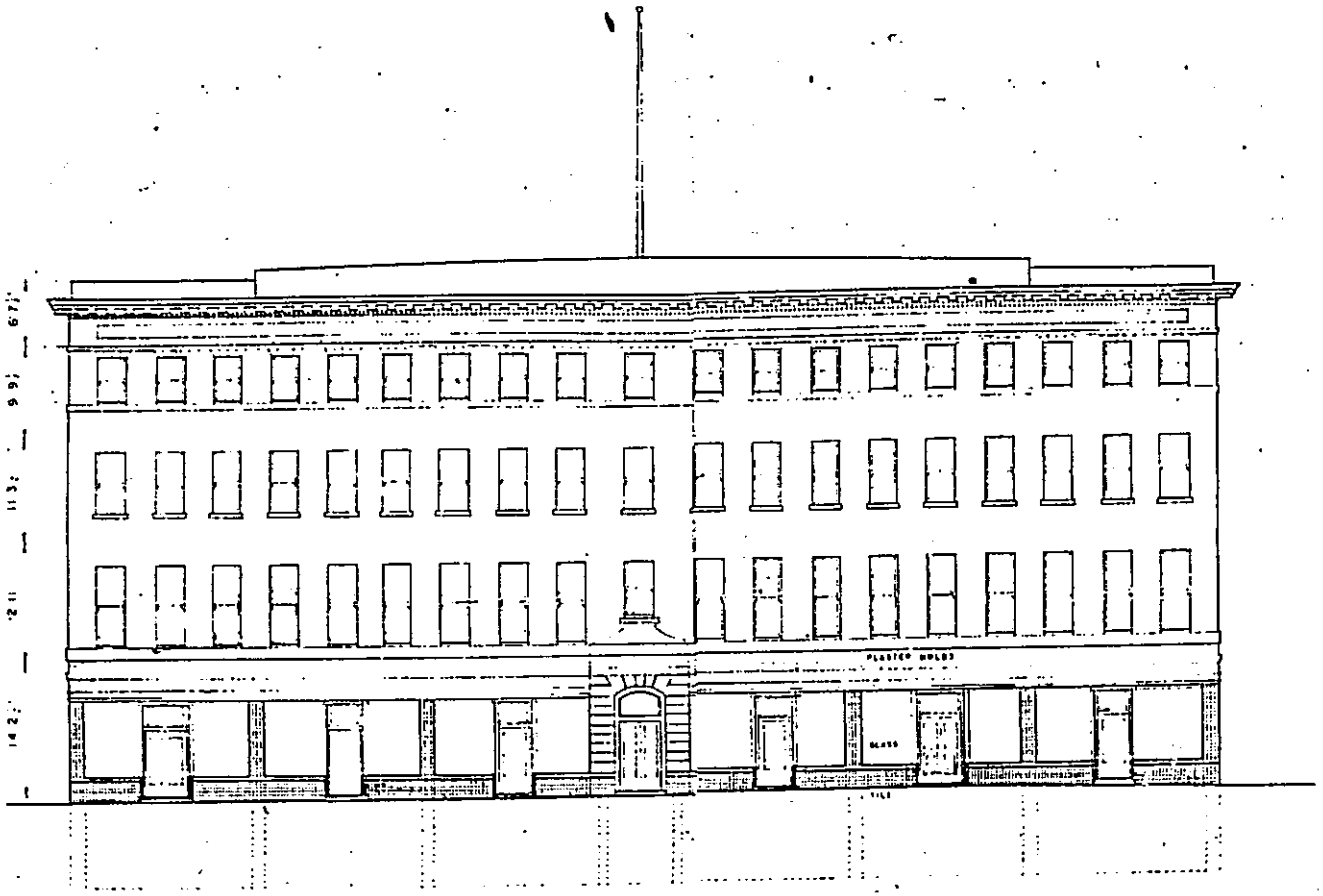

NOTE: STONE TRIM AND PLASTER MOLDS REMOVED AFTER 1906.

WEST ELEVATION

SCALE 1/8" = 1'-0"

SCALE IN FEET
10 4 8 12 16 20

SCALE IN METERS
1 0 1 2 3 4 5

MYRLE HUGHES - DEL.

THIS PROJECT WAS FINANCED FROM FUNDS OF THE "MISSION 66" PROGRAM

NAME OF STRUCTURE
MONTGOMERY BLOCK
628 MONTGOMERY STREET - SAN FRANCISCO - SAN FRANCISCO COUNTY - CALIFORNIA

SURVEY NO.

HISTORIC AMERICAN BUILDINGS SURVEY
SHEET 5 OF 13 SHEETS

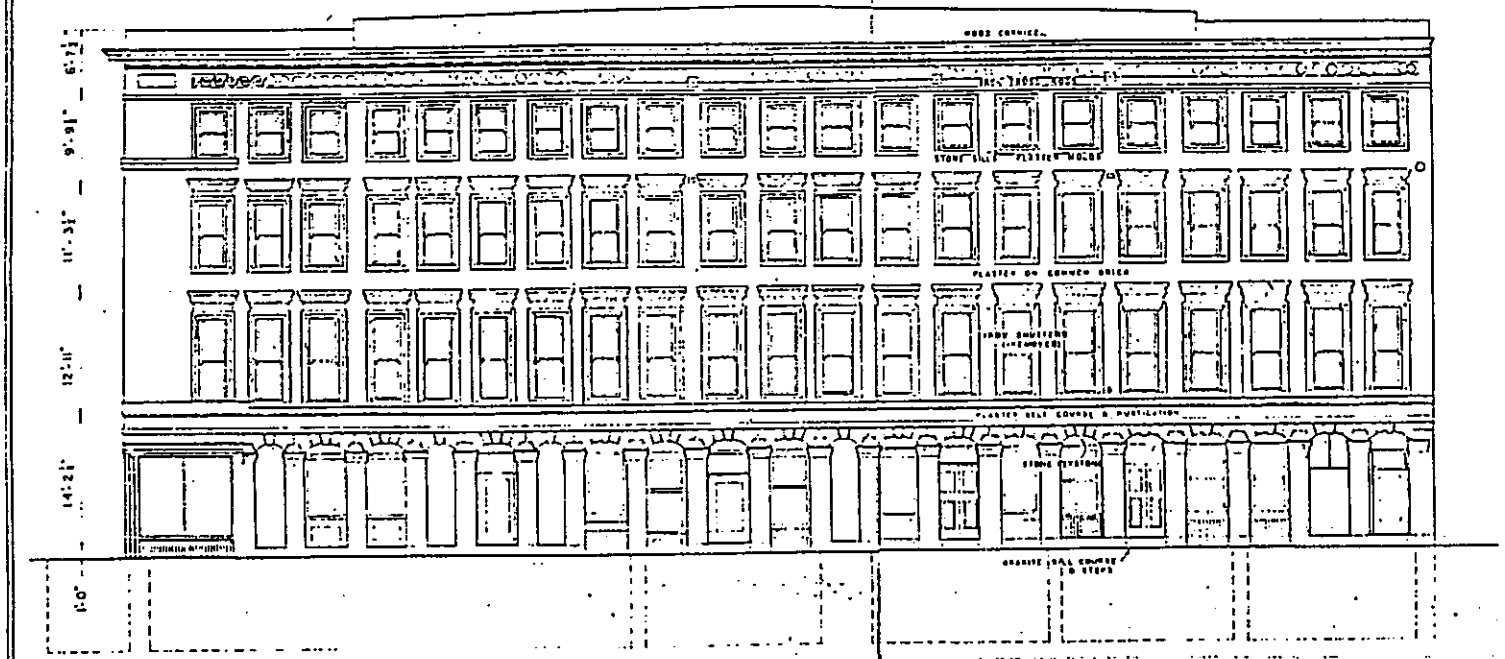

SOUTH ELEVATION

SCALE: 1/8"=1'-0"

SCALE IN FEET

0 2 4 6 8

SCALE IN METERS

0 1 2 3 4 5

W. L. WEBER - DEL.

THIS PROJECT WAS FINANCED FROM FUNDS OF THE "MISSION 66" PROGRAM

NAME OF STRUCTURE

MONTGOMERY BLOCK

628 MONTGOMERY STREET - SAN FRANCISCO - SAN FRANCISCO COUNTY - CALIFORNIA

SURVEY NO.

HISTORIC AMERICAN BUILDINGS SURVEY

SHEET 6 OF 13 SHEETS

Plan 6
140

Plan 7
141

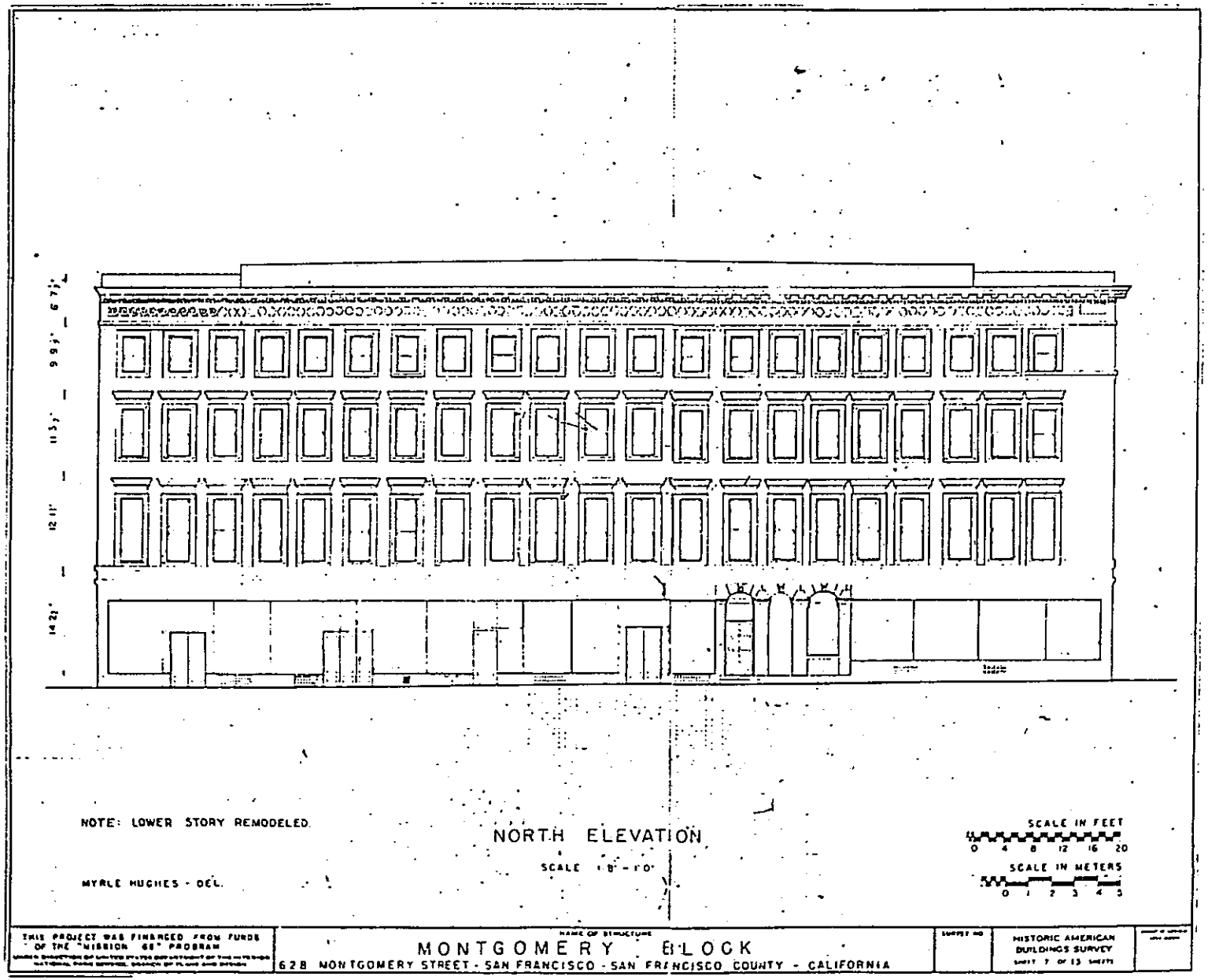
NOTE: LOWER STORY REMODELED.
NORTH ELEVATION
SCALE 1/8" = 1'0"
MYRLE HUGHES - DEL.
SCALE IN FEET
0 4 8 12 16 20
SCALE IN METERS
0 1 2 3 4 5
THIS PROJECT WAS FINANCED FROM FUNDS OF THE "MISSION 66" PROGRAM
NAME OF STRUCTURE
MONTGOMERY BLOCK
628 MONTGOMERY STREET - SAN FRANCISCO - SAN FRANCISCO COUNTY - CALIFORNIA
SHEET NO
HISTORIC AMERICAN BUILDINGS SURVEY
SHEET 7 OF 13 SHEETS

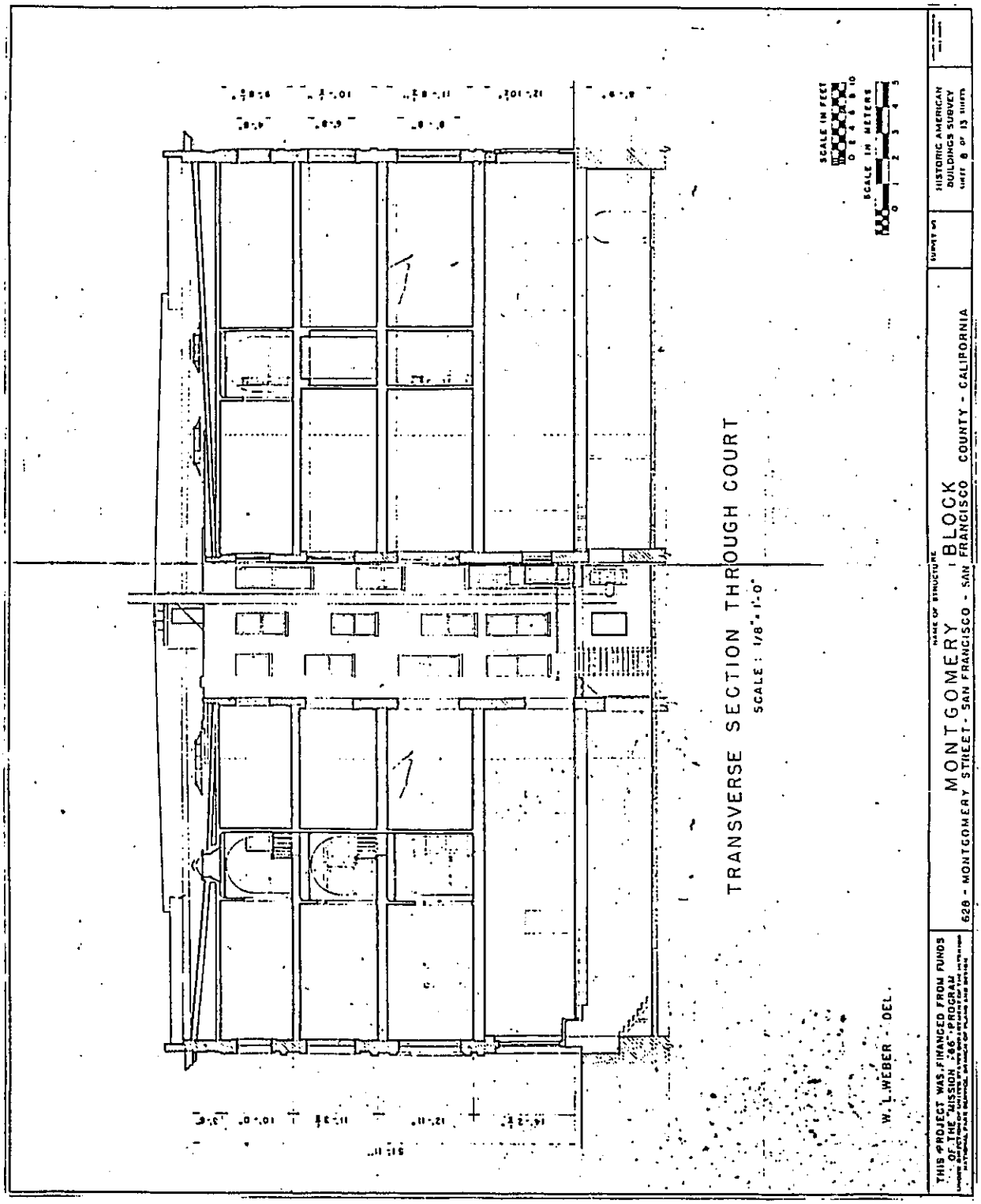
TRANSVERSE SECTION THROUGH COURT
SCALE : 1/8"-1'-0"
MONTGOMERY BLOCK
628 - MONTGOMERY STREET - SAN FRANCISCO - SAN FRANCISCO COUNTY - CALIFORNIA
W. L. WEBER - DEL.
HISTORIC AMERICAN BUILDINGS SURVEY

Plan 8

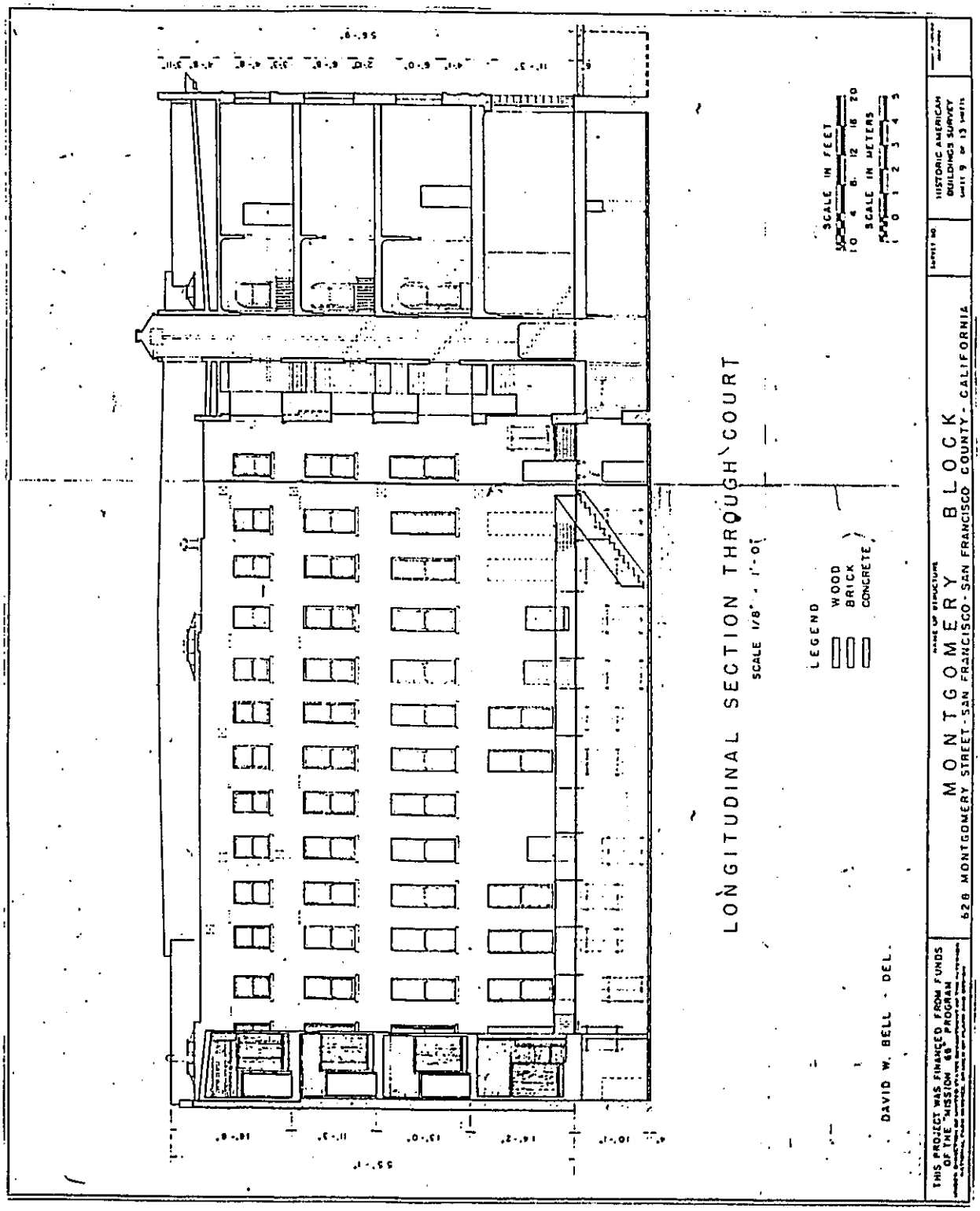
LONGITUDINAL SECTION THROUGH COURT
SCALE 1/8" = 1'-0"
LEGEND
WOOD
BRICK
CONCRETE
SCALE IN FEET
SCALE IN METERS
NAME OF STRUCTURE
MONTGOMERY BLOCK
628 MONTGOMERY STREET - SAN FRANCISCO - SAN FRANCISCO COUNTY - CALIFORNIA
HISTORIC AMERICAN BUILDINGS SURVEY
DAVID W. BELL - DEL.
THIS PROJECT WAS FINANCED FROM FUNDS OF THE "MISSION 66" PROGRAM

Plan 9

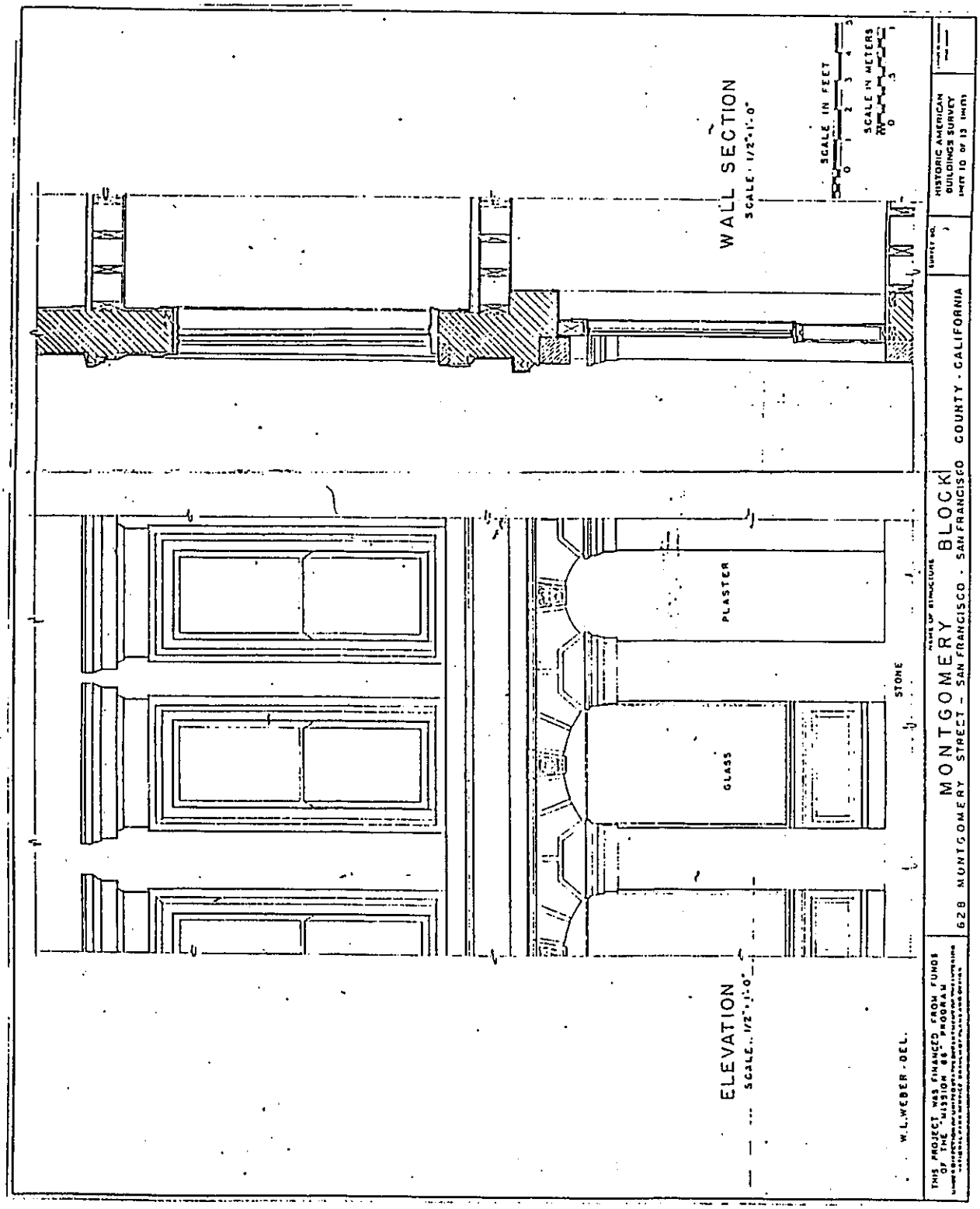
WALL SECTION
SCALE: 1/2"=1'-0"
SCALE IN FEET
SCALE IN METERS
ELEVATION
SCALE: 1/2"=1'-0"
PLASTER
GLASS
STONE
W.L.WEBER - DEL.
MONTGOMERY BLOCK
628 MONTGOMERY STREET - SAN FRANCISCO - SAN FRANCISCO COUNTY - CALIFORNIA
HISTORIC AMERICAN BUILDINGS SURVEY
THIS PROJECT WAS FINANCED FROM FUNDS OF THE "MISSION 66" PROGRAM

Plan 10
144

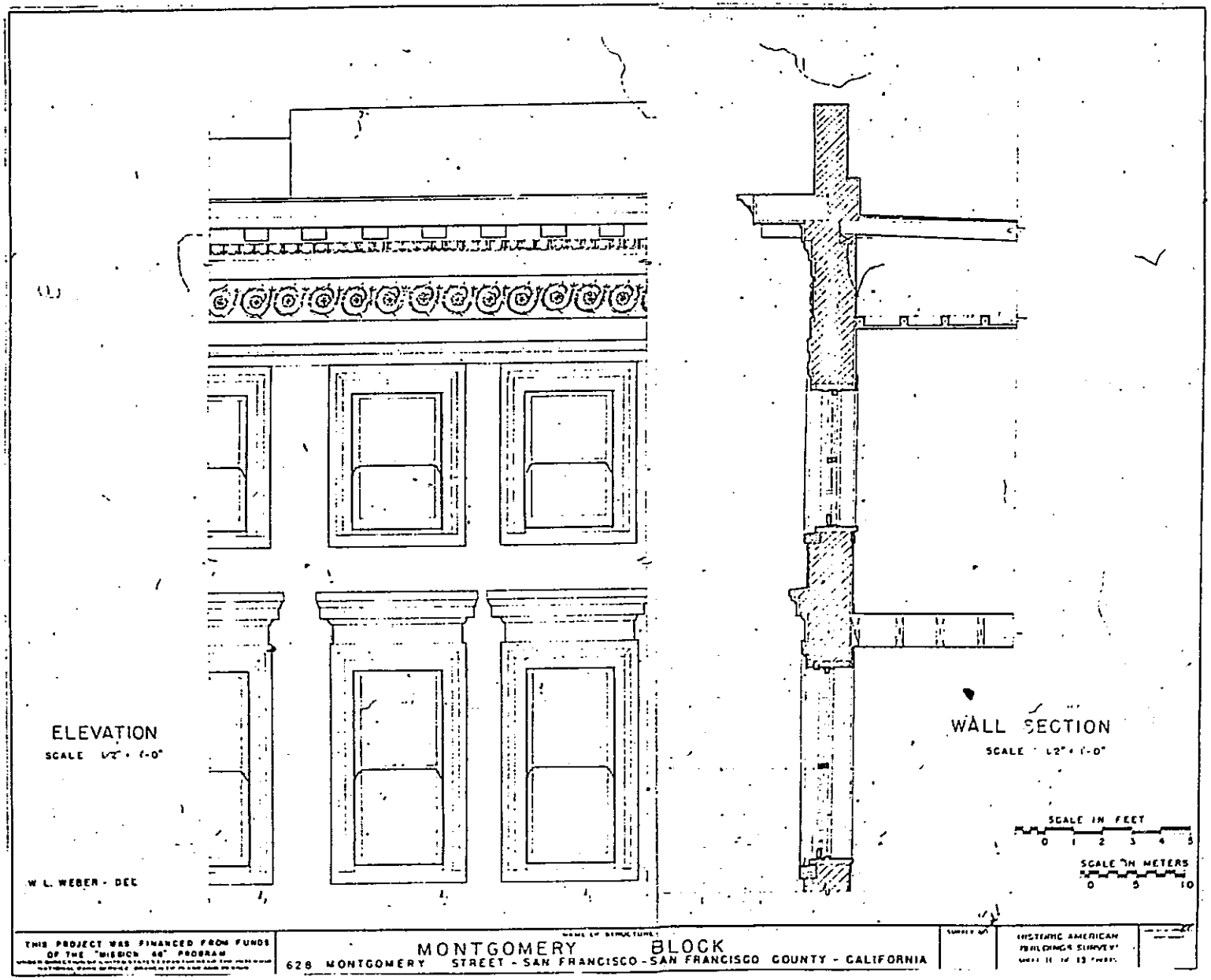
ELEVATION
SCALE 1/2" = 1'-0"
W. L. WEBER - DEL
WALL SECTION
SCALE 1" = 1'-0"
SCALE IN FEET
0 1 2 3 4 5
SCALE IN METERS
0 5 10
THIS PROJECT WAS FINANCED FROM FUNDS OF THE "HABER 66" PROGRAM
MONTGOMERY BLOCK
628 MONTGOMERY STREET - SAN FRANCISCO - SAN FRANCISCO COUNTY - CALIFORNIA
HISTORIC AMERICAN BUILDINGS SURVEY

Plan 11
145

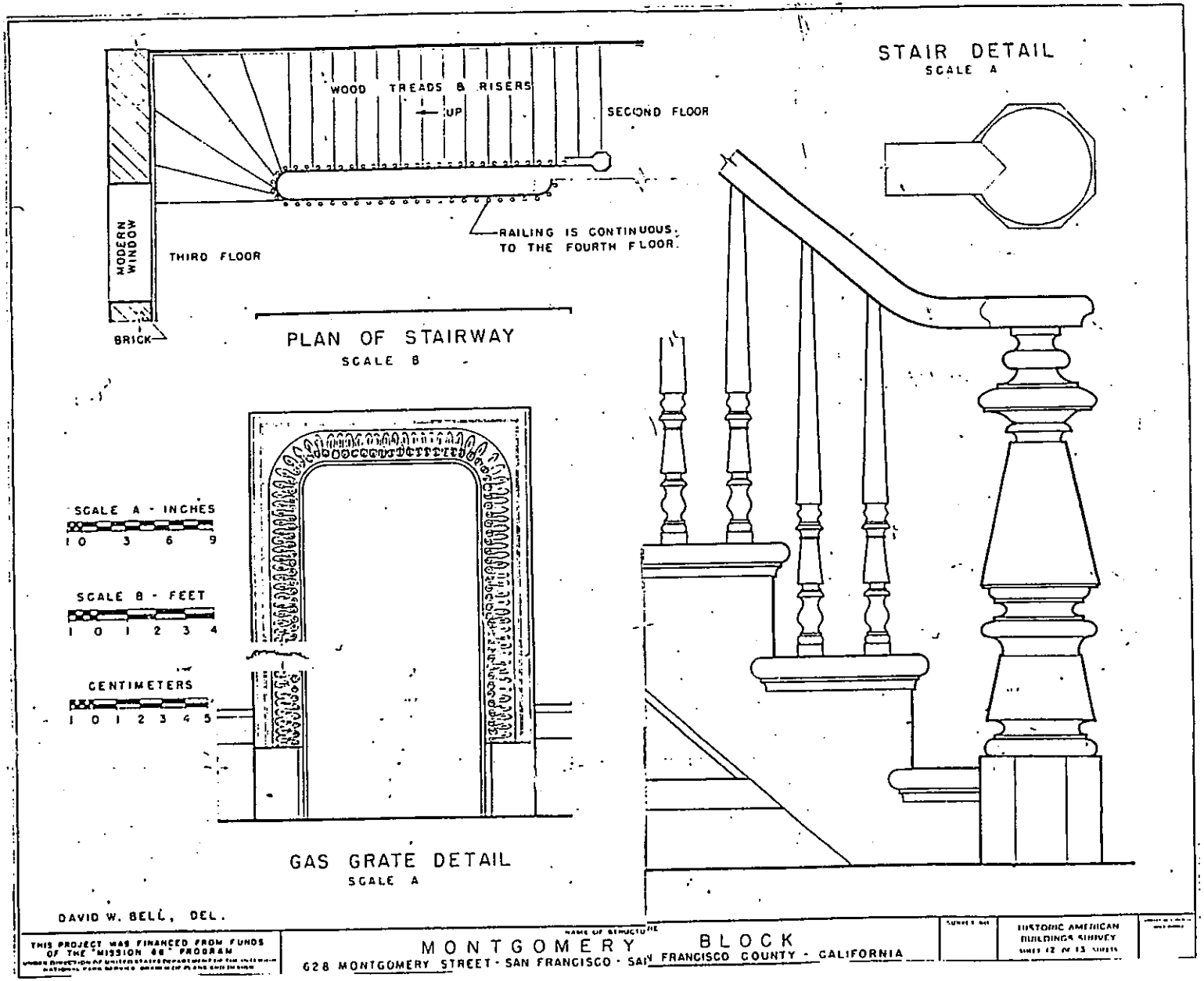
STAIR DETAIL
SCALE A
WOOD TREADS & RISERS
UP
SECOND FLOOR
RAILING IS CONTINUOUS TO THE FOURTH FLOOR.
MODERN WINDOW
THIRD FLOOR
BRICK
PLAN OF STAIRWAY
SCALE B
SCALE A - INCHES
0 3 6 9
SCALE B - FEET
0 1 2 3 4
CENTIMETERS
0 1 2 3 4 5
GAS GRATE DETAIL
SCALE A
DAVID W. BELL, DEL.
THIS PROJECT WAS FINANCED FROM FUNDS OF THE "MISSION 66" PROGRAM
NAME OF STRUCTURE
MONTGOMERY BLOCK
628 MONTGOMERY STREET · SAN FRANCISCO · SAN FRANCISCO COUNTY · CALIFORNIA
HISTORIC AMERICAN BUILDINGS SURVEY

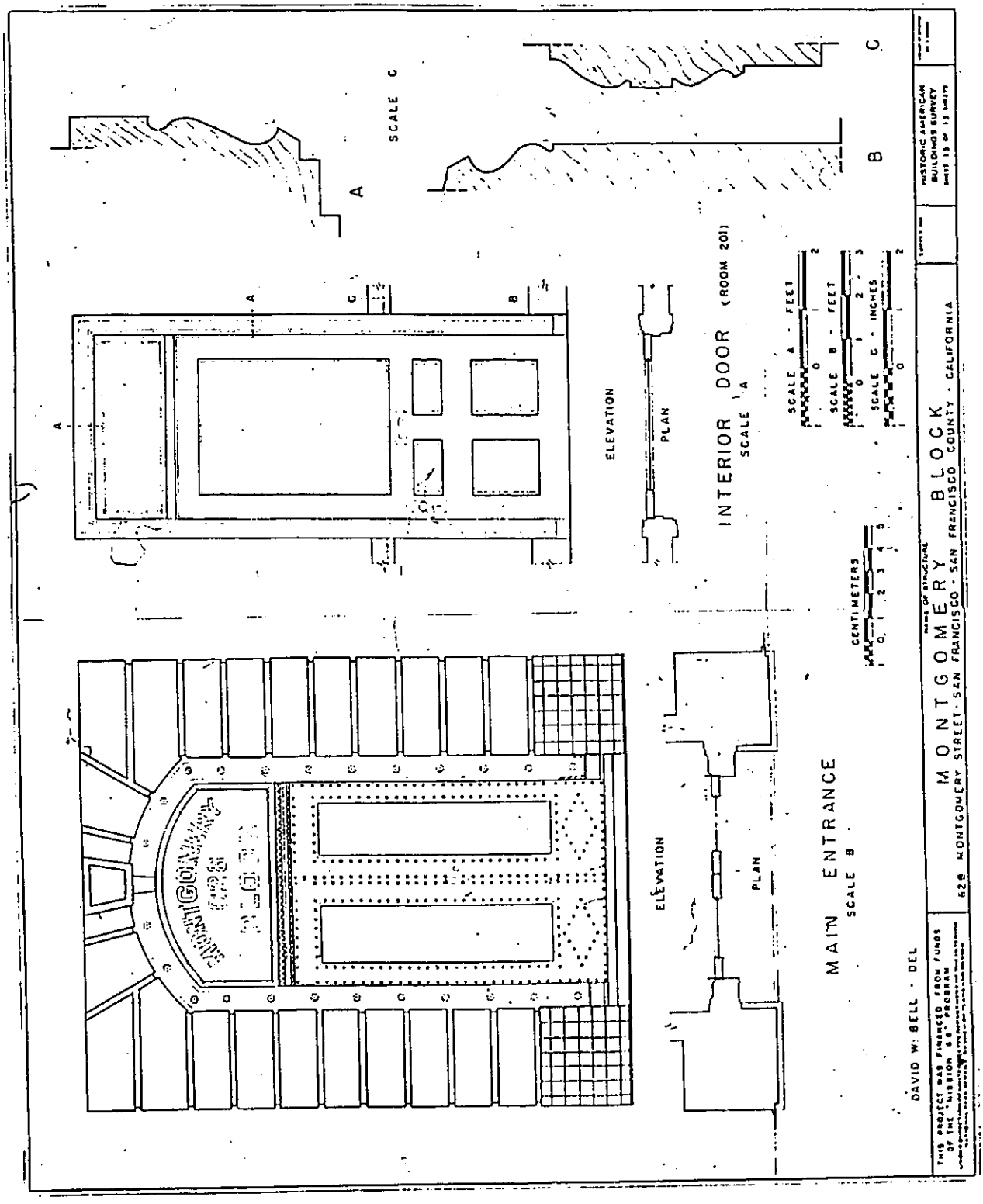
SCALE C
A
B
C
INTERIOR DOOR (ROOM 201)
SCALE A
ELEVATION
PLAN
SCALE A - FEET
SCALE B - FEET
SCALE C - INCHES
CENTIMETERS
MAIN ENTRANCE
SCALE B
ELEVATION
PLAN
MONTGOMERY BLOCK
628 MONTGOMERY STREET · SAN FRANCISCO · SAN FRANCISCO COUNTY · CALIFORNIA
DAVID W. BELL · DEL
HISTORIC AMERICAN BUILDINGS SURVEY

Plan 13
147

Appendix B

Step #	# of Damaged Elements	Damaged Elements	V_{max}(KN)	Fundamental Period: T(s)
1	1	89	171.5	0.49991
2	2	90	136.02	0.50609
3	3	91	129.5	0.51686
4	4	88	166.6	0.52648
5	5	92	161.1	0.53508
6	6	87	156.4	0.54418
7	7	93	150.7	0.55377
8	8	94	146.3	0.56155
9	9	86	140.4	0.57161
10	10	99	134.7	0.58304
11	11	98	128.7	0.59502
12	12	97	122.8	0.60804
13	13	85	116.7	0.62220
14	14	96	111.1	0.63757
15	15	84	105.0	0.65501
16	16	83	99.3	0.67329
17	17	82	93.6	0.69329
18	18	95	94.9	0.71577
19	19	81	87.8	0.74865
20	20	108	128.3	0.78184

Table B.1: Lateral load capacities and corresponding periods of the frame model without rigid offsets (F.T. is always dominant).

Step #	# of Damaged Elements	Damaged Elements	V_{max}(KN)	Fundamental Period: T(s)
21	21	109	106.5	0.78852
22	22	110	99.4	0.80002
23	23	107	135.1	0.81007
24	24	111	130.3	0.81848
25	25	106	126.2	0.82752
26	26	112	121.0	0.83725
27	27	105	116.0	0.84782
28	28	113	110.7	0.85931
29	29	114	105.3	0.87190
30	30	115	99.6	0.88569
31	31	118	93.9	0.89755
32	32	104	89.2	0.91309
33	33	117	84.3	0.93144
34	34	103	78.7	0.95207
35	35	102	73.73	0.97520
36	36	101	68.7	1.00114
37	37	116	70.2	1.03068
38	38	100	62.9	1.07352
39	39	127	123.9	1.11881
40	40	128	106.7	1.12371

Table B.1: (continued)

Step #	# of Damaged Elements	Damaged Elements	V_{max}(KN)	Fundamental Period: T(s)
41	41	129	97.8	1.13212
42	42	11	128.7	1.13935
43	44	120,121	128.7	1.15219
44	46	139,140	128.7	1.15749
45	47	71	120.6	1.15979
46	48	75	115.8	1.17174
47	49	137	105.0	1.18359
48	50	126	109.1	1.18822
49	51	125	106.3	1.19683
50	52	55	102.3	1.20625
51	53	130	95.2	1.22095
52	54	131	82.5	1.23159
53	55	124	90.3	1.24180
54	56	59	89.0	1.25547
55	57	63	86.2	1.27261
56	58	123	83.6	1.29114
57	59	134	78.8	1.30804
58	60	135	66.9	1.31582
59	61	76	77.5	1.33304
60	62	56	77.3	1.33703

Table B.1: (continued)

Step #	# of Damaged Elements	Damaged Elements	V_{max}(KN)	Fundamental Period: T(s)
61	63	122	80.2	1.34283
62	64	72	71.1	1.37020
63	65	64	69.1	1.37830
64	66	60	66.8	1.38722
65	67	119	81.3	1.40052
66	68	40	79.9	1.42550
67	69	80	53.0	1.49279
68	70	52	58.7	1.50628
69	71	48	59.2	1.52464
70	72	44	56.8	1.54403
71	73	36	59.2	1.59377
72	74	32	55.4	1.61952
73	75	28	51.6	1.64796
74	76	24	44.1	1.70980
75	77	20	42.6	1.74855
76	78	16	38.8	1.78865
77	79	68	38.3	1.83458
78	80	4	44.3	1.89720
79	81	8	41.2	1.93885
80	82	12	41.2	1.93885

Table B.1: (continued)

Step #	# of Damaged Elements	Damaged Elements	V_{max}(KN)	Fundamental Period: T(s)
1	1	89	297.8	0.34684
2	2	90	217.4	0.35309
3	3	91	192.6	0.36385
4	4	88	246.2	0.37369
5	5	92	235.7	0.38172
6	6	87	226.7	0.39033
7	7	93	215.8	0.39952
8	8	86	206.3	0.40946
9	9	94	195.2	0.42018
10	10	95	184.3	0.43190
11	11	85	173.0	0.44468
12	12	96	161.7	0.45884
13	13	84	150.3	0.47445
14	14	83	140.0	0.49201
15	15	97	128.8	0.51176
16	16	82	124.1	0.53441
17	17	98	112.9	0.56081
18	18	99	137.9	0.59177
19	19	81	123.6	0.62698
20	20	38	206.7	0.67263

Table B.2: Lateral load capacities and corresponding periods of the frame model with rigid offsets (F.T. is always dominant).

Step #	# of Damaged Elements	Damaged Elements	V_{max}(KN)	Fundamental Period: T(s)
21	21	109	148.4	0.68826
22	22	110	140.9	0.69201
23	23	37	184.2	0.70189
24	24	108	113.3	0.72101
25	25	128	12.4	0.72379
26	26	107	164.4	0.72450
27	27	127	157.0	0.73155
28	28	111	180.0	0.73244
29	29	106	171.9	0.74018
30	30	146	137.1	0.74855
31	32	40,44	137.1	0.74961
32	34	147,148	137.1	0.75023
33	35	112	176.8	0.75048
34	36	113	164.0	0.75966
35	37	114	152.7	0.77002
36	38	115	142.9	0.78164
37	39	105	134.0	0.79457
38	40	104	123.2	0.80940
39	41	103	112.9	0.82660
40	42	116	102.9	0.84649

Table B.2: (continued)

Step #	# of Damaged Elements	Damaged Elements	V_{max}(KN)	Fundamental Period: T(s)
41	43	102	93.7	0.86958
42	44	117	88.9	0.89741
43	45	101	78.8	0.93055
44	46	118	95.1	0.97283
45	47	100	84.1	1.02390
46	48	129	120.0	1.09569
47	49	11	119.0	1.10500
48	50	7	114.4	1.11723
49	51	71	110.4	1.12966
50	52	75	105.7	1.14335
51	53	15	101.3	1.15732
52	54	19	95.7	1.17274
53	55	23	90.6	1.18923
54	56	67	85.5	1.20689
55	57	63	79.8	1.22618
56	58	59	74.4	1.24719
57	59	27	69.2	1.27021
58	60	55	63.8	1.29556
59	61	31	60.0	1.32420
60	62	51	54.4	1.35574

Table B.2: (continued)

Step #	# of Damaged Elements	Damaged Elements	V_{max}(KN)	Fundamental Period: T(s)
61	63	3	52.3	1.39270
62	64	79	47.6	1.43334
63	65	47	41.9	1.47583
64	66	35	35.0	1.53928
65	67	41	97.1	1.63019
66	68	1	109.4	1.70426
67	69	73	107.1	1.73621
68	70	45	104.0	1.77032
69	71	33	98.3	1.80693
70	72	61	95.2	1.84625
71	73	17	90.0	1.88853
72	74	9	87.2	1.93430
73	75	69	81.7	1.98408
74	76	53	77.0	2.03849
75	77	25	71.5	2.09831
76	78	13	68.7	2.16453
77	79	65	63.0	2.23842
78	80	49	58.2	2.32166
79	81	29	52.2	2.41658
80	82	77	47.6	2.52636
81	83	21	43.0	2.63278
82	84	57	37.0	2.78398
83	85	43	34.1	2.97204
84	86	5	88.1	3.11613

Table B.2: (continued)